The Pennsylvania State University

The Graduate School

DEVELOPMENT OF ULTRAFILTRATION AND DIAFILTRATION PROCESSES FOR BATCH AND CONTINUOUS FORMULATION OF MONOCLONAL ANTIBODIES

A Dissertation in

Chemical Engineering

by

Mario Jabra

Submitted in Partial Fulfillment

of the Requirements

for the Degree of

Doctor of Philosophy

August 2022

The dissertation of Mario Jabra was reviewed and approved by the following:

Andrew Zydney
Bayard D. Kunkle Chair and Professor of Chemical Engineering
Dissertation Advisor
Chair of Committee

Wayne Curtis
Professor of Chemical Engineering

Darrell Velegol
Professor of Chemical Engineering

William Hancock
Professor of Biomedical Engineering

Seong Kim
Professor of Chemical Engineering
Director of the Graduate Program

Abstract

There is growing interest among biopharmaceutical companies in the development of fully integrated continuous processes for the manufacture of monoclonal antibodies (mAbs). These continuous processes have the potential to significantly reduce manufacturing costs, enhance product quality, and provide greater flexibility to respond to changes in market demands. The objective of this thesis was to explore the development of novel strategies for antibody concentration and buffer exchange, both of which are critical in the final formulation step, using membrane ultrafiltration (UF) and diafiltration (DF).

Diafiltration is currently used to perform buffer exchange and desalting. However, this is an inherently batch process, requiring prolonged recirculation of the antibody solution through a membrane module containing a highly retentive ultrafiltration membrane. Chapter 2 of this thesis presents results for a continuous 3-stage countercurrent diafiltration process that was able to provide 99.9% removal of a model impurity, with constant operation for 24 hrs. An alternative approach for buffer exchange was explored in Chapter 3 using a countercurrent dialysis process. This system was not only able to provide very high degrees of impurity removal, it also used less buffer and much less expensive membrane modules than current batch operations.

Single Pass Tangential Flow Filtration (SPTFF) systems have recently been developed for continuous inline concentration using ultrafiltration modules with a long flow path length used to achieve high conversion in a single pass. However, the high conversion in SPTFF modules leads to large variations in local flow rate, protein concentration, and transmembrane pressure drop through the module, significantly complicating the design of effective SPTFF processes. Chapter 4 examined the development of a numerical model for the filtrate flux and

conversion in SPTFF modules specifically accounting for the effects of intermolecular interactions on the viscosity and osmotic pressure of the antibody solution. Model predictions were validated using experimental data obtained with a highly purified monoclonal antibody product in several different SPTFF modules. This model was then used in Chapter 5 to examine the design and optimization of SPTFF modules to achieve specific process objectives.

There is growing interest in formulating monoclonal antibody products in low-buffered or bufferless media. One challenge with the use of diafiltration under these conditions is the large shift in pH and excipient concentrations that are commonly seen over the course of the diafiltration. The main objective of Chapter 6 was to develop a model for the pH and excipient concentration based on Donnan equilibrium and electroneutrality constraints that incorporates the effects of both pH and ionic strength on the mAb charge through the use of a charge regulation model. The model involves no adjustable parameters, with the protein charge evaluated directly from the protonation / deprotonation of the ionizable amino acids in the protein structure. Experimental results were shown to be in excellent agreement with model calculations for multiple mAb products over a range of conditions. This model was then extended to evaluate the pH shifts seen in both batch ultrafiltration and continuous SPTFF processes in Chapter 7.

In total, the results presented in this thesis provide important insights into the development of ultrafiltration and diafiltration processes for the concentration / formulation of monoclonal antibody products in both continuous and batch operations.

Table of Contents

List of Figures

List of Tables

Acknowledgments

I would like to sincerely thank and acknowledge my advisor Dr. Andrew L. Zydney for his mentoring, teaching, guiding, helping and supporting every step of my PhD journey. His intelligence, hard work, work ethic, heedfulness and patience inspired me to become a better researcher and a better person. He has his own ways of motivating his students as all of his students sincerely love working with him. I would have not had as successful a journey if it wasn't for Dr. Andrew Zydney.

I would like to thank all the members of Dr. Zydney's group (Fatemeh, Parinaz, Seon, Ivan, Zhao, Negin, Chris, Mirko, Matthew, Kaitlyn, Neil, Joshua, Vikram, Kevork, Zhuoshi, Liang, Mohammad).

I would like to acknowledge the donation of the Inline Concentrators and SPTFF modules by Pall Corporation and MilliporeSigma and the financial support provided through the Bayard D. Kunkle Chair, Eli Lilly, and through the Membrane, Science, Engineering and Technology (MAST) Center, which is funded by grant number 1841474 from the NSF IUCRC program. I also appreciate the technical guidance from representatives of Pall, MilliporeSigma, Biogen, Amgen, and in particular Hank Nguyen at Eli Lilly. I would like to thank Biogen for donation of the monoclonal antibody used in the experimental studies.

Chapter 1: Introduction

1.1 Continuous biopharmaceutical processing

The biopharmaceutical industry is one of the fastest growing and most profitable industries in the world. From the development of vaccines to the treatment of cancer, these industries keep expanding in order to satisfy the ongoing demand for improved healthcare. Many of these products are monoclonal antibodies (mAbs), each of which has a specially-designed binding site that interacts with specific receptors / cells / pathogens associated with specific diseases[1]. FDA approvals for different mAbs is increasing every year due to the effectiveness of mAbs as targeted therapeutics, particularly in the field of immunotherapy. The sales of mAbs increased by 90% from 2008 to 2013 and are projected to reach more than $130 billion dollars in annual sales by the year 2021[2]. The average price of most mAb treatments is $96,731 per patient per year where some treatments can go well above $150,000[3]. The increasing demand for new mAbs has highlighted the need for developing better upstream and downstream processes for manufacturing mAbs. This is particularly true for downstream processing which can provide between 50% to 80% of the total production cost[4,5]. A schematic of a typical downstream process is illustrated in Figure 1.1.

Monoclonal antibodies are produced in mammalian cell lines, most commonly Chinese Hamster Ovary (CHO) cells, using fed-batch or intensified fed-batch cell culture. Over recent years, there is growing interest in implementing continuous perfusion bioreactors for CHO cell culture. A perfusion bioreactor operates with continuous feed of nutrients / media and continuous recovery of product with removal of toxins. The CHO cells are recycled back to the perfusion bioreactor using some type of cell retention device, often based on semipermeable membrane systems[6]. Perfusion bioreactors are ideal for producing unstable biomolecules since the product is rapidly removed from the bioreactor, minimizing the possibility of product degradation or

aggregation. Perfusion bioreactors also have much higher productivity (in g product per liter of bioreactor per hr). However, the overall benefits of using a perfusion bioreactor are diminished when the downstream processing is performed in batch mode, making it difficult to process the large quantity of mAb produced in these systems.

Continuous processing provides many advantages. It can maintain product stability, improve product quality, reduce bioreactor size, increase the production rate, and can decrease the production cost[7]. In addition, it can open up the possibility of using single-use disposable equipment, e.g., single use bioreactors (SUB) based on plastic bags. These single use systems offer the opportunity of processing multiple monoclonal antibodies in the same facility without concern about product contamination.

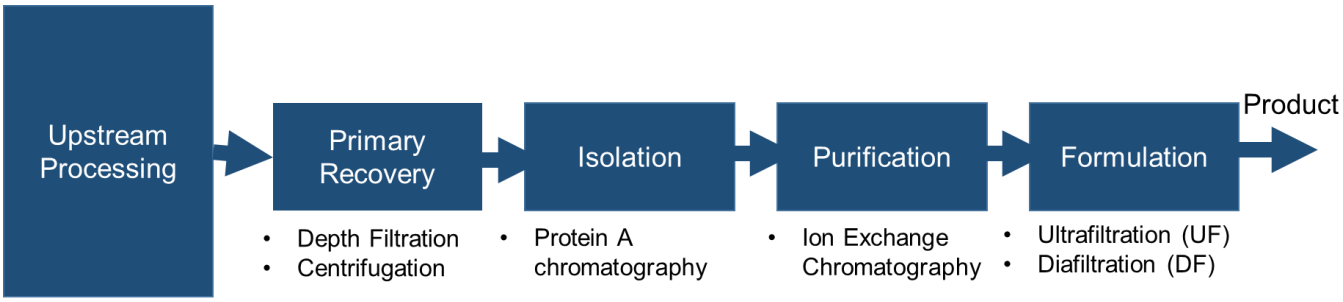

Figure 1.1: Schematic of downstream processing of therapeutics

1.2 Ultrafiltration and Diafiltration

Downstream processing steps include primary recovery (also known as clarification), isolation (or capture), purification (or polishing), and formulation. For the recovery, tangential flow filtration (TFF), alternating tangential filtration (ATF), depth filtration, and centrifugation are mainly used for the removal of cells and cell debris, with the product recovered in the liquid phase. Isolation and purification are commonly performed using Protein A affinity chromatography, ion

exchange chromatography, and hydrophobic interaction or mixed mode chromatography[8]. Formulation is typically performed by a combination of diafiltration (DF) and ultrafiltration (UF) which places the mAb in the desired buffer at a specific concentration appropriate for storage, transport, and delivery of the product to the patient. UF is a process which concentrates the mAb, with both water and other small solutes (e.g., buffer components) removed in the permeate. DF is used for buffer exchange, with the fresh buffer added continuously to the mAb solution while the previous buffer is removed through the membrane. Both UF and DF processes use membranes that have high retention of the mAb while allowing small solutes to pass through the membrane pores and into the permeate. A number of studies have examined different strategies for performing the chromatographic processing steps in a continuous format[9]. However, there is still a critical need to develop strategies for continuous UF/DF.

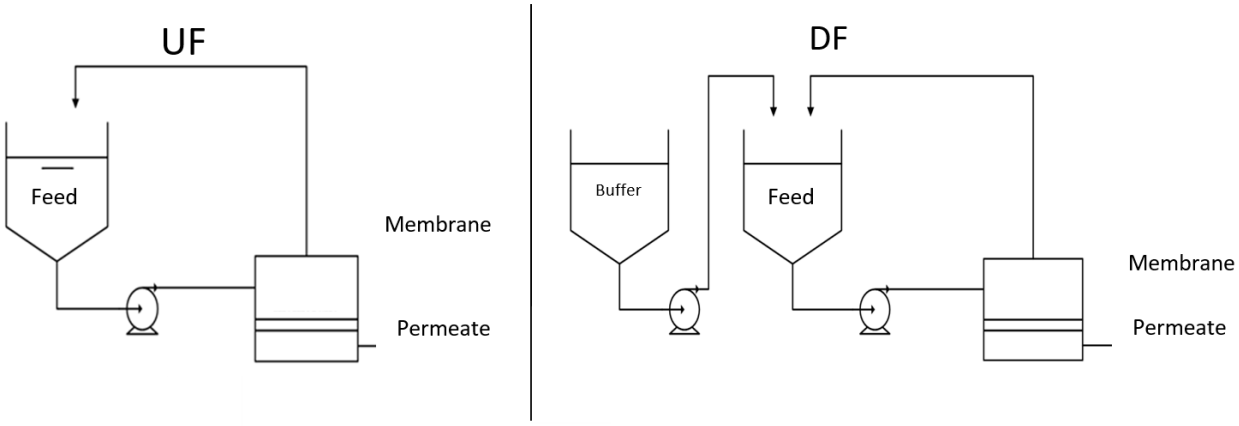

Figure 1.2: Schematic of the flow path in batch ultrafiltration (left) and diafiltration (right) processes.

Historically, UF and DF have been performed in a batch configuration as shown schematically in Figure 1.2. In batch UF, the feed is recirculated through the membrane module (with a membrane that is nearly fully retentive to the mAb) with permeate removed until the required concentration (or volume reduction) is achieved. The product is recycled many times through the membrane module because most current commercial UF modules have low conversion (≤10%), where the conversion is defined as the ratio of the cumulative permeate flow rate to the inlet (feed) flow rate. Batch DF is performed by recirculating the feed through the membrane while continuously adding buffer at the same rate as the permeate is removed, with the volume of the feed in the recycle tank maintained constant. Therefore, the concentration of the retained product is maintained while the species that pass through the membrane are diluted. The extent of diafiltration is typically described in terms of the number of diavolumes (N_D), equal to the volume of buffer added to the constant volume of the feed. The overall removal of impurities (R) during the diafiltration process is described by Equation (1.1)[10]:

$$R \equiv \frac{C_o}{C} = \exp(N_D\, S_o) \qquad (1.1)$$

where S_o is the observed sieving coefficient, equal to the ratio of the impurity concentration in the permeate to that in the bulk solution. C_o is the initial impurity concentration in the feed solution while C is the impurity concentration at any point during the diafiltration process.

The UF/DF process is time dependent with the number of diavolumes increasing as the filtration proceeds. Thus, the mAb is not obtained in the desired formulation buffer until the very end of the process. This type of batch operation creates a major bottleneck in the development of fully continuous processes for mAb production. In addition, the prolonged recirculation of the mAb through the membrane module can lead to mAb aggregation associated with the high shear rates and potential cavitation in the pump.

Several years ago, Pall Corporation released a single pass tangential flow filtration (SPTFF) module to the market sold under the tradename of Cadence™ Inline Concentrator (or ILC). The ILC provides significantly higher conversion than traditional TFF modules; thus, opening the possibility for continuous processing[11]. The module is designed so that there is a reduction of the cross-sectional area along the length of the module to compensate for the reduction in the retentate flow rate as permeate is removed (Figure 1.3).

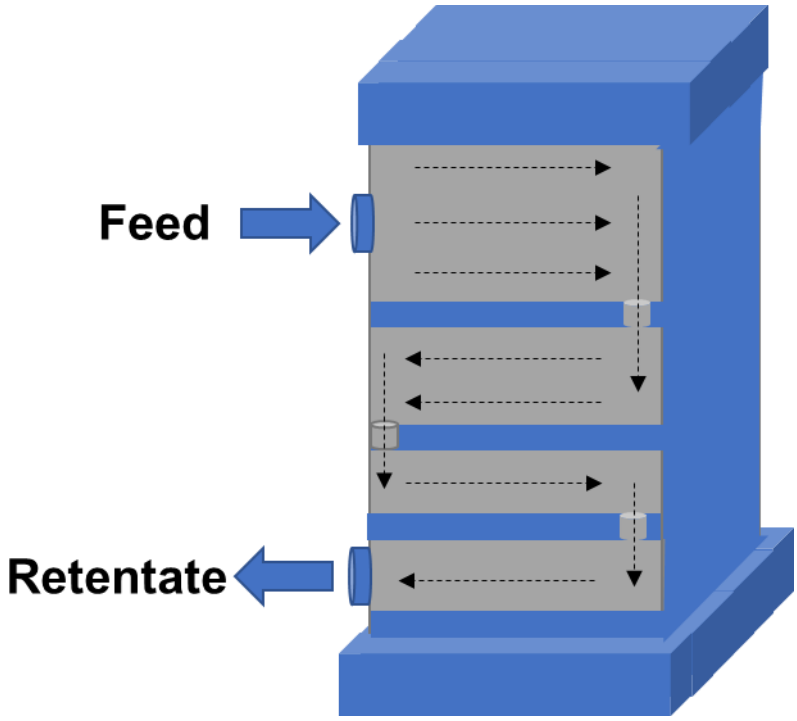

Figure 1.3: Schematic of the SPTFF design sold by Pall Corporation showing a reduction in the number of parallel channels along the length of the module.

1.5 pH and Excipient Shifts during UF/DF

MAbs are large charged macromolecules, with the net protein charge determined by the protonation / deprotonation of the various ionizable amino acids. Both the mAb charge and the existence of buffer non-idealities can cause partitioning of ions and pH shifts during ultrafiltration and diafiltration. These pH and excipient shifts cause challenges in obtaining the desired formulation conditions while adding the risk of mAb aggregation / degradation during excursions at low or high pH. Previous studies have examined the effects of volume exclusion[12] and Donnan equilibrium[13] (buffer partitioning) on the magnitude of these pH shifts as a function of buffer conditions, membrane properties, mAb concentration, mAb charge, mAb size and other parameters.[14] Bolton et al.[13] and Stoner et al.[15] developed models for UF/DF that accounted for the variation of the mAb charge with pH, however, the studies were limited to describing the pH and excipient concentrations at the end of the diafiltration process (where the system was assumed to reach equilibrium). Baek et al.[16] developed a model describing the pH throughout the diafiltration process by numerical integration of the governing species mass balances. Miao et al.[17] and Teeters et al.[18] solved the Poisson-Boltzmann equation to study pH and ion partitioning during DF.

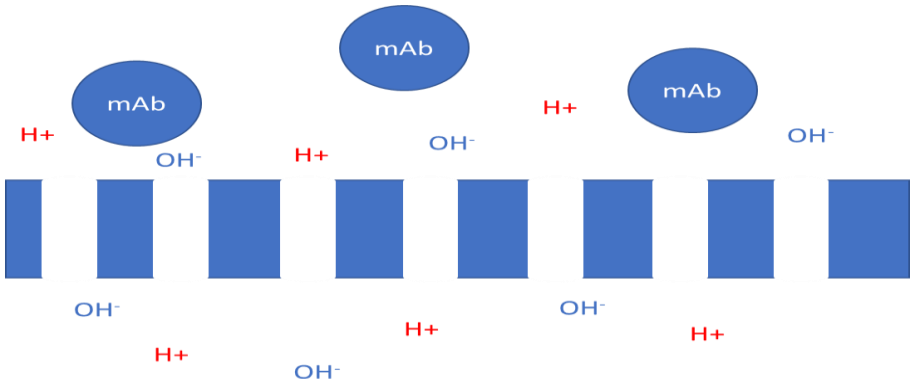

Figure 1.4: Schematic showing the different charged species on both sides of the membrane

As shown in Figure 1.4, since the charged mAb is present only on the retentate side of the membrane, a charge imbalance will occur between the retentate and permeate solutions. For instance, if the mAb is negatively charged, it would attract H^+ ions into the retentate to balance the charge on both sides of the membrane (typically referred to as Donnan equilibrium). This will cause a decrease in the pH of the retentate solution since the $pH = -\log_{10}[H^+]$. An opposite effect will occur with using a positively charged mAb. This will also affect the concentrations of other charged species in solution. The net result is that the final buffer concentration and pH in the product solution will not necessarily be the same as that in the diafiltration buffer even after a prolonged diafiltration process.

1.6 Thesis program

The overall objective of the thesis is to explore continuous and batch ultrafiltration and diafiltration methods for efficient monoclonal antibody processing and to provide a framework that can be used to better design and optimize antibody formulation processes.

In Chapter 2, experimental results are presented demonstrating the feasibility of using a 3 staged countercurrent setup for continuous diafiltration with operation for 24 hours without any degradation in performance. The results showed high levels of impurity removal and product recovery. In addition, model calculations explored the economic tradeoffs between staging and buffer consumption.

In Chapter 3, continuous countercurrent dialysis was explored as alternative approach for buffer exchange. Experiments demonstrated the feasibility of using low-cost hollow fiber hemodialysis modules for high levels of impurity removal with reduced buffer requirements

compared to both conventional batch diafiltration and countercurrent staged diafiltration processes.

In Chapter 4, a new mathematical model was developed capable of predicting the performance of SPTFF systems specifically accounting for the change in retentate flow rate and protein concentration, as well as the large pressure drops, due to flow through the retentate channel. The model was validated using experimental data obtained with a highly purified monoclonal antibody, with the key physical properties of the antibody solution (the viscosity and osmotic pressure) evaluated using independent experimental measurements over a wide range of antibody concentrations.

Chapter 5 examines the design and optimization of SPTFF systems for monoclonal antibody concentration using the model developed in Chapter 4. Model simulations explored the effects of module geometry, including channel length, width, and staging (variation in number of parallel channels along the module length) on the concentration factor and pressure drop.

Chapter 6 explores the pH and excipient shifts during batch diafiltration into low-buffered or bufferless media. A mathematical model was developed and shown to be in very good agreement with experimental data for the pH shift and the histidine and salt concentrations during batch diafiltration. The model explicitly accounts for the effects of charge regulation on the antibody charge as a function of pH and ionic strength, allowing *a priori* predictions of the diafiltration performance based on the amino acid sequence (composition) of the antibody.

Chapter 7 extends the models developed in Chapters 4 and 6 to evaluate the pH and excipient shifts in both batch ultrafiltration and SPTFF. The model uses the Nernst-Planck equation to calculate the local pH, excipient concentration, and solute flux across the membrane.

Chapter 8 provides a summary of the key conclusions from the work conducted in this thesis along with recommendations for future experimental and theoretical studies that would further advance our understanding of ultrafiltration and diafiltration processes for biomanufacturing.

Chapter 2: Multi-stage continuous countercurrent diafiltration for formulation of monoclonal antibodies

The work presented in this chapter is adapted from: Jabra, M. G., Yehl, C. J. & Zydney, A. L. Multistage continuous countercurrent diafiltration for formulation of monoclonal antibodies. *Biotechnol. Prog.* 35(4): e2810 (2019). doi:10.1002/btpr.2810. Mario Jabra and Christopher Yehl contributed equally to the experimental work with Mario Jabra taking the lead on preparation of the manuscript.

There is growing interest in the development of fully integrated and continuous biomanufacturing processes for the production of monoclonal antibody products. Recent studies have demonstrated the feasibility of using countercurrent staged diafiltration for continuous product formulation, but the 2 staged system examined previously did not provide sufficient levels of buffer exchange for most applications. The objective of the work presented in this Chapter was to design and test a 3-stage countercurrent diafiltration system that could achieve at least 99.9% buffer exchange over 24 hours of continuous operation. Experimental data were obtained using concentrated solutions of human Immunoglobulin G as a model protein, with the extent of vitamin B_{12} removal used to track the extent of diafiltration. Pall Cadence™ Inline Concentrators with Delta 30 kD regenerated cellulose membranes were used in each stage to achieve high conversion in a single pass. The 3-stage system showed stable operation with >99.9% vitamin B_{12} removal and minimal increase in pressure over the full 24 hours. Modules were effectively cleaned using NaOH, with nearly complete recovery of water permeability. A simple economic analysis was presented showing that the 3-stage system provides the optimal configuration for this type of countercurrent staged diafiltration process for typical buffer and membrane costs. The results

provide important insights to the design and operation of a continuous process for antibody formulation.

2.1 Introduction

Monoclonal antibodies (mAbs) are the largest class of biopharmaceutical products, with significant applications in immunotherapy and in the treatment of cancer. Annual sales of mAbs increased by 90% from 2008 to 2013 and are projected to reach $125 billion / yr by 2020[2]. Although mAbs are currently produced using batch processes, there is growing interest in the development of fully integrated continuous processes using perfusion bioreactors[9]. These continuous processes have the potential to significantly reduce cost of goods, increase manufacturing flexibility, and enhance product quality[9].

Buffer exchange / desalting is a critical step in the downstream process to place the mAb into the appropriate formulation buffer to insure stability during storage and safe delivery to the patient. Diafiltration (DF) is the most common approach for product formulation, with the feed solution re-circulated through a tangential flow filtration module (with a membrane that is highly retentive to the product) in a batch or fed-batch process[19]. As many as 100 pump passes are needed to obtain the high degree of buffer exchange appropriate for final formulation in this batch process.

Rucker-Pezzini et al.[20] examined the potential for doing continuous inline diafiltration using a series of sequential concentration and dilution steps, with each concentration performed using a Cadence Inline Concentrator (ILC) that can achieve high conversion in a single pass. Data obtained with a monoclonal antibody (mAb) using a 3-stage system showed 99.75% impurity removal; however, the process required nearly 4 times as much buffer as a corresponding batch diafiltration (performed at the same mAb concentration) due to the addition of fresh buffer in each of the repeated dilution steps.

Pall recently released the Cadence™ Inline Diafiltration (ILDF) device, which is an integrated system specifically designed to provide continuous (single-pass) diafiltration. The ILDF uses a series of 6 stages with the feed diluted with approximately 2.2x buffer in each stage to achieve an overall impurity removal of 99.9%. The buffer requirement for the ILDF is still somewhat greater than that for a batch DF. However, the simplicity and minimization of pump passes can outweigh the additional buffer consumption requirement.

In order to reduce the buffer requirements in a continuous diafiltration process, Nambiar et al.[21] used two Pall Cadence Inline Concentrators in a countercurrent staged configuration that effectively "re-used" the diafiltration buffer between stages. Steady-state operation with >98% product yield was obtained over a 2-hr process[21]. However, the two-stage system only provided 99% buffer exchange, which is well below the level required in most bioprocessing formulations (target exchange of at least 99.9%). Model calculations showed that a 3-stage countercurrent arrangement could provide the desired degree of buffer exchange with very similar buffer requirements as a traditional batch DF.

The objective of the work presented in this Chapter was to demonstrate the performance of a 3-stage countercurrent continuous diafiltration process with target impurity removal of at least 99.9%. Concentrated solutions of human serum immunoglobulin (polyclonal IgG) were used as the feed, with the degree of buffer exchange tracked using vitamin B_{12} as a model impurity. Stable steady-state operation was obtained over 24 hours, without the need for any membrane cleaning or process interruption. The performance of the multi-stage diafiltration process was also evaluated using a simple economic analysis accounting for the trade-offs between buffer requirements (i.e., buffer costs) and number of membrane stages (modules).

2.2 Materials and Methods

2.2.1 Buffer and Antibody solutions

All experiments were performed using human serum IgG obtained from Nova Biologics (Oceanside, CA) as a solid powder and then dissolved in 10 mM acetate buffer at the desired concentration. Vitamin B_{12}, obtained from MilliporeSigma (Burlington, MA), was used as a model impurity. In contrast to most fluorescent dyes which are electrically-charged, vitamin B_{12} is electrically neutral at pH 7. This eliminates issues associated with excipient partitioning (discussed in more detail in Chapter 6) and also reduces the likelihood of binding to the charged IgG. IgG and vitamin B_{12} concentrations were determined from the absorbance using a NanoDrop 2000c Spectrophotometer (Thermo Fisher Scientific, Waltham, MA) at wavelengths of 280 and 550 nm, respectively. Solute concentrations were determined from calibration curves constructed from standards of known concentrations accounting for the absorbance of both IgG and vitamin B_{12} at the respective wavelengths.

2.2.2 System and Module Setup

Countercurrent staged diafiltration was performed using the 3-stage system shown in Figure 2.1. Flow was driven by two Masterflex L/S Precision roller pumps, each with multiple pump heads, one that controlled the initial feed and retentate exits for each stage and one that controlled the buffer flow rate. Masterflex L/S Tygon E-LFL pump tubing size 16 was used in all experiments. This high-performance tubing provided consistent flow rates over long operating times (up to at least 24 hr). Flow rates were measured by timed collection using digital scales (LEADZM). Pressures gauges were placed at the feed, retentate, and permeate locations shown in Figure 2.1. The fresh diafiltration buffer (10 mM acetate without any vitamin B_{12}) was introduced

in Stage 3, with the permeate from each stage cycled back to the feed inlet for the previous stage to achieve the desired countercurrent staging. The permeate from Stage 1 was directed to waste.

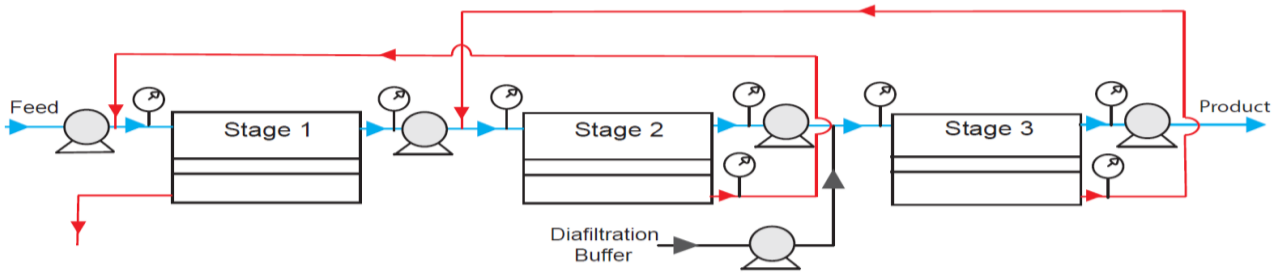

Figure 2.1: Schematic of the 3-stage countercurrent diafiltration system

2.2.3 SPTFF operation

After assembling the system, the pumps were started and the entire system was flushed with approximately 4 L of deionized water followed by 4 L of acetate buffer while manually adjusting the pumps to obtain the desired flow rates in the countercurrent configuration. The feed reservoir was then replaced with a solution of concentrated IgG spiked with vitamin B_{12}. Samples were obtained from the retentate exit from Stage 3 (the formulated product) throughout the experiment for off-line analysis of the IgG and vitamin B_{12} concentrations. At the end of the experiment, the entire system was flushed with 4 L of buffer followed by deionized water (for 40 minutes). The modules were then cleaned using 2 L of 0.5 N NaOH at room temperature followed by 2 L of 0.25 N NaOH at 40^{o}C. The modules were then filled with 0.1 N NaOH and stored at 4^{o}C until subsequent use.

2.3 Results and Discussion

2.3.1 Pressure profile for 3 staged countercurrent system

Figure 2.2 shows results for both the feed side pressure drop ($P_{feed} - P_{retentate}$) and the transmembrane pressure (average feed side pressure minus the permeate pressure) for the three stages (in-line concentrators) as a function of time during operation of the countercurrent staged diafiltration process. The experiment was performed using a feed containing 140 g/L IgG and 2.6 g/L vitamin B_{12}. The feed flow rate was kept constant at 4.0 ± 0.4 mL/min, with the diafiltration buffer added at a flow rate of 46 mL/min (corresponding to $\alpha = q_{DF}/q_F = 11.5$). Thus, the total feed flow rate into each module (stage) was 50 mL/min, corresponding to a feed flux (feed flow rate normalized by the membrane area) of 46 $L/m^2/h$. Each module provided a single pass conversion of 92 ± 1%, with the conversion defined as the ratio of permeate to feed flow rates. The feed was processed in single-pass mode (no recycle), with the conditions used in this experiment providing the formulation of slightly more than 800 g of IgG over the 24-hr run.

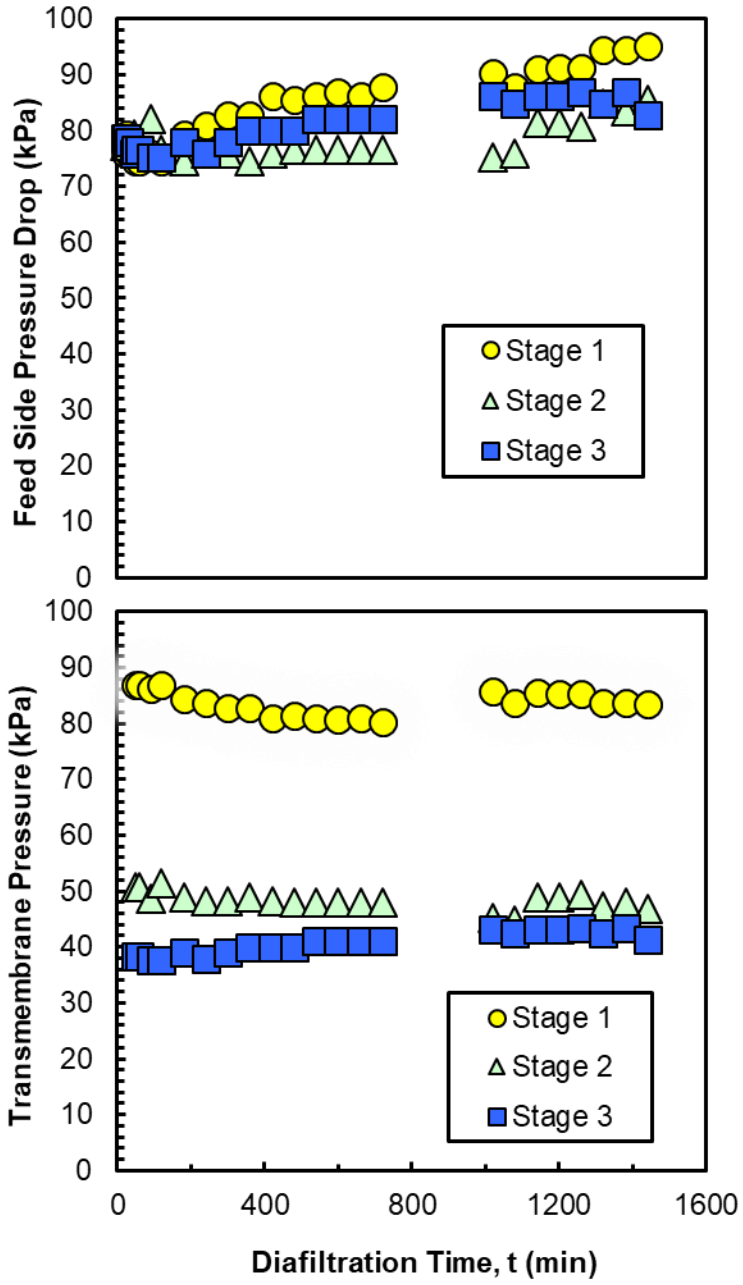

Figure 2.2: Feed side pressure drop and transmembrane pressure (TMP) for each stage of the countercurrent 3-staged diafiltration system. Feed contained 140 g/L of IgG at a flow rate of 4.0 ± 0.4 mL/min. Data obtained using Cadence Inline Concentrators with 650 cm^2 membrane area.

The feed side pressure drop (top panel) and the transmembrane pressure (bottom panel) both remained relatively stable throughout the diafiltration process after a short initial equilibration period (<10 min). The feed-side pressure drop in Stage 1 does show about a 20% increase over the course of the 24-hr run, which may be due to a low level of membrane fouling. The feed side pressure drop was approximately 80 kPa (12 psi) for all three stages, consistent with the use of identical modules for each stage. However, the transmembrane pressure was significantly higher in Stage 1, which is the stage where the permeate flow is unrestricted. In contrast, the permeate flow from Stages 2 and 3 are recycled back to the feed of the previous stage using Y-connectors, creating a back-pressure on the permeate flow in both of these modules. This led to small differences in the conversion in the 3 modules, with the slightly higher conversion (flux) in Stage 1 resulting in the higher transmembrane pressure.

2.3.2 Impurity removal for 3 staged countercurrent diafiltration

The effectiveness of the countercurrent staged diafiltration process is shown in Figure 2.3. The top panel shows the IgG concentrations in the formulated product collected in the retentate exit from the final stage of the 3-stage system as a function of time, while the bottom panel shows the corresponding vitamin B_{12} concentrations. In both cases, the data points represent the means and standard deviations determined from 3 consecutive samples. The IgG and vitamin B_{12} concentrations both remained very stable throughout the diafiltration, similar to the results for the pressures. The average exit IgG concentration was 120 g/L, which is somewhat lower than the feed concentration of 140 g/L. This difference is due to a small dilution of the feed (the average exit flow rate was 4.9 mL/min compared to the feed flow rate of 4 mL/min). The calculated IgG yield, accounting for the dilution effect, was 103 ± 6%. The average vitamin B_{12} concentration in

the formulated product was less than 3 mg/L, corresponding to 99.9% removal. This is equivalent to the value that would be obtained in a constant volume batch diafiltration process after approximately 7 diavolumes. However, the 3-stage process required only 0.082 L of buffer per g of protein. A batch diafiltration performed at 120 g/L would require slightly less buffer, although this high a concentration would lead to a very low filtrate flux. More typical operation of the batch DF at a feed concentration of 60 g/L would require 0.12 L/g [21]. Note that the Cadence Inline Diafiltration system (ILDF) employing 6 sequential dilution and concentration steps requires 0.094 L/g for the same degree of impurity removal (for a feed concentration of 140 g/L), which is 15% more than that the countercurrent staged process.

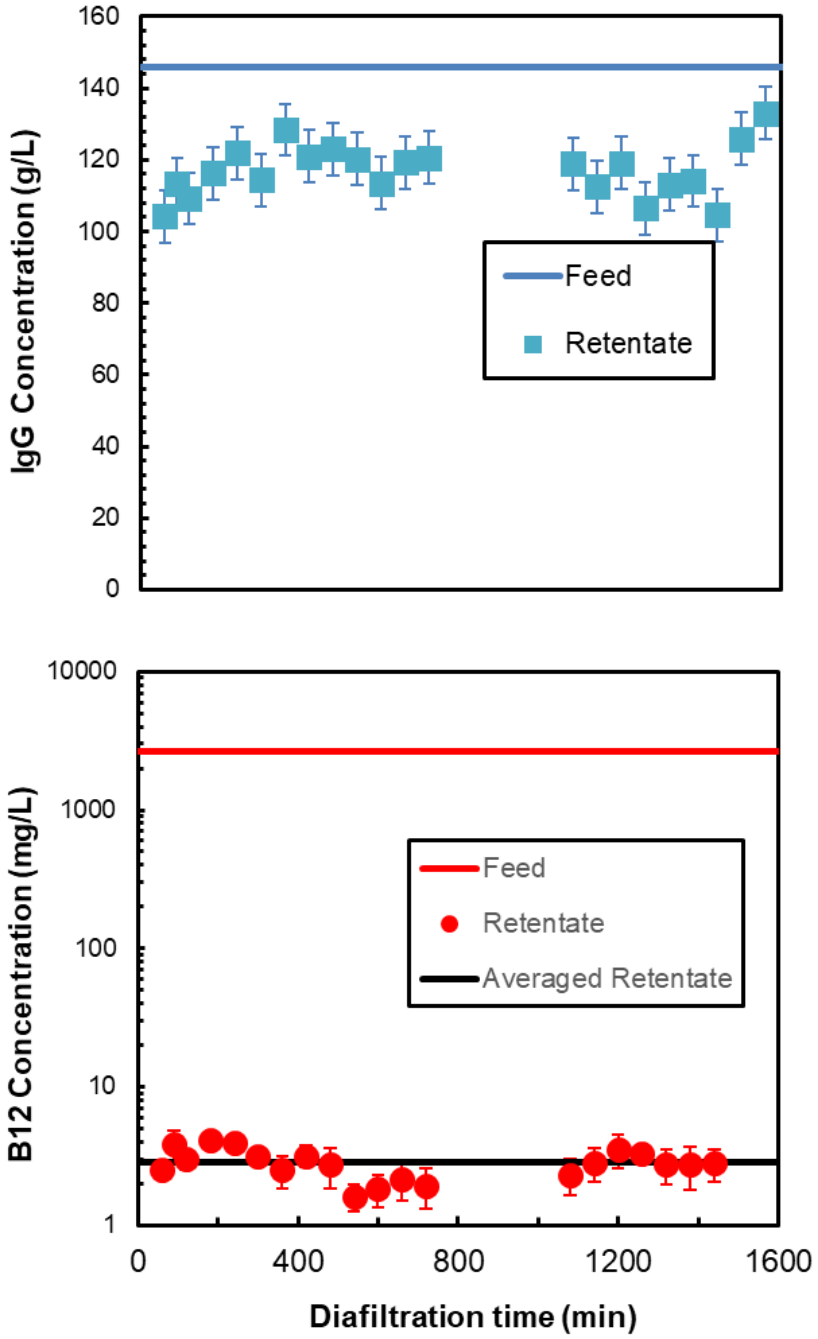

Figure 2.3: IgG (top panel) and vitamin B12 (bottom panel) concentrations in the feed and formulated product during the 24 hr diafiltration. Feed contained 140 g/L of IgG at a flow rate of 4.0 ± 0.4 mL/min. Each stage used Cadence Inline Concentrators with 650 cm^2.

2.3.3 Effect of staging and flow ratio on impurity removal

The extent of diafiltration for this type of countercurrent staged diafiltration was evaluated theoretically by Nambiar et al.[11] as:

$$R = \frac{C_{Feed}}{C_N} = \frac{\alpha^{N+1} - 1}{\alpha - 1} \qquad (2.1)$$

where C_{Feed} is the initial impurity concentration in the feed, C_N is the impurity concentration in the retentate exit from the N-stage system, and α is the ratio of the buffer flow rate to the feed flow rate. The 3-stage diafiltration examined in Figure 2.3 would thus provide R = 1700 compared to the experimental value of R = 1100 ± 400 in this study. This difference may simply be due to errors in evaluating the small concentration of vitamin B_{12} in the final product, although it could also arise from the dilution effect and the discrepancies in the internal (recirculation) flow rates. Note that R = 1100 would correspond to α = 10 for the 3-stage system, which is approximately equal to the ratio of the buffer flow rate to the average of the feed and retentate (exit) flow rates.

The solid curves in Figure 2.4 show the effects of the number of stages and the flow ratio on the overall impurity removal based on Equation (2.1). The symbols are experimental results obtained in this thesis and from the literature[21]. The model calculations are in good agreement with the experimental data, confirming that the performance of the countercurrent staged diafiltration can be well described using classical models for staged systems. An impurity removal of R = 1000 (99.9%) can be achieved with a 2-stage system using a flow ratio of α = 31, while the 3-stage system only requires α = 9.6. A 4-stage system could achieve the same degree of impurity removal using α = 5.4. These differences in α correspond to large differences in the amount of buffer required for the formulation per gram of protein:

$$V_{DF} = \frac{\alpha}{C_F} \qquad (2.2)$$

where C_F is the protein concentration in the feed. Thus, the 2-stage system would require 0.22 L/g while the 3-stage system only requires 0.069 L/g assuming that both processes operate with C_F = 140 g/L.

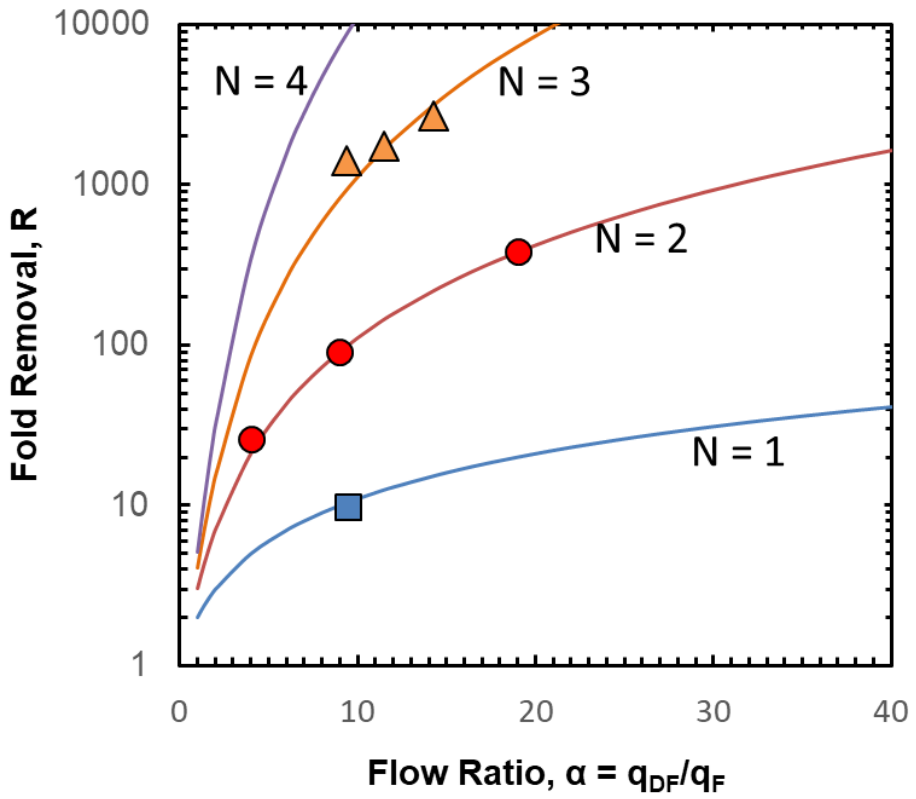

Figure 2.4: Impurity removal (R) as a function of flow ratio for countercurrent diafiltration processes using different numbers of stages. Solid symbols are experimental data. Results from the 2-stage system were obtained by Nambiar et al.[21]

2.3.4 Membrane cleanability and reusability

The data in Figure 2.4 were obtained with the same Inline Concentrator modules, with the modules cleaned in between each experiment with 2 L of 0.5 N NaOH at room temperature followed by 2 L of 0.25 N NaOH at 40°C. The cleaning cycle was highly effective at restoring the

clean water permeability for the modules, with typical data for one of the modules (used as Stage 1 in the 3-stage system) shown in Figure 2.5. The clean water permeability of the membrane, evaluated as the ratio of the filtrate flux to the transmembrane pressure, was 1.79 L/m^2/hr/kPa. The permeability after both 5 and 10 cycles (5 separate diafiltration experiments, each using different flow rates and IgG feeds) was within ± 4% of this value. Additional studies would be needed to determine the ultimate lifetime for these modules in this type of countercurrent staged diafiltration process.

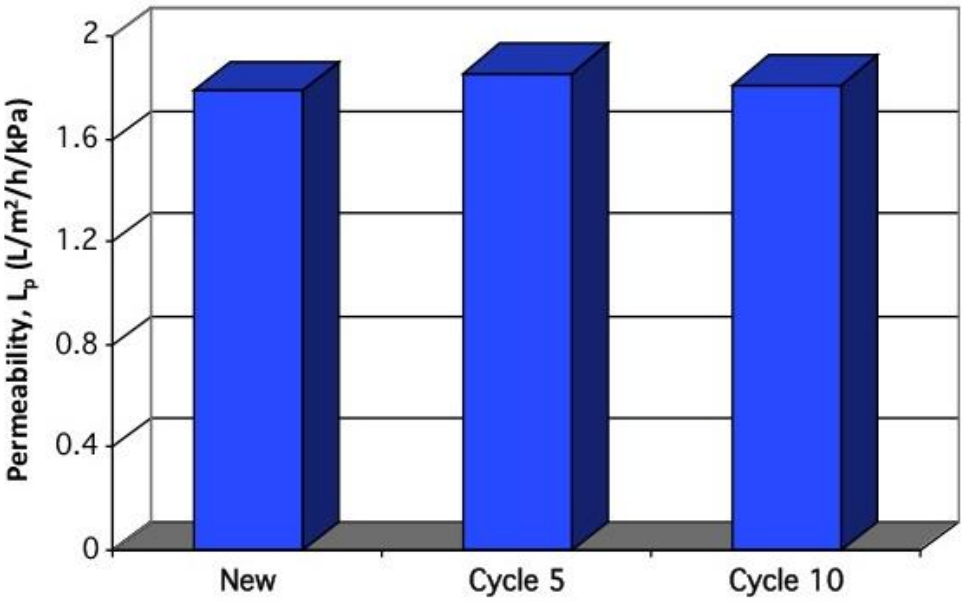

Figure 2.5: Permeability of the Pall InLine Concentrator (Stage 1) new, after 5 cycles of use, and after 10 cycles.

2.3.5 Economic analysis

In order to obtain additional insights into the performance of the countercurrent staged diafiltration process, a simple economic analysis was performed with the cost per gram of formulated protein evaluated as:

$$C_{total} = E_{buffer} V_{DF} + E_{module} N \tag{2.3}$$

The coefficients E_{buffer} (in \$ / L of buffer) and E_{module} (in \$ / g product) are related to the cost of the buffer and membrane modules, respectively. Typical buffer costs are E_{buffer} = \$1 - \$10 per L. The cost of the module depends upon the cost of the membranes (in \$ / m^2) and the total amount of protein that can be processed before the module needs to be replaced, with the latter equal to the product mass flow rate multiplied by the total module lifetime. Each of these has considerable uncertainty. The 24-hr diafiltration experiment conducted in this thesis was performed at a feed flow rate of 4 mL/min using 140 g/L IgG using membranes with 650 cm^2 membrane area, giving 12 kg product per m^2 membrane area per module. Thus, a membrane cost of ~\$7,000 / m^2 would correspond to E_{module} = \$1 / g of formulated IgG. This cost would be further reduced if the modules were able to operate for significantly more than 24 hr. In addition, larger scale commercial systems would be expected to have much lower membrane costs per m^2.

Figure 2.6 summarizes the results using E_{buffer} = \$2 and \$8 per L in the bottom and top panels, respectively, for several values of E_{module}. In each case, the model calculations were performed assuming an extent of diafiltration of 99.9% (R = 1000), with V_{DF} calculated from Equation (2.2) using the value of α given by Equation (2.1). The cost for the single stage system is prohibitively high due to the very large quantity of buffer needed to achieve the 99.9% buffer exchange. The cost decreases significantly for the 2-stage system due to the large reduction in α. The lowest cost for E_{buffer} = \$8 / L and E_{module} = \$1 and \$0.5 / g is achieved with the 3-stage system, with further increases in the number of stages causing an increase in the total cost due to the greater cost of the modules. The optimal system design shifts to N = 4 and N=5 as the cost of the modules decrease to \$0.1 and \$0.05 / g, i.e., as the modules themselves become less expensive or as the

module lifetime increases. Decreasing the buffer cost to $2 / L also causes the optimal configuration to shift to 2 stages for a module cost $0.5 /g and above and to 3 stages when the module cost is $0.1 /g as seen in the lower panel of Figure 2.6.

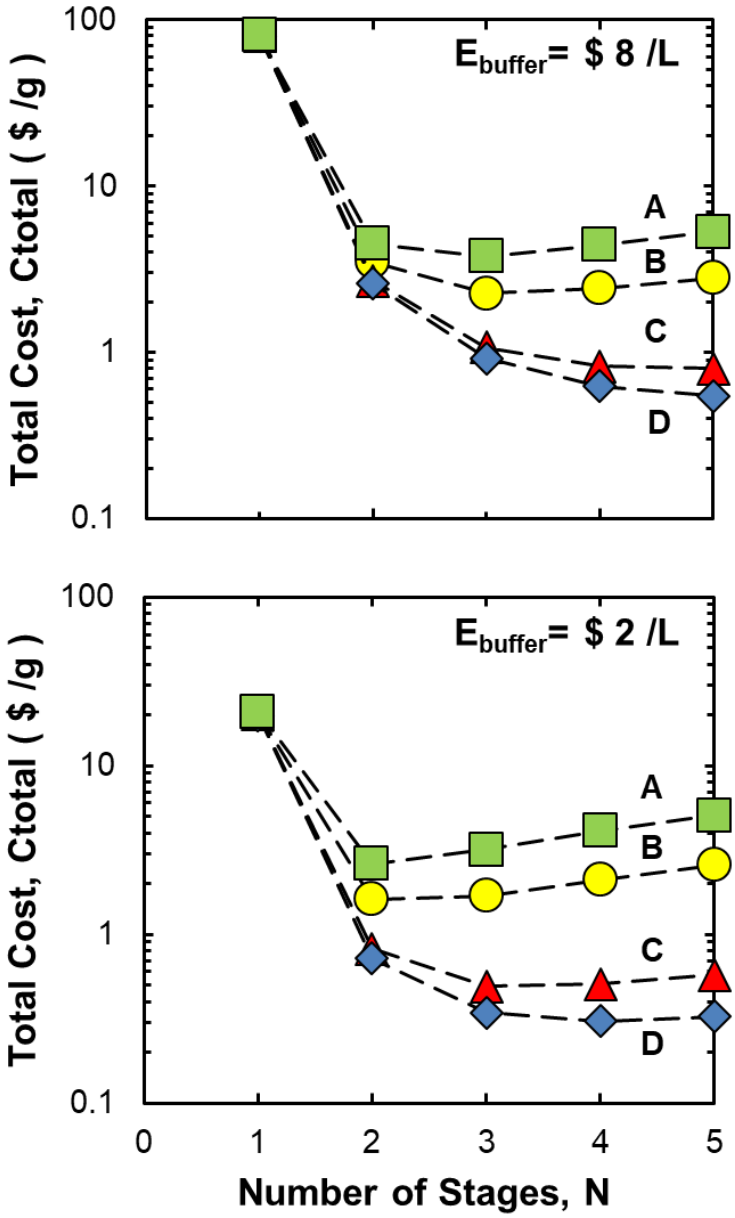

Figure 2.6: Economic analysis comparing the total diafiltration cost per gram of formulated protein as a function of the number of stages for E_{buffer} = \$8 / L (top panel) and E_{buffer} = \$2 / L. Curves A, B, C and D are constructed using E_{module} = \$1, \$0.5, \$0.1 and \$0.05 /g respectively.

2.4 Conclusions

The development of truly integrated continuous bioprocesses requires a re-evaluation of many of the standard unit operations used in current batch manufacturing. In this Chapter, we have examined the performance of a continuous staged countercurrent diafiltration system suitable for the final formulation of monoclonal antibody products and other biotherapeutics. Experimental studies demonstrated that a 3-stage countercurrent diafiltration could provide 99.9 % impurity removal ($R > 1000$) for a full 24-hr run with nearly constant exit concentrations and pressures throughout the process. The protein yield was essentially 100%, but there was a 15% dilution due to the inability to maintain identical feed / retentate flow rates in each stage. The implementation of this technology in commercial manufacturing would likely require the use of appropriate process automation and control to maintain the desired flow rates and product concentration.

The 3-stage countercurrent DF system examined in this Chapter provided equivalent buffer exchange as that given by the commercial Pall Cadence Inline Diafiltration system which operates using $\alpha = 2.2$ but with 15% less buffer; this is directly due to the more effective use of the diafiltration buffer associated with the countercurrent staging. In addition, the countercurrent DF system provided a formulated product at a concentration >100 g/L, which would likely eliminate the need for a final ultrafiltration (concentration) step as used by Rucker-Pezzini et al. in their DF process[20].

A simple economic analysis of the effects of staging showed that the 3-stage countercurrent diafiltration process yielded the lowest overall cost per gram of product for typical values of the buffer and module costs. Increasing the number of stages (modules) does reduce the amount of buffer required, but this was not sufficient to compensate for the greater cost of the modules except when operating with expensive buffers or very low-cost modules. Reducing the cost of the buffer

or increasing the cost of the modules shifted the optimal system configuration to the 2-stage system.

One of the critical factors determining the overall economics of the countercurrent staged diafiltration is the total quantity of protein that can be processed by the modules. The data obtained in this Chapter showed very low levels of fouling over 24-hr of operation, corresponding to the formulation / processing of more than 12 kg per m^2 of membrane. In addition, the modules could be effectively cleaned at least 10 times, with nearly complete restoration of the original permeability. This indicates that it would be possible, at least in principle, to periodically remove and clean the modules, enabling the 3-stage system to process as much as 120 kg of product per m^2. Note that a 2000 L perfusion bioreactor producing a monoclonal antibody at 2 g/L concentration with one volume exchange per day would yield approximately 360 kg of product over 3 months of operation, indicating that a single countercurrent diafiltration system with 3 m^2 of membrane area per module could potentially process this entire quantity of product. Additional studies will be required to demonstrate the effectiveness of this type of continuous formulation step as part of an actual commercial manufacturing process.

Chapter 3: Hollow Fiber Countercurrent Dialysis for Continuous Buffer Exchange of High Value Biotherapeutics

The work presented in this chapter is adapted from: Yehl, C. J., Jabra, M. G. & Zydney, A. L. Hollow Fiber Countercurrent Dialysis for Continuous Buffer Exchange of High Value Biotherapeutics. *Biotechnol. Prog.* 35(2): e2763 (2018). doi:10.1002/btpr.2763 Mario Jabra and Christopher Yehl contributed equally to the experimental work with Christopher Yehl taking the lead on preparation of the manuscript.

Buffer exchange, desalting, and formulation of high value biotherapeutics are currently performed using batch diafiltration; however, this type of tangential flow filtration process may be difficult to implement as part of a fully continuous biomanufacturing process. The objective of the work described in this Chapter was to explore the potential of using countercurrent dialysis for continuous protein formulation and buffer exchange. Experiments were performed using concentrated solutions of serum Immunoglobuin G (IgG) with commercially available hollow fiber dialyzers having 1.5 and 1.8 m^2 membrane surface area. More than 99.9% buffer exchange was obtained over a range of conditions, as determined from the removal of a model impurity (vitamin B_{12}). The dialyzers were able to process more than 0.5 kg of IgG per day in an easily scalable low-cost process. In addition, buffer requirements were less than 0.02 L of buffer per g IgG, which is several times less than that used in current batch diafiltration processes. These results clearly demonstrate the potential of using low-cost hollow fiber dialyzers for buffer exchange and product formulation in continuous bioprocessing.

3.1 Introduction

Buffer exchange is a critical processing step in the commercial production of all biotherapeutics and other protein-based products[10]. Buffer exchange is used to precondition in-process streams to enhance the performance of subsequent unit operations, e.g., desalting prior to ion exchange chromatography[22]. More significantly, buffer exchange is required to place the protein product in the desired formulation buffer for long-term storage and delivery.

The dominant method for performing buffer exchange in large-scale bioprocessing is batch diafiltration (DF), which involves a simultaneous dilution (buffer addition) and concentration, with the latter performed by tangential flow ultrafiltration in which the liquid phase is removed by pressure-driven filtration through a semipermeable membrane. Constant volume batch DF is the most common process configuration, with the product solution continuously recirculated through the tangential flow ultrafiltration module while fresh (DF) buffer is added at a rate equal to that at which the filtrate is removed. Commercial systems for batch DF can involve several hundred square meters of membrane area housed in a specially-designed stainless steel skid[19].

Although current bioprocessing operations are almost all performed in batch mode, increasing concerns about cost of goods and manufacturing flexibility has led to growing interest in the potential of continuous bioprocessing. These continuous bioprocesses can provide significant reductions in production time and facility size, improved product quality (due to the reduction in residence time throughout the process), and increased productivity.[5] Pall Corporation has recently introduced the Cadence Inline DF module, the first commercial system designed for continuous buffer exchange[20]. The DF involves multiple sequential (inline) dilutions and concentration steps, each performed using single pass tangential flow filtration (SPTFF)

modules[11]. 1000-fold removal of impurities can be achieved using 3-stages, each with 10-fold dilution. Although these modules do provide continuous buffer exchange, the system requires considerably larger buffer volumes to achieve the same level of buffer exchange as a corresponding batch system, and the fluid needs to be managed through a more complicated (and expensive) multi-head pumping system.

Nambiar et al. [21] also used SPTFF modules for continuous DF, but the individual modules (stages) were arranged in a countercurrent configuration to significantly reduce the buffer requirements. Data obtained with a polyclonal IgG showed 99% removal of a small impurity using a 2-stage system with similar buffer requirements as a batch process. Even higher degrees of impurity removal above 99.9 % with lower buffer consumption can be obtained for processes employing 3 or 4 stages as discussed in Chapter 2. However, the requirement for multiple pumps, multiple SPTFF modules, and the complex countercurrent staging might limit commercial applications of this technology.

An alternative approach for buffer exchange is to use dialysis in which the buffer components diffuse across a semipermeable membrane that separates the product solution from the dialysate. Dialysis bags or tubes are used extensively for laboratory-scale (batch) buffer exchange with the protein dialyzed against water or an appropriate buffer solution. In addition, hemodialysis (i.e., "blood" dialysis) is one of the largest commercial applications of membrane technology[23]. Current hemodialyzers consist of a parallel array of nearly 10,000 hollow fiber membranes, approximately 200 μm in inner diameter and 40 μm thick.[24] Most dialyzers use synthetic polysulfone membranes which are highly retentive to albumin (MW = 67 kDa) but allow rapid removal of small solutes like urea, creatinine, and uric acid.[24] Clinical hemodialysis is typically performed with blood flow rates of 300 – 500 mL/min with dialysate flow rates of 600

mL/min; these dialyzers remove about 90% of the urea in a single pass while also providing significant removal of middle molecular weight proteins like β_2-microglobulin which is associated with dialysis-related amyloidosis.[25]

Kurnik et al.[10] examined the use of countercurrent dialysis for large-scale buffer exchange in bioprocessing applications as part of a more general study comparing the performance of dialysis, DF, and size exclusion chromatography. The results demonstrated that DF provided the best overall performance, although the analysis was limited to batch processes employing very dilute protein solutions (in this case 1 g/L bovine serum albumin). In addition, the countercurrent dialysis was performed using Cuprophan regenerated cellulose membranes that have much poorer transport characteristics than the high performance synthetic polysulfone membranes that now dominate the hemodialysis market[23,26].

The objective of the work presented in this Chapter was to examine the potential of using countercurrent hollow fiber dialyzers for continuous buffer exchange of a highly concentrated protein solution, typical of what would be expected for a continuous bioprocess used for monoclonal antibody production. Experiments were performed using off-the-shelf hollow fiber cartridges developed for hemodialysis; these membranes only provide ≤90% impurity removal in hemodialysis applications which employ much higher feed flow rates than what were used in this study. The results clearly demonstrate that countercurrent continuous dialysis can readily achieve the high degrees of buffer exchange required for final product formulation using less buffer than a corresponding batch system with relatively simple / straightforward and low-cost operation.

3.2 Materials and Methods

3.2.1 Dialysis Module

All experiments were performed using either Nipro Polynephron® or Fresenius Optiflux F180B polysulfone hollow fiber dialyzers with properties summarized in Table 3.1.

Table 3.1: Properties of hollow fiber dialyzers

Dialyzer	Manufacturer	Polymer	Membrane Area	Inner Diameter	Fiber Length
Polynephron	Nipro	Polyethersulfone	1.5 m^2	200 µm	0.26 m
Optiflux F180B	Fresenius	Polysulfone	1.8 m^2	185 µm	0.25 m

A new dialyzer was used for each experiment. The dialyzer was mounted in a vertical orientation with the dialysate buffer introduced into the shell side from the top port (Figure 3.1). The feed (product solution) was introduced into the lumen-side inlet at the bottom of the dialyzer to achieve countercurrent flow. Feed and buffer flow rates were controlled using Masterflex L/S peristaltic pumps (Cole-Parmer) fitted with platinum-cured silicone tubing (Cole-Parmer). The dialysate inlet and outlet flows were controlled using a single pump fitted with two pump-heads; a separate pump was used for the feed inlet. The pumps were calibrated before each experiment by timed collection using a digital balance. Pressures were monitored throughout the experiment using Ashcroft pressure gauges located immediately before and after the inlet / outlet ports. Dialyzers were flushed with buffer solution before the experiment. The feed flow was then started to fill the dialyzer, with

the dialysate flow started as soon as the feed had stabilized. Experiments were performed at room temperature (21 ± 2 ^{o}C) without any external temperature control.

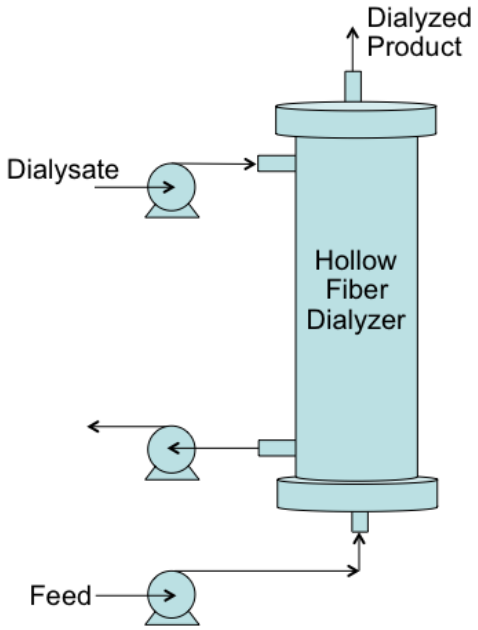

Figure 3.1: Schematic of continuous countercurrent dialysis system.

3.2.2 Buffer and Antibody solutions

Dialysis was performed using solutions of human serum immunoglobulin G (IgG – NovaBiologics, Oceanside, CA) with vitamin B_{12} (Caymen Chemicals, Ann Arbor, MI) used as a model impurity. The IgG was dissolved in a 10 mM sodium acetate buffer at pH 5; the same buffer (without any vitamin B_{12}) was used as the dialysate. All solutions were pre-filtered through 0.2 μm mixed cellulose and/or 0.45 μm polyvinylidene fluoride (PVDF) membranes prior to use to remove any insoluble aggregates. When necessary, the IgG solutions were centrifuged at 4800 g before the pre-filtration to remove undissolved (particulate) material.

All experiments were performed using constant feed and buffer flow rates in single pass operation (no recycle of either the IgG or the dialysate). Small samples were obtained periodically from both the dialysate and feed exits for off-line evaluation of the IgG and vitamin B_{12} concentrations using a NanoDrop 2000c Spectrophotometer (Thermo Scientific) based on the absorbance at 550 and 280 nm; these wavelengths have strong absorbance for vitamin B_{12} and IgG, respectively. Vitamin B_{12} was used due to its low binding to the IgG and the membrane as well its easy quantification. Appropriate calibration curves were constructed using standard solutions with known concentrations of both components to account for the non-zero absorbance of both species at the two wavelengths.

3.3 Results and Analysis

3.3.1 Vitamin B_{12} removal

Typical data for the vitamin B_{12} concentration in the product (exit) stream from a countercurrent dialysis experiment are shown in Figure 3.2. Data were obtained with the Optiflux F180B dialyzer using a feed flow rate of $q_F = 4.0 \pm 0.3$ mL/min and a dialysate buffer flow rate of $q_D = 9.0 \pm 0.3$ mL/min, corresponding to $\alpha = q_D/q_F = 2.25$. The pressure drop across the dialyzer (feed inlet minus retentate outlet) was <2 kPa (0.3 psi); the very low pressure drop is directly related to the low flow rates used in these experiments compared to the 300 – 600 mL/min flow rates used in clinical applications of the Optiflux module for hemodialysis. The feed contained IgG and vitamin B_{12} at concentrations of 100 ± 2 g/L and 3300 ± 100 mg/L, respectively. This system thus processed 0.4 g of IgG per min or about 0.5 kg / day. This is comparable to the level of protein produced by a 500 L perfusion bioreactor operated continuously using one bioreactor volume exchange per day and a mAb titer of 1 - 1.5 g/L, which are typical of the values expected

for continuous bioprocessing for small-scale manufacturing.[9] The initial feed volume of 800 mL was fully processed in 200 min. No data were obtained during the first 30 min since it required almost this much time to fully washout the ≈100 mL hold-up volume in the dialyzer and tubing.

The vitamin B_{12} concentration in the final dialyzed product fluctuated between values of 0 and 1.2 ± 0.6 mg/L, corresponding to 99.98 ± 0.04% buffer exchange; the values plotted in Figure 3.2 are the average of 3 consecutive measurements taken at 10-minute intervals (plotted at the mean time). The large error bars are due to the very low absorbance of B_{12} at these low concentrations; these values are just beyond the limit of quantification for the spectrophotometric assay. Note that these dialyzers typically provide only 60-90% solute removal in a single pass when used in hemodialysis applications; the much higher level of vitamin B_{12} removal in this study is due to the much lower flow rates used in our experiments.

The average IgG concentration in the collected product stream was 103 ± 4 g/L (data not shown), which is nearly identical to the feed concentration of 100 ± 2 g/L. The slight increase in IgG concentration was due to a small filtration flow rate across the membrane; the retentate exit flow rate was 3.74 mL/min compared to 3.97 mL/min for the feed. The overall IgG yield was 101 ± 4% after accounting for the slight concentration of the product stream. There was no evidence of any IgG in the dialysate solution, nor was there any evidence of IgG adsorption to the membrane. This is consistent with the application of these hollow fiber membranes in hemodialysis in which there is nearly complete recovery of albumin and larger plasma proteins. Note that the buffer exchange in Figure 3.2 was accomplished using 0.023 L of buffer per g of IgG, which is several times less than that for a conventional batch DF process (0.058 L/g for DF performed at 120 g/L and 0.12 L/g for DF at the more commonly used 60 g/L). This is discussed in more detail subsequently.

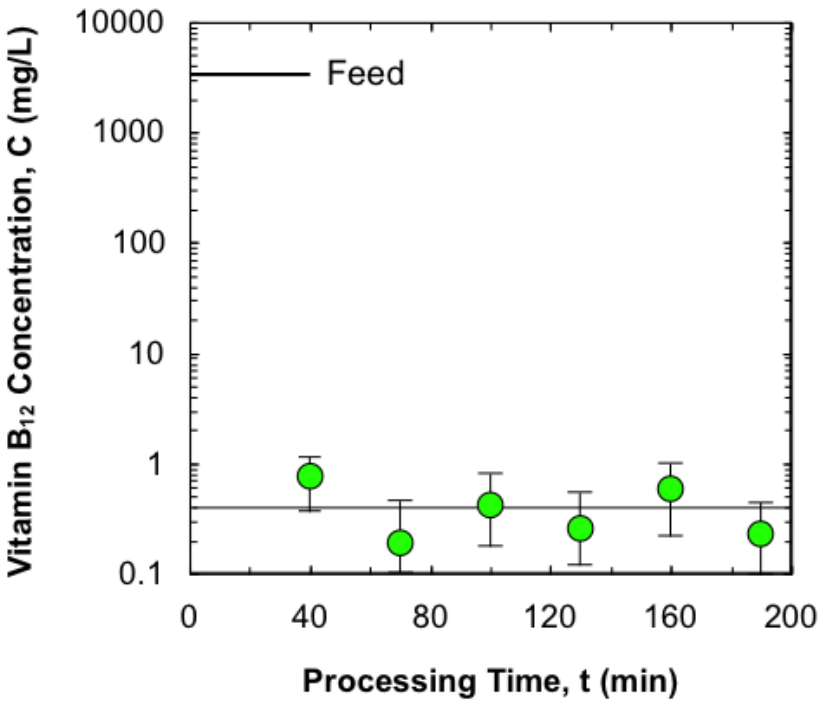

Figure 3.2: Vitamin B12 concentration in the diafiltered product stream using the Optiflux F180B dialyzer operated with a 3.97 mL/min feed ($\alpha = 2.25$) containing 100 ± 2 g/L IgG and 3300 ± 100 mg/L vitamin B_{12}.

3.3.2 Effect of IgG feed concentration

Figure 3.3 shows the degree of vitamin B_{12} removal, defined as the ratio of the vitamin B_{12} concentration in the feed to the measured concentration in the buffer exchanged product, as a function of the IgG concentration in the feed solution. Results with both the Optiflux 180B and Nipro Polynephron® dialyzers were essentially identical, with R = 1000 ± 200 independent of the IgG concentration. This is in sharp contrast to the behavior of a tangential flow diafiltration process in which the filtrate flux decreases significantly with increasing protein concentration.[14] However, increasing the IgG concentration in the feed leads to a corresponding reduction in the amount of buffer required for the buffer exchange, with the run at 120 g/L IgG using less than 0.019 L of buffer per g of IgG processed. Note that the pressure drop through the hollow fiber module

remained below 2 kPa (0.3 psi) even at an IgG concentration as high as 120 g/L, consistent with the very low feed flow rate used in these experiments.

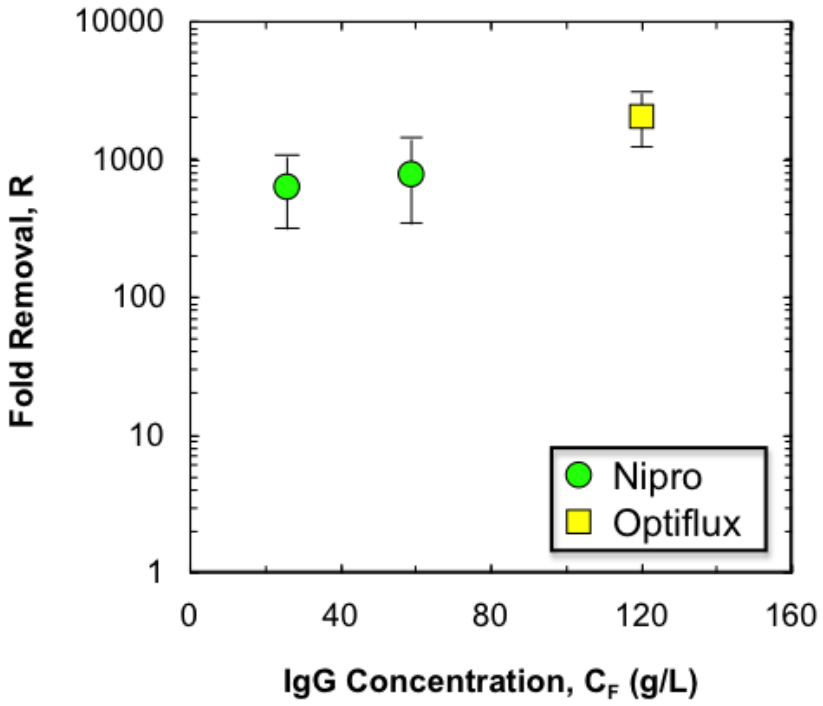

Figure 3.3: Fold-removal of vitamin B_{12} as a function of IgG concentration for countercurrent dialysis performed using the Optiflux F180B and Nipro Polynephron® dialyzers using a feed flow rate of 4 mL/min and $\alpha = 4.5$.

3.3.3 Model calculations

The effect of the dialysate (buffer) flow rate on the removal of vitamin B_{12} is examined in Figure 3.4 for data obtained with the Optiflux F180B dialyzer using $q_F = 4$ mL/min and IgG feed concentrations between 90 and 120 g/L. In this case the vitamin B_{12} concentration in the formulated product was evaluated as the average of samples obtained over the entire length of the continuous dialysis. More than 99.9% buffer exchange ($R > 1000$) was obtained at $q_D = 9$ and 18 mL/min, but

the vitamin B_{12} removal decreased significantly when the dialysate flow rate was reduced to 6 mL/min. The lower rate of buffer exchange is due to the reduction in the concentration driving force between the feed and dialysate solutions (associated with the greater build-up of vitamin B_{12} in the dialysate at small q_D) in combination with the smaller overall mass transfer coefficient (associated with the slower flow rate and smaller shear rate in the dialysate region of the dialyzer).

The solid curve in Figure 3.4 is a model calculation for the fold-removal in a countercurrent dialyzer adapted from Michaels[27]:

$$R = \frac{a \exp(b) - 1}{a - 1} \tag{3.1}$$

where

$$b = \frac{k_o A}{q_F}\left(1 - \frac{1}{a}\right) \tag{3.2}$$

and $\alpha = q_D/q_F$ with k_oA equal to the product of the overall mass transfer coefficient and the membrane area. Equation (3.1) properly describes the reduction in the rate of solute removal with decreasing α using k_oA = 38 mL/min (determined by a fit to the eye), although more rigorous comparison between the model and data would require information on the flow rate dependence of the dialysate-side mass transfer coefficient as discussed by Wickramasinghe et al.[28]

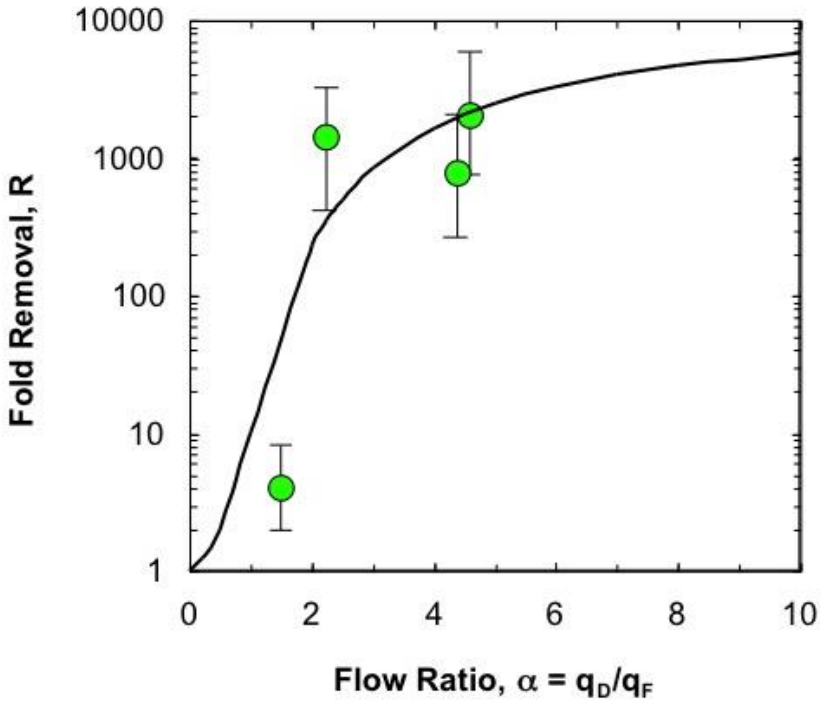

Figure 3.4: Fold-removal of vitamin B_{12} as a function of the ratio of the dialysate to feed flow rates (α) for data obtained with the Optiflux F180B dialyzer using a feed flow rate of 4 mL/min. Solid curve is model calculation given by Equation (3.1) with k_oA = 38 mL/min.

3.3.4 Buffer requirements

In addition to providing high degrees of impurity removal, the countercurrent dialysis system uses significantly less buffer than alternative processes. The volume of buffer used in the countercurrent dialysis per mass of protein is simply:

$$V_D = \frac{a}{C_F} \tag{3.3}$$

The data in Figure 3.4 with α = 2.25 provided R = 1000, which is the typical target for the extent of buffer exchange in the formulation of most biotherapeutics. This corresponds to V_D = 0.019 L/g

assuming a feed concentration of 120 g/L; it is likely that even higher protein concentrations could be used in these dialyzers to further reduce the buffer requirements.

The corresponding expression for the buffer requirement in a conventional batch diafiltration process is[21]:

$$V_D = \frac{N_D}{C_F} = \frac{\ln(R)}{S_o C_F} \tag{3.4}$$

where N_D is the number of diavolumes and S_o is the observed sieving coefficient for the solute of interest. A batch diafiltration process with R = 1000 and S_o = 1 (valid for a small impurity) would thus require 0.058 L/g if it were performed with C_F = 120 g/L. However, this high a feed concentration would yield a very low filtrate flux; thus, most commercial diafiltration processes are performed with $C_F \approx 60$ g/L giving V_D = 0.12 L/g, which is more than 6 times the amount of buffer required for the countercurrent dialysis system examined in this study.

The experimental data presented in Chapter 2 using the same IgG and vitamin B_{12} feed solution demonstrated that it is also possible to perform continuous buffer exchange using a countercurrent staged DF process with Pall Inline Concentrator (SPTFF) modules. The buffer required for this type of countercurrent staged system is:

$$V_D = \frac{a}{S_o C_F} \tag{3.5}$$

where in this case α is equal to the ratio of the DF buffer to feed flow rates. A 3-stage configuration with α = 9.7 could provide R = 1000 using vitamin B_{12} as a model impurity, but this would still require 4 times the amount of buffer than the countercurrent dialysis even if the SPTFF could be performed at the same protein concentration. A summary of the different buffer requirements is provided in Table 3.2. Note that the use of very high protein concentrations in the batch and 3-

stage diafiltration systems gives low filtrate flux and large feed-side pressure drops, which would likely create significant challenges in the implementation of a 3-stage process for long term continuous operation.

Table 3.2: Comparison of buffer requirements for continuous countercurrent dialysis, batch diafiltration, and countercurrent staged diafiltration processes (with 1000-fold buffer exchange)

	Countercurrent Dialysis (α = 2.25)	**Batch**	**3-stage DF**
60 g/L	0.038 L/g	0.12 L/g	0.16 L/g
120 g/L	0.019 L/g	0.058 L/g	0.081 L/g

4. Conclusions

The data obtained in this Chapter clearly demonstrate the feasibility of using countercurrent hollow fiber dialysis for buffer exchange and final formulation of high value biotherapeutics. The countercurrent dialysis can provide high levels of buffer exchange ($R \geq 1000$) in a fully continuous single-pass process by operating at much lower feed flow rates (<10 mL/min) than that used in hemodialysis ($q_F \geq 300$ mL/min) where the goal is to achieve approximately 70-90% removal of small solutes like urea. In addition, the product is processed with only a single pump pass, compared to the 10-100 pump passes in current batch diafiltration processes; this could lead to significant improvements in product quality, particularly for highly labile products. The results in Figure 3.2 show stable operation over 3 hr, but similar dialyzers have been used for more than 96 hr of continuous operation in continuous renal replacement therapy. This long-term operation with

minimal fouling is likely due to the absence of any transmembrane filtrate flow; additional studies will be required to determine the potential for even longer-term continuous processing using these hollow fiber dialyzers.

Although it is always difficult to perform detailed economic analyses of different processes before they have been deployed in actual commercial manufacturing, the results presented in this Chapter suggest that there could be very substantial cost-savings associated with the use of continuous countercurrent dialysis for antibody formulation. First, the countercurrent dialysis system requires several-fold less buffer than either traditional batch or countercurrent staged diafiltration processes. Second, the hollow fiber dialyzers used in this study cost less than $20 (approximately $10 / m^2) for a pre-sterilized cartridge suitable for direct integration in an extracorporeal blood circuit[29], suggesting that they could also be directly implemented in a continuous downstream biomanufacturing process. If these dialyzers could be used for the 96-hr operating time commonly obtained in hemodialysis applications, the cost would be less than $0.01 / g of formulated protein (assuming operation at q_F = 4 mL/min and C_F = 120 g/L).

Although we operated these dialyzers at low feed flow rates to obtain the high levels of buffer exchange needed in bioprocessing, these systems still processed nearly 0.7 kg of protein per day (based on q_F = 4 mL/min and C_F = 120 g/L). This is similar to the mass of monoclonal antibody that would be produced by a 500 L perfusion bioreactor operated continuously with one bioreactor volume exchange per day and a titer of ≈1 g/L. This suggests that a relatively small number of these hollow fiber dialyzer cartridges operated in parallel could process sufficient material to handle the product generated by continuous operation of a 500 - 2000 L perfusion bioreactor, which is typical of current targets for large-scale continuous biomanufacturing[30]. In addition, these modules come pre-sterilized and are intended for single-use applications, both of which are highly

attractive in bioprocessing. Additional studies will clearly be needed to demonstrate the effectiveness and economics of this type of continuous countercurrent hollow fiber dialysis in commercial bioprocesses.

Chapter 4: Single Pass Tangential Flow Filtration of Monoclonal Antibodies: Experimental Studies and Theoretical Analysis

The work presented in this chapter is adapted from: Jabra, M. G.; Lipinski, A. M.; Zydney, A. L. Single Pass Tangential Flow Filtration (SPTFF) of Monoclonal Antibodies: Experimental Studies and Theoretical Analysis. J. Memb. Sci. 637: 119606 (2021). https://doi.org/10.1016/j.memsci.2021.119606.

Single Pass Tangential Flow Filtration (SPTFF) enables continuous ultrafiltration and diafiltration for inline concentration and buffer exchange in downstream bioprocessing of monoclonal antibody (mAb) products. However, the high conversion in SPTFF modules leads to large variations in local flow rate, protein concentration, and transmembrane pressure drop, significantly complicating the design of effective SPTFF processes. In this Chapter, a recently developed concentration polarization model for the filtrate flux in protein ultrafiltration that accounts for protein-protein interactions has been extended to the analysis of SPTFF, specifically including the effects of the mAb and membrane properties as well as the long path-length. Model calculations are in good agreement with experimental data for the filtrate flux and pressure drop in two commercial SPTFF systems with very different module geometries. The model was then used to analyze the design of SPTFF processes for inline mAb concentration, providing additional insights into the underlying physical phenomena governing the performance and optimization of SPTFF modules for bioprocessing.

4.1 Introduction

Monoclonal antibodies (mAbs) are used to treat patients with cancer and a range of immunological diseases, with more than 100 FDA-approved mAbs currently available. The global market for mAbs is over $100 billion / yr and is expected to exceed $180 billion by 2025.[31] The development of mAb therapeutics for Covid-19 (and future pandemics) has created even greater pressures on mAb manufacturing, including the development of ultrafiltration (UF) systems for protein concentration, buffer exchange, and final formulation. Ultrafiltration is typically performed as a batch operation [32], although several studies have demonstrated that continuous (inline or single pass) ultrafiltration can be effectively incorporated in downstream processing.[33,34] These Single Pass Tangential flow Filtration (SPTFF) systems can reduce tankage constraints,[33] improve the performance of subsequent chromatographic processes,[35] and minimize protein aggregation due to repeated pump passes.

A number of commercial systems have been developed specifically for SPTFF, beginning with the module developed by SPF Innovations,[36] now licensed to Pall and sold under the tradename Cadence™. The Pall Cadence™ SPTFF consists of several internal stages with the number of parallel flow channels decreasing along the length of the module to balance the reduction in retentate flow rate at high conversions.[37] The Pellicon® SPTFF system developed by MilliporeSigma uses conventional UF modules arranged in series by a specially designed stainless steel holder with appropriate diverter plates.[38]

Given the growing interest in SPTFF, Huter and Strube[39] and Huter et al.[40] have recently presented models for the filtrate flux and conversion (ratio of permeate to feed flow rates) for these long pathlength modules. The SPTFF module was described using a series of membrane units and junctions, with the filtrate flux evaluated using either a concentration polarization / osmotic

pressure model or a boundary layer resistance model. Model calculations based on the boundary layer resistance model for the filtrate flux were shown to be in good agreement with experimental data obtained with both bovine serum albumin (BSA) and human serum immunoglobulin (IgG). However, the boundary layer resistance needed to be fit to the experimental data for the filtrate flux in the SPTFF system using an empirical power law expression,[40] which significantly limits the overall applicability of the model.

The objective on the work described in this Chapter is to extend the ultrafiltration model developed by Binabaji et al.[41] and Baek et al.[42] for mAb ultrafiltration to the analysis of SPTFF systems. The resulting model specifically accounts for the effects of protein-protein interactions on protein diffusion, viscosity, and osmotic pressure, while also including the variation in local concentration, pressure, and flow rate on the performance of the long path length SPTFF module. Model calculations were validated using experimental data obtained for a model monoclonal antibody product in two different experimental systems: a conventional UF module operated at low feed flow rates and a specially designed SPTFF module. In both cases, all of the key physical properties of the mAb were evaluated from independent experimental measurements. The model was then used to examine the design of an SPTFF module for inline concentration of a mAb, demonstrating how this theoretical framework can be used to obtain important insights into the performance and optimal design of SPTFF systems for bioprocessing.

4.2 Materials and Methods

4.2.1 Protein Solution

A model monoclonal antibody (mAb) was provided to our laboratory by Biogen (Cambridge, MA) at a concentration of 10 g/L in a 20 mM histidine and 150 mM arginine buffer at pH 5. The IgG1 mAb was produced by fed-batch culture in CHO cells and purified by Protein A and ion exchange chromatography before shipping. The protein molecular weight was approximately 150 kDa and the isoelectric point was 6.55. The mAb was sterile filtered through a 0.22 μm Durapore membrane (MilliporeSigma, Bedford, MA) before each experiment to remove any large aggregates.

The hydrodynamic radii and surface charge of the mAb were determined by dynamic light scattering (DLS) using a Zetasizer Nano (Malvern, UK). The surface charge was determined to be around 6.5 and the antibody's hydrodynamic radius was 6.5 nm with less than 2% high molecular weight (HMW) aggregates before the experiments and up to 5% HMW after the SPTFF experiments. mAb concentrations were evaluated from the UV absorbance at 280 nm using a Tecan Infinite m200 Pro microplate reader (Switzerland) based on appropriate calibration curves. The osmotic pressure and viscosity were evaluated as a function of the mAb concentration using a membrane osmometer[43] and a Cannon-Fenske capillary viscometer.

4.2.2 SPTFF modules

Experiments were performed with Pellicon® 3 cassettes with Ultracel 30 kDa membranes and C screen (provided by MilliporeSigma) and Cadence® SPTFF modules with 30 kDa Delta membranes (provided by Pall Corp., Port Washington, NY). The key physical properties of the

two systems are summarized in Table 4.1; the membrane width was calculated directly from the area using the measured channel length. The Pellicon® 3 module is designed for traditional ultrafiltration applications, but high conversion can be achieved by operation at low feed flow rates. A special holder and manifold (MilliporeSigma) were used to double the total path length and increase the conversion. The Cadence® SPTFF is a module specifically designed for single pass ultrafiltration. The module was assembled with 4 "stages" with a 3-2-1-1 configuration (number of parallel cassettes in each stage) as shown in Figure 4.1. The hydraulic diameter and mesh length for the cassettes were estimated by cutting open the modules and examining the internal retentate spacer using a digital caliper.

Table 4.1: Key physical properties of the Pellicon® 3 and Cadence® SPTFF modules

	Pellicon® 3	Cadence®
Length	20 cm (per channel)	68 cm
Width	2.2 cm	2.7 cm
Area	88 cm^2 or 176 cm^2	650 cm^2
Configuration	1 or 1-1	3-2-1-1
Hydraulic diameter	100 µm	100 µm
Mesh length	500 µm	340 µm
Membrane permeability	8.2 LMH/psi	10 LMH/psi

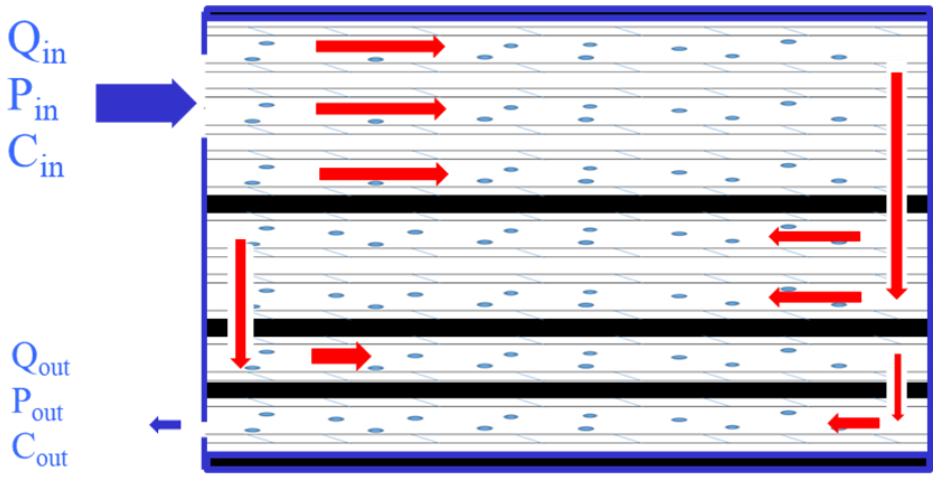

Figure 4.1: Schematic showing flow path for Pall Cadence® SPTFF

The feed flow rate was controlled using a Masterflex® L/S® peristaltic pump with size 16 Tygon tubing. The retentate line was partially clamped to adjust the transmembrane pressure, with the feed inlet and retentate exit pressures measured using Ashcroft® digital pressure gauges; the permeate exit was open to the atmosphere. Filtration was performed in full recirculation mode, with the retentate and permeate lines both recycled back to the 1 L feed reservoir. The system was allowed to equilibrate for a minimum of 10 min before evaluating the permeate flux using simple timed collection.

The membrane permeability was evaluated by measuring the buffer flux (J_o) as a function of transmembrane pressure (TMP) using a feed flow rate of 50 mL/min. The slope of the J_o vs TMP data is equal to the permeability (L_p) divided by the buffer viscosity. The pressure flow parameter (β), defined subsequently in Equation (4.8), was evaluated from the pressure difference

between the feed inlet and retentate exit over a range of buffer flow rates with the permeate line clamped to maintain zero net ultrafiltration.

At the end of each experiment, i.e., after evaluating the permeate flux as a function of transmembrane pressure for a given feed flow rate and feed concentration, the modules were cleaned by flushing with at least 2 L of DI water followed by circulation of a 0.25 N NaOH solution for 45 min. Modules were stored in 0.1 N NaOH at 4° C between experiments. Modules were discarded whenever the permeability had decreased by more than 20% from that of the clean (new) module.

4.2.3 Protein viscosity and osmotic pressure profile

The viscosity of the mAb was measured using a Cannon-Fenske viscometer based on the time required for the flow to pass through a narrow capillary. Antibody solutions of different concentration were obtained by ultrafltration through a 30 kDa Biomax® membrane. The viscosity data were fit to the Mooney equation[44]:

$$\frac{\eta_p}{\eta_0} = e^{\left(\frac{b\,C_p}{1-\frac{C_p}{C_{max}}}\right)} \qquad (4.1)$$

with b = 0.0162 L/g and C_{max} = 800 g/L as shown in Figure 4.2.

The osmotic pressure was evaluated in a stirred cell osmometer using the procedure described by Binabaji et al.[43] Data were obtained with a Biomax® 30 kDa membrane, with the osmotic pressure evaluated as the transmembrane pressure at which there was zero permeate flux across the membrane. The data were fit to a modified 3rd order virial expansion[45,46]:

$$\Pi_p = \mathrm{RT}\left\{2\left[\left(\frac{\mathrm{Z}\,C_p}{2\,\mathrm{M_w}}\right)^2 + \mathrm{m_s}^2\right]^{0.5} - 2\,\mathrm{m_s}\right\} + \mathrm{RT}\left(B_1 C_p + B_2 C_p^2 + B_3 C_p^3\right) \qquad (4.2)$$

where Z = 6.2 is the protein charge (evaluated from the electrophoretic mobility) and m_s is the molal salt concentration. The viral coefficient B_1 was set equal to $1/M_{w,mAb}$ based on ideal solution behavior, with $B_2 = 1.62 \times 10^{-5}$ m^3.mol/kg^2 and $B_3 = 1.03 \times 10^{-6}$ m^6.mol/kg^3 based on a fit to the experimental data in the lower panel of Figure 4.2.

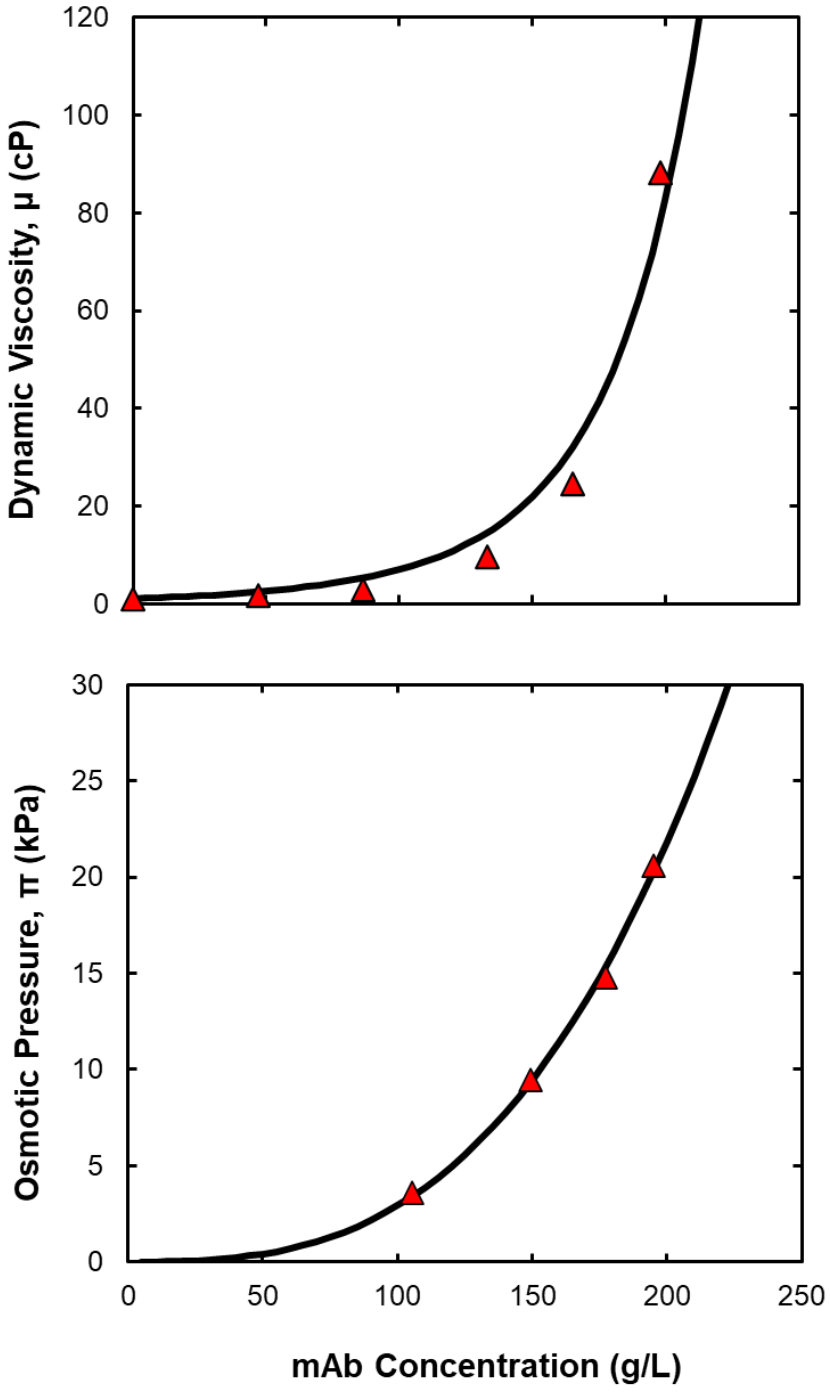

Figure 4.2: Dynamic viscosity (top panel) and osmotic pressure (bottom panel) as a function of mAb concentration. Solid curves represent model fits given by Equations (4.1) and (4.2).

4.3 Model development

The local filtrate flux was evaluated using the mathematical model developed by Binabaji et al.[41] for protein ultrafiltration, which specifically accounts for the effects of protein-protein interactions on flow and antibody transport. At high transmembrane pressures, the filtrate flux was assumed to be mass transfer-limited and given by a modified concentration polarization model, developed by solution of the steady-state one-dimensional diffusion equation:

$$N_s = J_v C - D\left(\frac{dC}{dy}\right) \tag{4.3}$$

where Ns is the protein flux, J_v is the volumetric filtrate flux, and C is the local protein concentration at position y measured from the membrane surface into the bulk solution.

The diffusive solute flux in highly concentrated solutions is proportional to the gradient of the chemical potential (μ) instead of the gradient in the solute concentration, thus Equation (4.3) becomes:

$$N_s = J_v C - \frac{DC}{RT}\left(\frac{d\mu}{dy}\right) \tag{4.4}$$

The gradient in the chemical potential can be rewritten in terms of the protein osmotic pressure (Π) as:

$$\left(\frac{d\mu}{dy}\right) = \frac{M_p}{C}\left(\frac{d\Pi}{dC}\right)\left(\frac{dC}{dy}\right) \tag{4.5}$$

The diffusion coefficient can be described as function of protein concentration based on the dependence of the protein mobility on the local solution viscosity:

$$D = D_0\left(\frac{\eta_0}{\eta}\right) \tag{4.6}$$

Equations (4.5) and (4.6) are substituted into Equation (4.4) which is then integrated over the concentration boundary layer thickness (δ) to obtain the following expression for the filtrate flux:

$$J_{lim} = \frac{D_0}{\delta}\int_{C_b}^{C_w}\left(\frac{M_p}{RT}\right)\left(\frac{\eta_0}{\eta}\right)\left(\frac{d\Pi}{dC}\right)\frac{dC}{C} \qquad (4.7)$$

The boundary layer thickness typically depends on $Sc^{1/3}$ where Sc is the Schmidt number. Equation (4.7) can thus be rewritten as:

$$J_{lim} = k_0\left(\frac{\eta_b}{\eta_0}\right)^{\frac{1}{3}}\int_{C_b}^{C_w}\left(\frac{M_p}{RT}\right)\left(\frac{\eta_0}{\eta}\right)\left(\frac{d\Pi}{dC}\right)\frac{dC}{C} \qquad (4.8)$$

where C, C_w, and C_b are the local, wall, and bulk protein concentrations; η, η_o, and η_b are the local, solvent, and bulk viscosities; M_p is the protein molecular weight; R is the ideal gas constant, and T is the absolute temperature. Equation (4.8) reduces to the classical concentration polarization model when the viscosity is constant and the osmotic pressure is given by the ideal Van't Hoff equation. The bulk mass transfer coefficient, k_o, was evaluated using the correlation presented by Da Costa et al.[47]

$$Sh = \frac{k_o d_h}{D_p} = 0.664 Re^{0.5} Sc^{0.33}\left(\frac{d_h}{l_m}\right)^{0.5} \qquad (4.9)$$

where $Re = \frac{U d_h}{v}$ is the local Reynold number and $Sc = \frac{v}{D_p}$ is the local Schmidt number with U the local velocity, d_h the hydraulic diameter, and ν the kinematic viscosity. The Reynold's number was well within the laminar regime for all experiments with values of $Re \leq 30$. The local values of the velocity and viscosity were used to evaluate the local mass transfer coefficient at position 'z' in the module. The protein diffusivity at infinite dilution, $D_p = 2.8 \times 10^{-11}$ m^2/s, was evaluated using the Stokes-Einstein equation based on the measured hydrodynamic diameter of the mAb as determined by DLS.

Equation (4.8) will not be valid at low transmembrane pressures where the filtrate flux is instead determined by the permeability of the membrane (L_p):

$$J_{mem,} = \frac{L_p}{\eta_0} (\Delta P_{TM} - \Delta\Pi) \quad (4.10)$$

where ΔP_{TM} is the local transmembrane pressure difference and $\Delta\Pi$ is the local osmotic pressure difference, both of which will vary with position in the module. The filtrate flux at arbitrary transmembrane pressures was evaluated by simple interpolation between Equations (4.8) and (4.10) using the expression originally presented by Yeh et al.[48]

$$\frac{1}{J_v} = \frac{1}{J_{lim}} + \frac{1}{J_{mem}} \quad (4.11)$$

The membrane limited flux is more important in the low concentration region where the membrane creates a high enough resistance compared to the polarization layer. The flux in SPTFF is typically dominated by concentration polarization effects as described by the mass transfer limited flux.

The performance of the SPTFF module was determined by integrating the overall mass and momentum balances, Equations (4.12) and (4.13), along the length (z) of the module:

$$\frac{dQ}{dz} = -2\, Nw\, J_v \quad (4.12)$$

$$\frac{dP}{dz} = -\frac{\beta}{N}\eta Q \quad (4.13)$$

where Q and P are the local retentate flow rate and pressure at position 'z' in the module, N and w are the number and width of the channels in each stage of the module and β is a geometric factor describing the pressure drop due to flow through the channel. The geometric factor is dependent on the module and spacer geometry and accounts for parasitic pressure losses. Numerical

integration was performed in Mathematica using a minimum of 1000 steps along the length of the module.

4.4 Results and Analysis

4.4.1 Pellicon® 3 module

Figure 4.3 shows data for the filtrate flux (top panel) and concentration factor (bottom panel) as a function of the mean transmembrane pressure drop in the Pellicon® 3 module for a 20 g/L mAb feed. Data were obtained at feed flow rates of 5, 10, and 20 mL/min, corresponding to feed flux (feed flow rate divided by the membrane area) of 34, 68, and 136 L/h/m^2. In each case, the mean transmembrane pressure was evaluated as:

$$TMP = \frac{P_{feed}+P_{exit}}{2} - P_{permeate} \qquad (4.14)$$

with the permeate pressure assumed to be atmospheric. There was no evidence of any antibody in the permeate samples, corresponding to a mAb retention of >99.9%, nor was there any measurable loss of mAb during the experiment (mass balance closure better than 95%). In addition, the permeability of the membrane evaluated at the end of the filtration was within 20% of the original (clean) permeability, suggesting that fouling was negligible. Dynamic light scattering profiles of the initial and final retentate were essentially identical, indicating that there was minimal mAb aggregation.

The solid curves in Figure 4.3 are model calculations, developed from numerical solution of Equations (4.8) to (4.13) using the correlations for the osmotic pressure and viscosity presented in Equations (4.1) and (4.2). The membrane permeability (L_p) and geometric factor (β) were

determined from buffer flux and pressure measurements based on Equations (4.10) and (4.13), respectively; there were no model parameters fit to any of the data in Figure 4.3. The model is in good agreement with the data over the entire range of experimental conditions. The filtrate flux initially increases with increasing TMP as the flux transitions from the membrane-limited to mass transfer-limited regimes. The x-intercept, corresponding to zero filtrate flux, occurs at a small positive value of the TMP due to the osmotic pressure of the mAb solution. The filtrate flux at high TMP increases with increasing feed flow rate due to the increase in the mass transfer coefficient given by Equation (4.9). In contrast, the concentration factor (defined as the mAb concentration in the retentate exit normalized by that in the feed) decreases with increasing Q_{feed} since k_o depends on $Q_{feed}^{0.5}$ (Equation 4.9). The maximum concentration factor of X = 1.9 was obtained at a feed flow rate of 5 mL/min; higher concentration factors would require the use of even lower feed flow rates or the addition of a second cassette to increase the overall path length.

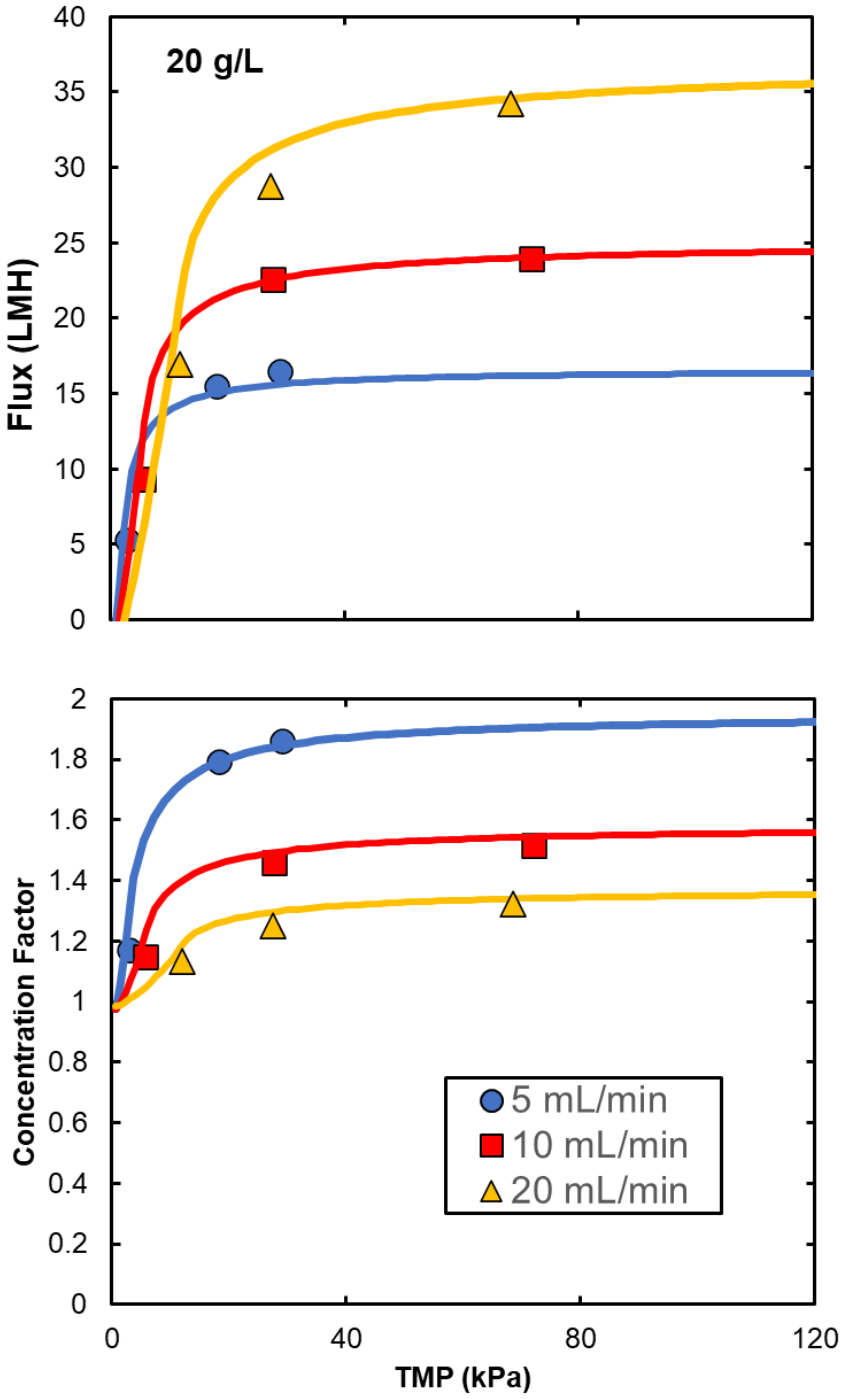

Figure 4.3: Filtrate flux (top panel) and concentration factor (bottom panel) as a function of the mean transmembrane pressure during ultrafiltration of a 20 g/L mAb solution in the Pellicon® 3 cassette at feed flow rates of 5, 10 and 20 mL/min. Solid curves are model calculations as described in the text.

Figure 4.4 shows a comparison of the experimental results and model predictions for the filtrate flux (top panel) and concentration factor (bottom panel) for the one- and two-stage Pellicon® 3 cassettes using a 20 g/L mAb feed. The two-stage system is simply constructed with two cassettes in series, creating a module with an effective path length of 40 cm. The results at feed flow rates of 5 and 10 mL/min were obtained at a transmembrane pressure of 28 kPa while those at 20 mL/min were at a TMP = 50 kPa, both of which are near the start of the pressure independent regime. The model predictions are in good agreement with the experimental data under all conditions with deviations of less than 2.8%. The filtrate flux is uniformly higher in the one-stage system since the second cassette in the two-stage module has a lower retentate flow rate and higher mAb concentration than that entering the first stage. In contrast, the concentration factors achieved with the two-stage system were uniformly higher since the increased path length allows for greater relative removal of permeate. The maximum concentration factor in the two-stage system, X = 2.5, was obtained at the lowest feed flow rate (5 mL/min), compared to X = 1.9 with the one-stage cassette under the same conditions. The two-stage system also has a much larger feed-side pressure drop (ΔP = 63 kPa at the highest feed flow rate of 20 mL/min), which is slightly more than twice that in the one-stage cassette. The increase in viscosity of the more concentrated mAb more than compensates for the reduction in retentate flow rate in the second cassette, and there is also a small pressure drop in the manifold that connects the two stages of the Pellicon® 3 cassettes.

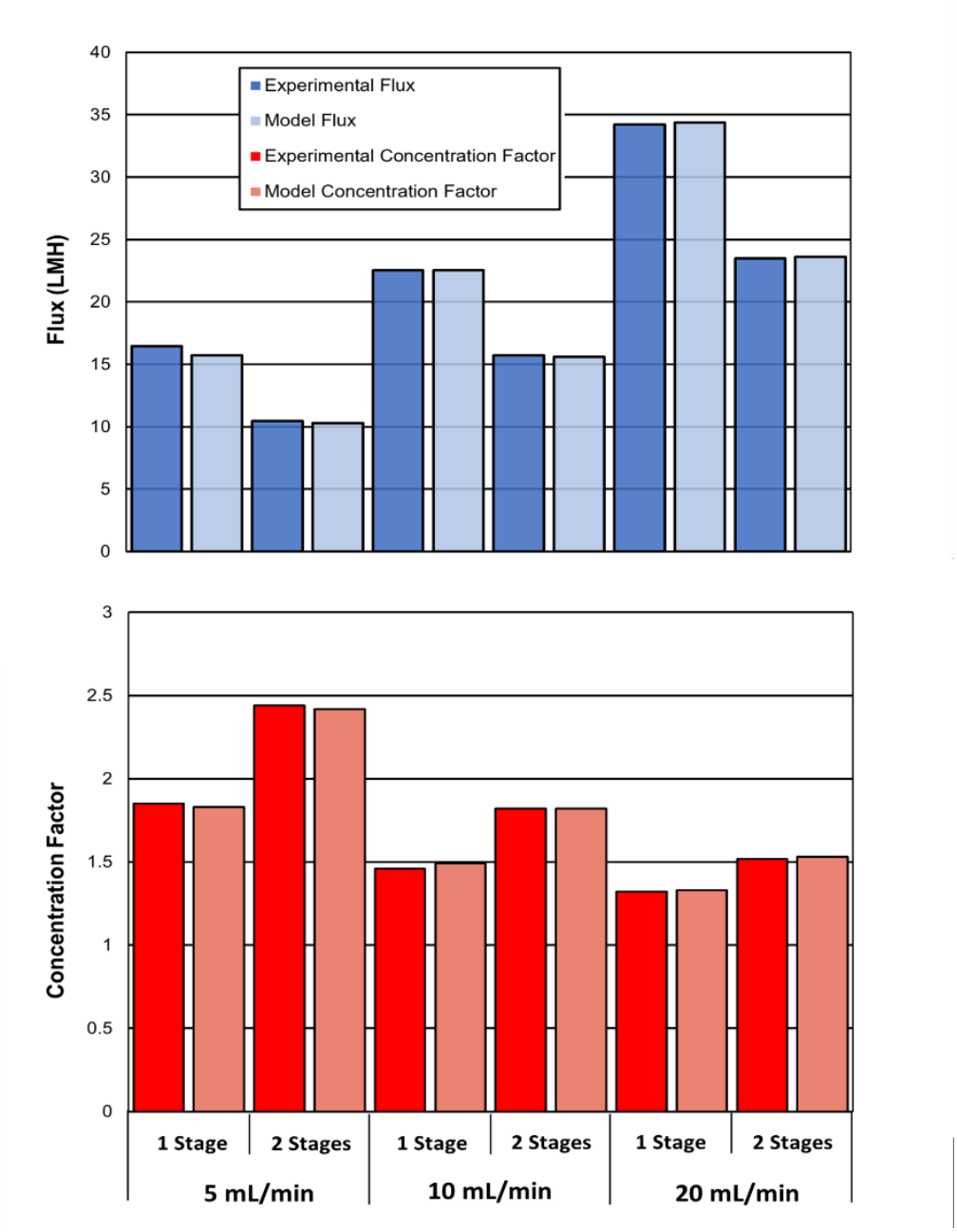

Figure 4.4: Comparison of experimental data and model predictions for the filtrate flux (top panel) and concentration factor (bottom panel) for the one- and two-stage Pellicon® 3 modules at different feed flow rates. Results at 5 and 10 mL/min were obtained at TMP = 28 kPa while results at 20 mL/min were at 50 kPa. The model to experimental error bar is less than 2.8% for all cases.

4.4.2 Cadence® module

Corresponding data for the Pall Cadence® module are shown in Figure 4.5 at feed flow rates of 10, 20, and 40 mL/min (corresponding to feed flux of 9, 18, and 37 L/h/m^2). Although the qualitative behavior is similar to that seen in the Pellicon® 3 module, the concentration factors are significantly higher due to the much larger membrane area (650 vs 88 cm^2) and the longer path length (L = 68 cm vs 20 and 40 cm in the one and two-stage Pellicon® 3). The concentration factor at Q_{Feed} = 10 mL/min is X > 6 for TMP above 30 kPa. In contrast, the filtrate flux in the Cadence® module was significantly less than that in the Pellicon® 3, e.g., the maximum flux at 10 mL/min was only 8 LMH in the Cadence® compared to 24 LMH in the one-stage Pellicon® 3 and 17 LMH in the two-stage system. In addition, it was difficult to obtain data for the Cadence® module in the membrane-limited regime due to the large feed-side pressure drop, which was more than 37 kPa in the Cadence® module compared to only 12 kPa in the Pellicon® 3 at the same feed flow rate of 10 mL/min (Table 4.2). The model calculations are again in very good agreement with the data over the full range of feed flow rates and TMP. Similar agreement was obtained at other feed concentrations.

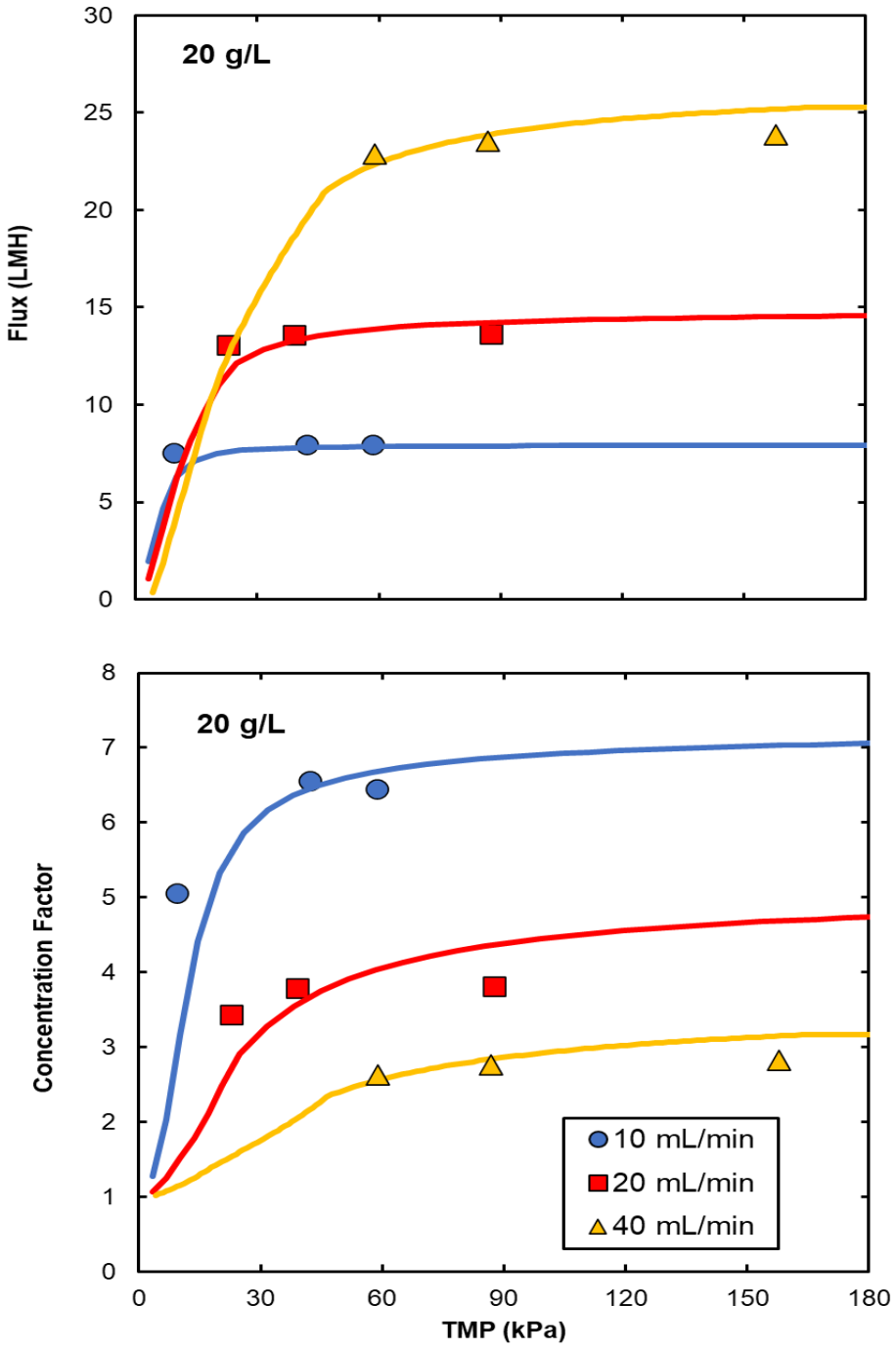

Figure 4.5: Filtrate flux (top panel) and concentration factor (bottom panel) as a function of mean transmembrane pressure at feed flow rates of 10, 20 and 40 mL/min for a 20 g/L mAb feed.

The flux profile as a function of position in the module for the 1 stage Pellicon® 3 cassette and the Pall Cadence® SPTFF module as shown in Figure 4.6. The SPTFF modules exhibit a lower average flux due to the much higher conversion and pressure drop in the module. The local filtrate flux decreases along the length of the module due to the increase of mAb concentration and the decrease in local mass transfer coefficient; the discontinuities in the flux in the Pall SPTFF module are due to the increase in local flow rate (and thus the local mass transfer coefficient) when the module goes from the 3 cassettes in parallel to 2 cassettes in parallel and then from 2 to 1 cassette for the final half of the overall path length.

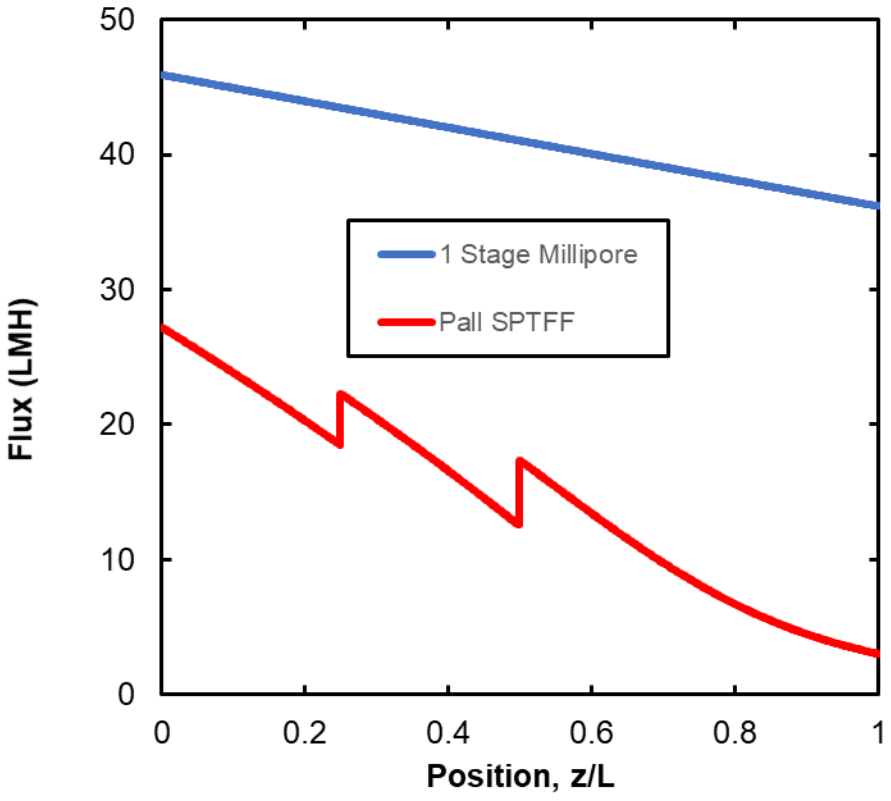

Figure 4.6: Filtrate flux as a function of position in the Pall SPTFF module and 1 stage Millipore Pellicon® 3 cassette at a feed flow rate of 20 mL/min and feed concentration of 10 g/L.

The model was further verified using experimental data at mAb concentrations of 10 and 40 g/L as shown in Figure 4.7. Again, the model predictions are in good agreement with the experimental data for the filtrate flux across the full range of transmembrane pressures, with some deviations seen at 10 g/L at 40 mL/min, possibly due to discrepancies in the value of the membrane permeability used in the model. The filtrate flux for the 10 g/L solutions was approximately 50% larger than that with the 40 g/L feed at high TMP. Operation at higher feed flow rates and concentrations requires a higher transmembrane pressure in order to reach the pressure independent region.

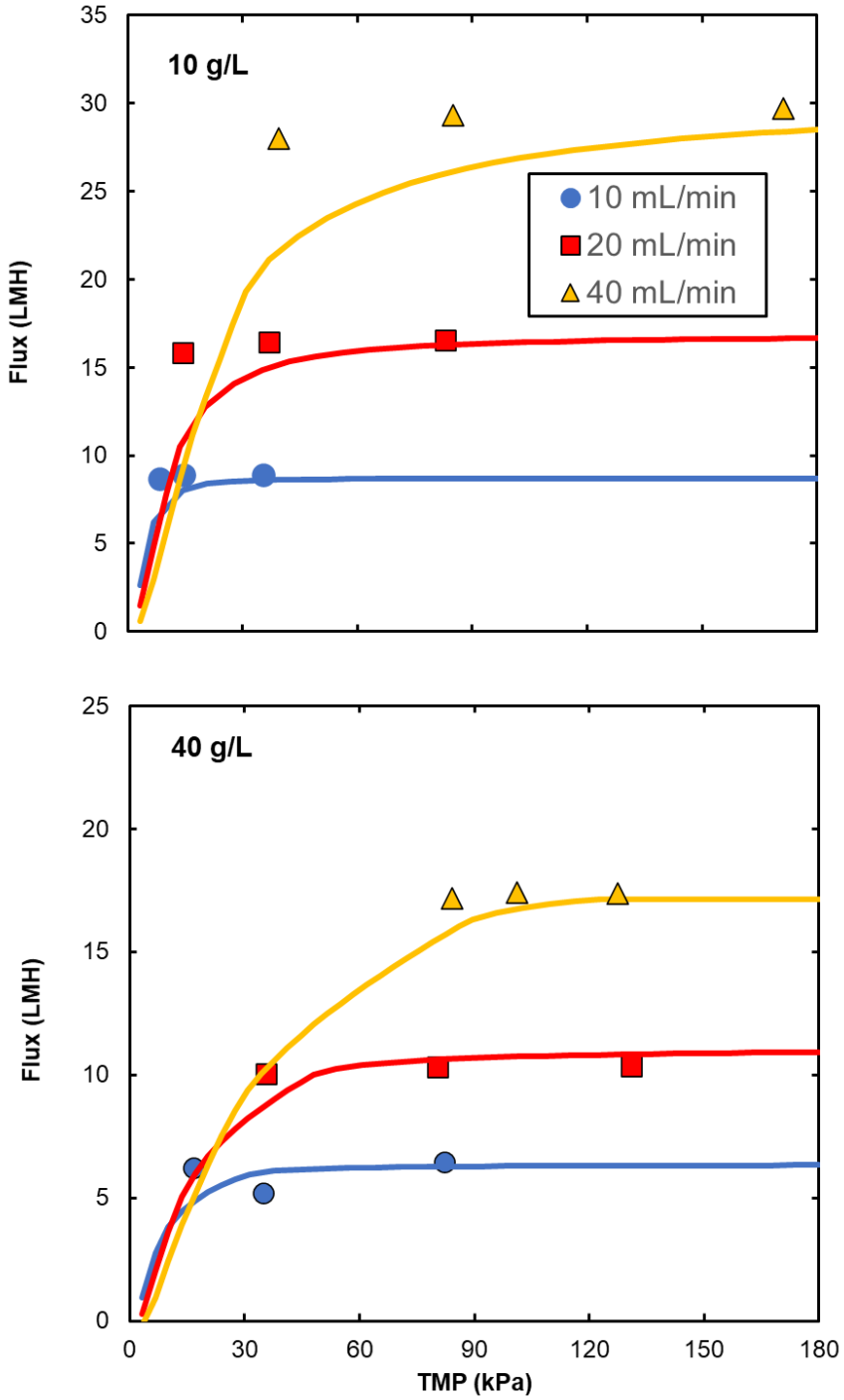

Figure 4.7: Filtrate flux as a function of mean transmembrane pressure at feed flow rates of 10, 20 and 40 mL/min for a mAb feed concentration of 10 g/L (top panel) and 40 g/L (bottom panel) using the Cadence® SPTFF module. Solid curves are model calculations.

The performance characteristics of the one- and two-stage Pellicon® 3 cassettes and the Cadence® SPTFF module are compared in Table 4.2. The results are shown in the pressure-independent regime (at a mean transmembrane pressure of 40 kPa), with the experimental values determined by linear interpolation where needed. The filtrate flux decreases with increasing channel length (going from the one- to two-stage Pellicon® 3 and then to the Cadence® module), with a corresponding increase in the feed-side pressure drop. The model calculations are in excellent agreement with the data, with all of the values within 5% (except for ΔP for the two-stage Pellicon® 3). The small discrepancy in the pressure drop for the two-stage Pellicon® 3 is likely due to the pressure loss in the manifold that connects the two cassettes, an effect that is not currently accounted for in the model.

Table 4.2: Performance characteristics of the Pellicon® 3 and Cadence® SPTFF modules at a feed flow rate of 10 mL/min using a 20 g/L mAb feed and TMP ≈ 40 kPa.

		Filtrate Flux (LMH)		**Volumetric Concentration Factor**		**Pressure Drop (kPa)**	
	Path-length	**Expt**	**Model**	**Expt**	**Model**	**Expt**	**Model**
1 stage Pellicon® 3	20 cm	23	22	1.5	1.5	12	12
2 stage Pellicon® 3	40 cm	15	15	1.8	1.8	26	24
Cadence® SPTFF	68 cm	8.0	7.8	7.5	6.5	37	38

Figure 4.8 shows results for the filtrate flux and concentration factors in the Cadence® SPTFF module as a function of the mAb concentration in the feed solution at feed flow rates of 20

and 40 mL/min at a fixed transmembrane pressure of approximately 80 kPa. The solid curves are the model calculations. The flux and concentration factor both decrease with increasing mAb concentration due to concentration polarization effects, although the exit mAb concentration increases slightly with increasing feed concentration. For example, the exit concentration at a feed flow rate of 20 mL/min is just under 100 g/L for C_F = 10 g/L but this increases to around 110 g/L at C_F = 41 g/L. The increase in the exit concentration with increasing C_F is more pronounced at the higher feed flow rate due to the smaller concentration factor under these conditions.

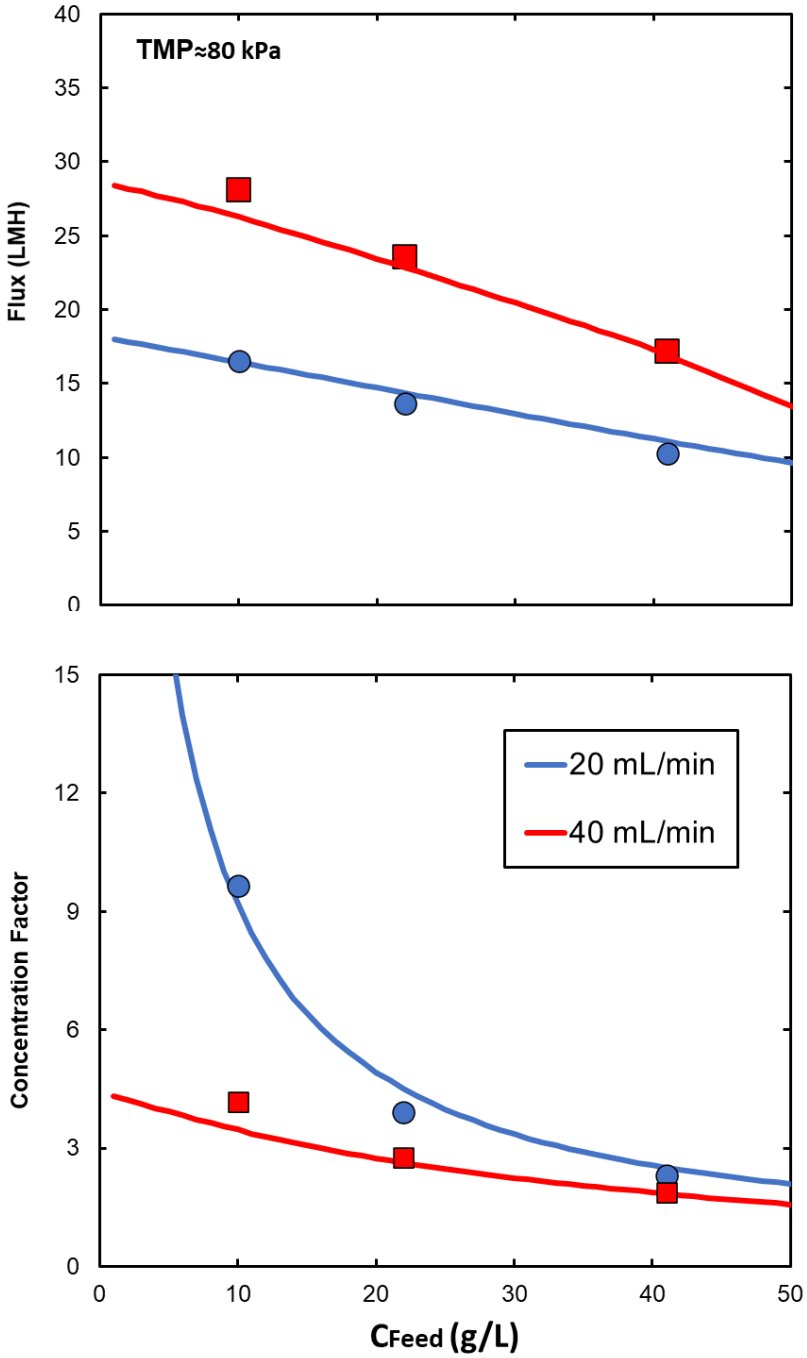

Figure 4.8: Filtrate flux (top panel) and concentration factor (bottom panel) as a function of mAb feed concentration at feed flow rates of 20 and 40 mL/min at a transmembrane pressure of approximately 80 kPa in the Cadence® SPTFF module.

Further confirmation of the model was obtained by collecting data for the cumulative filtrate flow rate from the two permeate outlets in the Cadence® SPTFF module. The first permeate exit primarily collects the filtrate flow from the first 3 cassettes in parallel (Q_{f1}) while the second exit primarily collects the filtrate from the latter 3 stages in the 2-1-1 arrangement (Q_{f2}). The gasket in the Cadence® module is unlikely to provide perfect division of the permeate flow, but the data should be representative of the spatial variation in permeate flow rate within the module. The filled symbols in Figure 4.9 are the experimental results while the model calculations for Q_{f1} and Q_{f2} are shown as the solid and dashed curves, respectively. At Q_{Feed} = 10 mL/min, the filtrate flow rate in the first section of the module is larger than that in the latter region because the high conversion causes a significant reduction in the retentate flow rate, and thus the mass transfer coefficient, in the final cassettes; this effect is more significant than the increase in local velocity due to the reduction in the number of parallel cassettes. The difference between Q_{f1} and Q_{f2} at 10 mL/min increases with increasing TMP since the higher transmembrane pressure near the inlet of the module increases the conversion in the first region, thereby reducing the mass transfer coefficient and filtrate flux near the exit of the module. In contrast, the filtrate flow rate in the latter region of the module is larger than that in the first section at Q_{Feed} = 40 mL/min since the lower overall conversion (Figure 4.9) reduces the variation in feed flow rate over the length of the module. The net result is that both Q_{f1} and Q_{f2} increase with increasing TMP at the highest feed flow rate, in contrast to the behavior at Q_{Feed} = 10 mL/min where Q_{f2} actually goes through a maximum before decreasing at the highest TMP. The plots intercept the x-axis at TMP values equal to the osmotic pressure of the mAb solution.

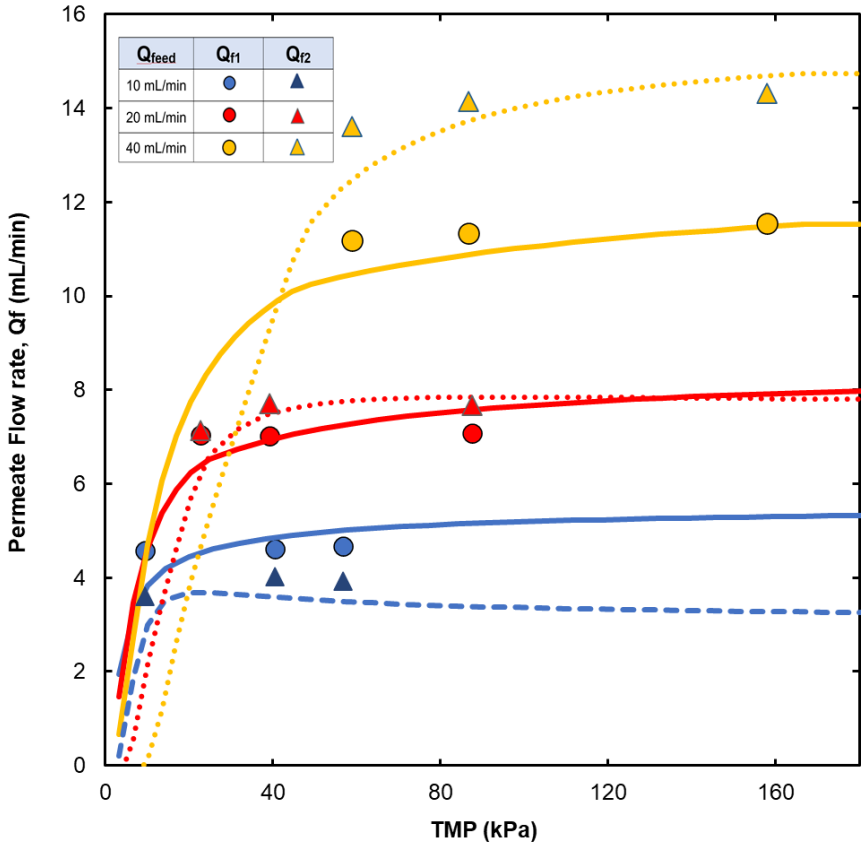

Figure 4.9: Filtrate flow rate from the two ports of the Pall Cadence® SPTFF module as a function of the mean transmembrane pressure at feed flow rates of 10, 20, and 40 mL/min. Solid and dashed curves are model calculations for Q_{f1} and Q_{f2}, respectively.

4.4.3 Design Calculations

One of the advantages of the validated model is that it can be used to examine the performance of SPTFF modules that are not currently available for experimental evaluation. In this case, we performed a series of model simulations for an SPTFF module designed for inline concentration of a mAb stream from 10 to 20 g/L (top panel of Figure 4.10) and from 10 to 100 g/L (bottom panel), both at a feed flow rate of 20 mL/min. The retentate exit pressure was fixed at 14 kPa (2 psi), with iterations performed on both the feed (inlet) pressure and filter length to achieve the target exit transmembrane pressure and concentration factor (X = 2 or X = 10). Results are shown for the required membrane area:

$$A = 2(w+w_c)L \tag{4.15}$$

where w_c is the unavailable (blocked) width of membrane that is lost in the formation of the flow channel in the cassette. Calculations are shown as a function of the available width (w) for w_c = 0, 0.5, and 1 cm. The dashed portion of the curves at small values of the membrane width correspond to conditions where the inlet feed pressure is greater than 300 kPa (3 bar), which is likely to be the maximum permissible pressure for operation of an SPTFF system.

Much larger membrane areas are required for the high conversion (X = 10) as expected. In both cases, the calculated area increases monotonically with increasing width when w_c = 0 due to the reduction in the filtrate flux arising from the decrease in crossflow velocity which causes a reduction in the local mass transfer coefficient. The behavior is considerably different when $w_c \neq 0$. For example, the results for X = 2 show a minimum in the membrane area at $w \approx 1.9$ cm (with $L \approx 44$ cm) for w_c = 1 cm. Note that this geometry is very similar to the design of the two-stage Pellicon® 3 module which has w = 2.4 cm and L = 40 cm (total length). The presence of a minimum in the total area is a direct result of the very large “loss” in available (filtering) membrane

area for the long modules required to maintain X = 2 at small w. The location of the minimum area shifts to larger w at X = 10 since much longer channel lengths are required to achieve this high conversion. For example, the minimum area with w_c = 0.5 cm occurs at w = 0.8 cm at X = 2 but this shifts to w = 2 cm at X = 10; the minimum area for w_c = 1 cm does not occur until w = 4 cm when X = 10. A more detailed discussion of the design and optmization of staged systems with different numbers of parallel cassettes in each stage is presented in the next Chapter.

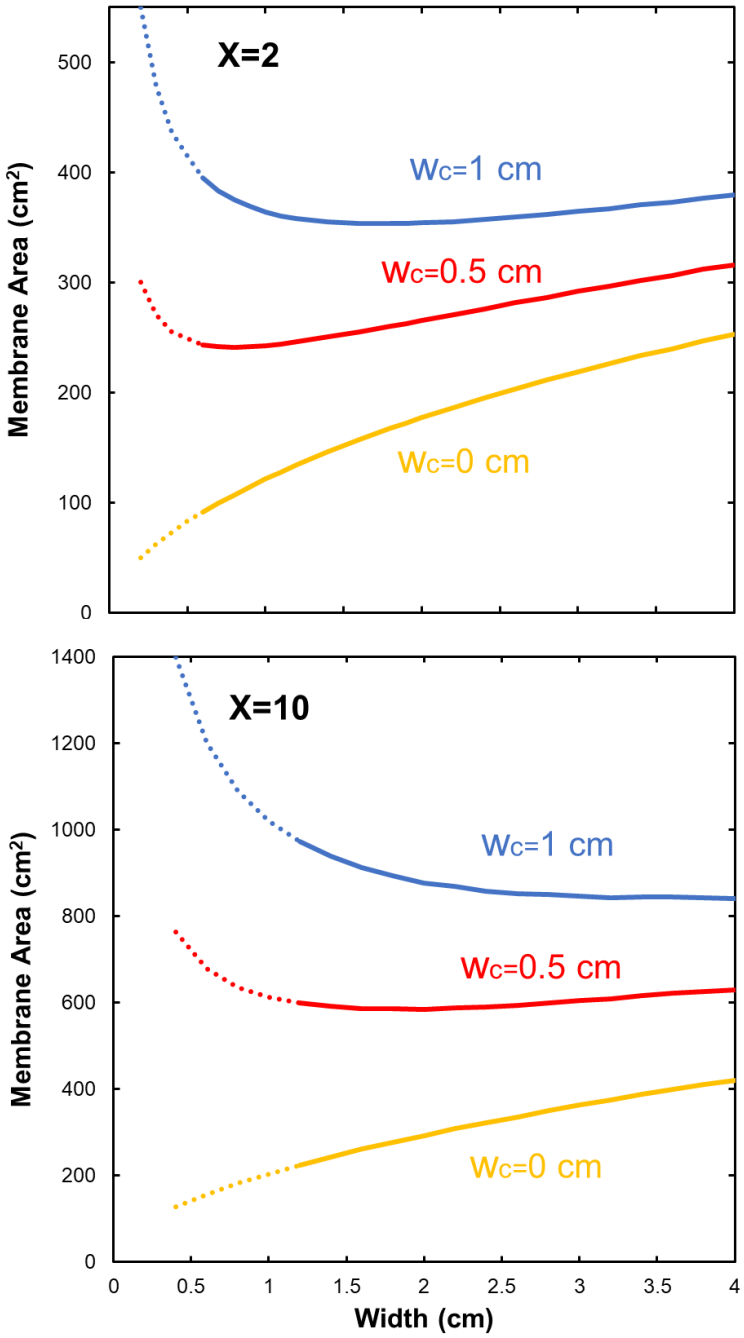

Figure 4.10: Membrane area as a function of channel width for an SPTFF module designed for concentration of a mAb from 10 to 20 g/L (top panel) and from 10 to 100 g/L (bottom panel) at a feed flow of 20 mL/min and an exit retentate pressure of 14 kPa. Results are shown for several values of w_c, which represents the width of membrane lost in forming the flow channel. Dashed portions of the curves show regions with a feed pressure >300 kPa.

4.5 Conclusions

There is growing interest in the application of single pass tangential flow filtration systems in bioprocessing. This Chapter examined the performance of these SPTFF systems using a combination of experimental studies and model simulations for a monoclonal antibody product. Data were obtained in both conventional Pellicon® 3 cassettes (one- and two-stage designs) and in the Cadence® SPTFF module, with the latter specifically designed with a long path length and staged configuration to achieve higher conversions but at the cost of a lower filtrate flux.

The filtrate flux and pressure drop data were compared with a mathematical model that specifically accounts for the variation in pressure, retentate flow rate, and bulk protein concentration along the length of the SPTFF module, with the local filtrate flux evaluated using a concentration polarization model that incorporates the effects of protein-protein interactions on both the solution viscosity and protein transport. All model parameters were evaluated from independent experimental measurements for the antibody (viscosity and osmotic pressure) and the module (membrane permeability and pressure drop factor). The model calculations were in very good agreement with the experimental results over a wide range of conditions in all 3 modules (one-stage Pellicon® 3, two-stage Pellicon® 3, and Cadence®). The model was even able to accurately predict the filtrate flow rate in different regions of the Cadence® SPTFF module, including the reduction in filtrate flow rate in the latter stages with increasing TMP at low feed flow rates, with the opposite behavior seen at high feed flow rates. This is the first reported analysis of this phenomenon in SPTFF modules.

The model was then used to examine the design of an SPTFF system for inline concentration of a monoclonal antibody product from 10 g/L to either 20 or 100 g/L at a given

feed flow rate. Model simulations performed with a single channel design showed a minimum in the total membrane area at an intermediate channel width, reflecting the tradeoff between the lower crossflow velocity (and mass transfer coefficient) at large widths and the significant loss of membrane area due to the sealing of the membranes to form the channel at small widths. The theoretical framework developed in this Chapter not only provides a framework for the design and optimization of SPTFF modules, it also provides important insights into the underlying physical phenomena governing the behavior of these systems.

Chapter 5: Design and Optimization of Single Pass Tangential Flow Filtration for Inline Concentration of Monoclonal Antibodies

The work presented in this chapter is adapted from: Jabra, M. G.; Zydney, A. L. Design and optimization of Single Pass Tangential Flow Filtration for inline concentration of monoclonal antibodies. J. Memb. Sci. 643: 120047 (2022). https://doi.org/10.1016/j.memsci.2021.120047.

A number of Single Pass Tangential Flow Filtration (SPTFF) systems have recently been commercialized for inline concentration of monoclonal antibodies and other biotherapeutics, both to resolve bottlenecks in existing processes and as part of the development of integrated continuous downstream processes. The objective of the analysis presented in this Chapter was to examine the design and optimization of SPTFF modules using a previously developed mathematical model for the filtrate flux and pressure drop that specifically accounts for the concentration dependence of the antibody viscosity and osmotic pressure as well as the variation of the flow rate and antibody concentration with position in the long pathlength SPTFF device. Model simulations were performed to examine the effects of channel width, length, and cassette staging (number of parallel cassettes in each stage) on SPTFF performance. The concentration factor (conversion) was greatest for a long thin channel configuration, but this also caused very large feed-side pressure drops. The use of cascade configurations, with a greater number of parallel channels near the feed inlet, significantly reduced the pressure drop but with a corresponding increase in total membrane area. These results provide important insights into the design and optimization of SPTFF systems for monoclonal antibody processing.

5.1 Introduction

There is considerable interest in the application of Single Pass Tangential Flow Filtration (SPTFF), both for intensification of (existing) batch processes and for development of new continuous downstream processes for the production of monoclonal antibodies (mAbs) and other biotherapeutics. For example, Dizon-Maspat et al.[33] explored the use of SPTFF for the inline reduction of process intermediate volumes, with the results demonstrating that SPTFF could help accommodate an increase in protein titer (mass throughput) using existing stainless steel tanks in a commercial manufacturing facility. Elich et al.[35] showed that SPTFF could be used to improve the performance of an anion exchange chromatography step, with the preconcentrated feed showing an improved binding isotherm leading to a 4-fold increase in antibody loading at the same level of host cell protein removal. Brinkmann et al.[49] used SPTFF to reduce the harvest volume from a fed-batch bioreactor, with the more concentrated feed stream providing a 5-fold increase in the productivity of the subsequent Protein A capture step. Perry and Rayat[50] discussed the potential application of SPTFF for enhanced production of lentiviral vectors for gene processing, although no experimental results were presented.

SPTFF can also be used for final concentration and formulation. Casey et al.[34] used SPTFF for final concentration of an IgG feed solution, increasing the IgG concentration from 45 g/L to approximately 200 g/L in a single pass. Rucker-Pezzini et al.[20] used a series of sequential dilution and concentration (SPTFF) steps for buffer exchange, with 99.75% removal of a trace impurity from a mAb. The results in Chapter 2 demonstrated that countercurrent staging of SPTFF modules could provide more effective buffer exchange by effectively “re-using” the diafiltration buffer between stages, with a 3-stage countercurrent system providing >99.9% removal of a small impurity over 24 hr of continuous operation.

A number of different approaches have been used to develop SPTFF modules for bioprocessing applications. The pioneering work by de los Reyes and Mir[36] used a cascade arrangement of tangential flow filtration channels, with the number of parallel channels decreasing as one moves from the feed inlet to the retentate exit to increase the local shear rate, and thus the filtrate flux, even as the retentate flow rate decreases. Pall Corporation has commercialized a number of SPTFF modules based on this technology, ranging from a 4-in-series configuration (with 3 cassettes followed by 2 then 1 and 1) to a 9-in-series module that uses a total of 21 channels[37]. In contrast, MilliporeSigma sells the Pellicon® SPTFF system which uses conventional UF modules arranged in series to obtain a longer effective channel length but without any change in the number of parallel channels (or effective membrane width) within the system[38]. Yehl and Zydney[51] took a very different approach, using low-cost hollow fiber modules that were only 26 cm long but operated at sufficiently low feed flow rates to achieve more than 10-fold concentration in a single pass.

The diversity of SPTFF configurations is due, at least in part, to the lack of detailed understanding of the key factors that govern the performance of these SPTFF modules for specific applications. The objective of the work described in this Chapter was to examine the design and optimization of SPTFF modules using the mathematical model presented in Chapter 4. This model accounts for the variation in both flow rate and mAb concentration with position due to the high conversion in these modules. A number of module geometries are explored, including the effects of module width / length as well as different cascade configurations. These results provide important insights into the development and optimization of SPTFF modules for specific target applications in bioprocessing.

5.2. SPTFF Model Development

The performance of the SPTFF module was described using the model developed in Chapter 4. The resulting equations involve no adjustable parameters (i.e., there are no parameters that must be fit to the filtrate flux data). This is in contrast to the models developed by Huter and Strube[39] and Huter et al.[40] in which the boundary layer resistance must be fit to data for the measured filtrate flux in the specific SPTFF module, making it unclear whether these equations can be directly extended to other module geometries. Similarly, Krippl et al.[52] developed a hybrid model for SPTFF incorporating a machine learning approach, although significant care would need to be taken in extrapolating this modeling approach outside the range of modules on which the system was trained.

The local filtrate flux was evaluated by interpolation between the membrane-limited (J_{mem}) and mass transfer limited filtrate flux (J_{lim}) using Equation (4.11). The local value of J_{lim} was evaluated in terms of the local bulk protein concentration (C_b) using the model equation presented by Binabaji et al.[41] using Equation (4.8). The membrane-limited flux was evaluated simply as the product of the effective pressure driving force (equal to the difference between the local transmembrane and osmotic pressures, $\Delta P_{TM} - \Delta\pi$) and the membrane permeability (L_p).

The variations in the retentate flow rate (Q), protein concentration (C), and pressure (P) along the length (z) of the module were evaluated using overall mass and momentum balances:

$$\frac{dQ}{dz} = -2\,Nw\,J_v \tag{5.1}$$

$$\frac{d(QC)}{dz} = -2\,Nw\,S_o J_v \tag{5.2}$$

$$\frac{dP}{dz} = -\frac{\beta}{N}\eta Q \tag{5.3}$$

where N and w are the number and width of the channels in each stage of the module, S_o is the protein sieving coefficient (assumed to be zero for a fully retentive membrane), and β is a geometric factor describing the parasitic pressure losses due to flow through the screened channel. Equations (5.1) to (5.3) can also be applied to hollow fiber modules with w replaced by πR where R is the fiber radius. Additional details on the model equations are provided in Chapter 4. The governing ordinary differential equations were integrated numerically in Mathematica version 12 (Wolfram).

Most of the model calculations were performed using modules that have properties similar to those of commercially available Pellicon® 3 cassettes with Ultracel 30 kDa membranes and C screen (MilliporeSigma, Bedford, MA) which have a mesh length of 500 μm and hydraulic diameter of 100 μm[13]. Model simulations were focused on exploring the effects of membrane geometry (length and width), total membrane area (A), and device configuration (internal staging) on the SPTFF performance, including the concentration factor (X = ratio of exit to inlet mAb concentrations) and the feed-side pressure drop ΔP.

5.3 Results and Discussion

5.3.1 Concentration factor and feed-side pressure drop for cassettes in series

Figure 5.1 shows results for the concentration factor and feed-side pressure drop for 1, 2, 3, and 4 Pellicon® 3 cassettes in series (corresponding to total lengths of L = 20, 40, 60, and 80 cm) at different feed flow rates for C_F = 20 g/L. In each case, the model calculations were performed with P_F = 310 kPa (45 psi), with the governing equations integrated numerically along the channel length until z = L. Also shown for comparison are experimental data for systems with

1 and 2 cassettes in series from Chapter 4; the experimental values are in good agreement with the model calculations for both the concentration factor and pressure drop. Note that the experimental data were obtained at a mean transmembrane pressure of 50 kPa, which is in the mass transfer-limited regime where the filtrate flux, and thus the concentration factor, are essentially independent of the transmembrane pressure.

The concentration factor decreases with increasing feed flow rate since the mass transfer coefficient varies with Reynolds number to the ½ power. Thus, a doubling of the feed flow rate will provide only about a 40% increase in the mass transfer-limited flux (and an even smaller change in the membrane-limited flux). The concentration factor also increases with increasing channel length due to the increase in membrane area. The concentration factors become greater than X = 5 for feed flow rates below 7 mL/min at L = 80 cm and below 1 mL/min at L = 20 cm. It is worth noting that the recommended feed fluxes (feed flow rate normalized by the membrane area) for the Pellicon® 3 cassettes are between 240 and 360 L/m^2/h (LMH) which is equivalent to a feed flow rate between 35 and 53 mL/min for N = 1 and between 140 and 210 mL/min for N = 4. However, these high feed flow rates provide relatively low conversion, requiring continued recirculation of the feed through the module as is typical in batch ultrafiltration processes.

The behavior of the feed side pressure drop is more complex (bottom panel of Figure 5.1). The pressure varies nearly linearly with Q_F at high feed flow rates, reflecting the small concentration factors under these conditions (top panel), which leads to a nearly constant retentate flow rate throughout the model. The increase in pressure drop at very low feed flow rates is a direct result of the large increase in viscosity of the concentrated mAb solutions that are generated under these conditions due to the high conversion (large X) in the SPTFF modules. Model calculations using the correlation developed for the viscosity of the mAb solution show that the product η^*Q

increases at very low flow rates. This effect is most pronounced for the module with 4 cassettes in series (L = 80 cm) since the conversion is greatest under these conditions.

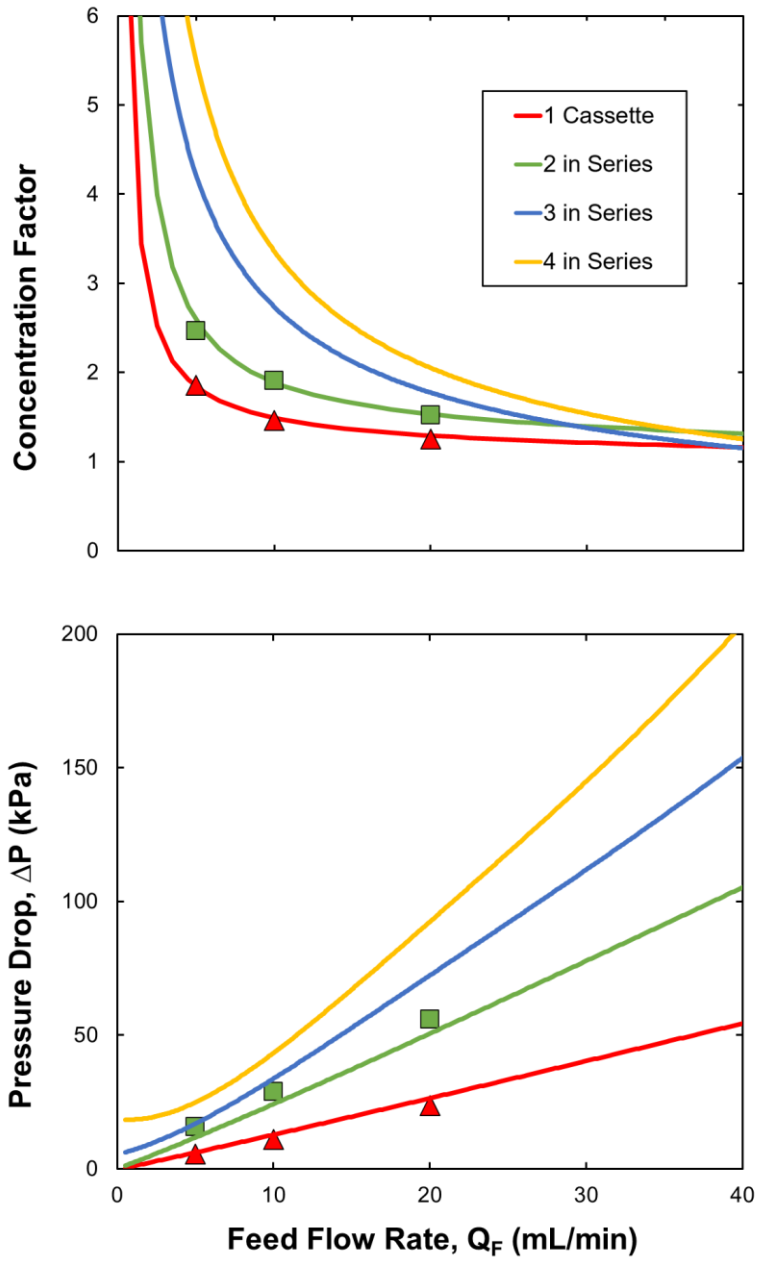

Figure 5.1: Concentration factor (top panel) and feed-side pressure drop (bottom panel) as a function of the feed flow rate for different numbers of Pellicon® 3 cassettes in series (L_{total} = 20 to 80 cm with w = 2.2 cm) at a mean transmembrane pressure of 50 kPa and C_F = 20 g/L. Experimental data for 1 and 2 cassettes in series are at a mean transmembrane pressure of 50 kPa.

5.3.2 Dimensionless pressure drop

In order to understand the pressure drop behavior in more detail, the results in Figure 5.1 were replotted as the scaled pressure drop $\Delta P/\Delta P_0$, where ΔP_0 is the pressure drop through the module evaluated assuming the flow rate and viscosity are constant at their exit values:

$$\Delta P_0 = -\frac{\beta}{N}\eta Q L \tag{5.4}$$

The results for the different module lengths tend to collapse to a single curve when plotted as the scaled pressure drop as a function of the mAb concentration at the device exit (C_R). The scaled pressure drop initially increases with increasing feed flow rate since the reduction in Q is more significant than the increase in viscosity at low mAb concentrations. The scaled pressure drop goes through a maximum around 50 g/L and then decreases at high feed flow rates due to the very high viscosity at the high mAb concentrations (η varies exponentially with C as given by Equation 4.1).

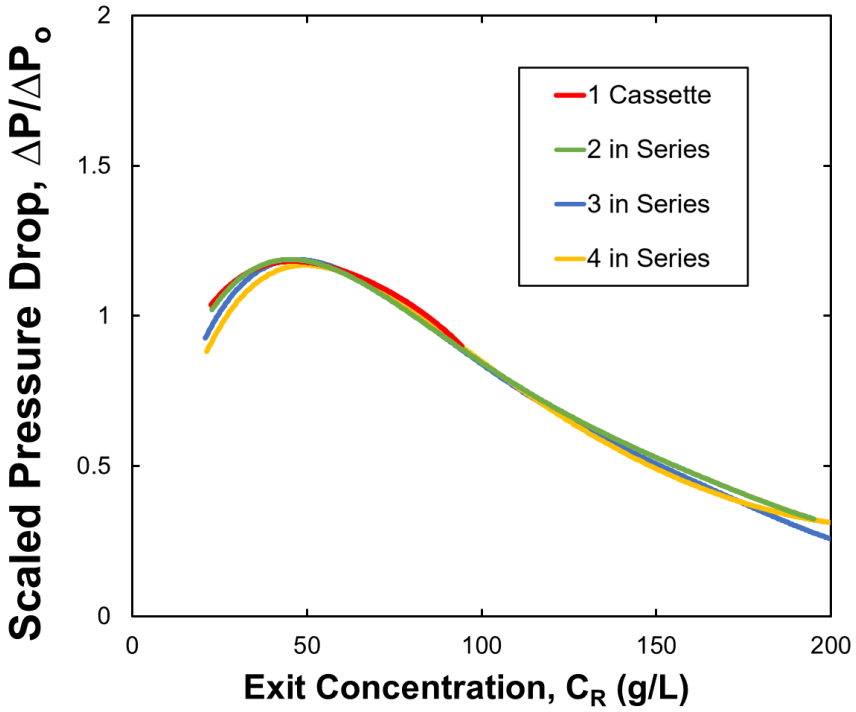

Figure 5.2: Plot of the dimensionless pressure drop versus the final retentate concentration at C_F = 20 g/L for different numbers of modules in series.

5.3.3 Cascade configurations

The effect of channel width and length on the performance of the SPTFF process was examined by performing calculations for a system with six cassettes, each 20 cm in length and 2 cm in width, arranged in different series and parallel configurations: (a) 6 channels in parallel (with total width of 12 cm), (b) 3 channels in parallel followed by a second 3 channels in parallel (total length of 40 cm and total width of 6 cm), (c) a 2-2-2 configuration (L = 60 cm and w = 4 cm), and (d) all 6 single channels in series giving a 1-1-1-1-1-1 configuration (L = 120 cm). All four configurations had the same total membrane area of A = 2wL = 480 cm^2. Simulations were performed over a range of feed flow rates with C_F = 10 g/L; similar results were obtained at other

mAb concentrations with the concentration factor decreasing with increasing C_F while the pressure drop increases. As shown in Figure 5.4, the concentration factor was greatest for the configuration with all 6 cassettes in series, which has the highest mass transfer coefficient due to the large Reynolds number (Equation 5.3). However, this configuration also has the largest pressure drop due to the very long channel length, and high velocity, with $\Delta P = 98$ kPa at a feed flow rate of 20 mL/min compared to only 3 kPa for the fully parallel cascade. The minimum pressure drop in the series configuration occurs at $Q_F = 13.5$ mL/min; operation at lower feed flow rates leads to a greater pressure drop due to the increase in viscosity that occurs at high conversion. The concentration factor decreases as one moves to a more highly parallel arrangement due to the reduction in the mass transfer coefficient caused by the lower Reynolds number. In addition, the minimum in the pressure drop shifts to smaller Q_F due to the corresponding reduction in the conversion. Figure 5.3 shows the pressure drop data for the different configurations which again collapse to a single curve when plotted in the form used previously in Figure 5.2.

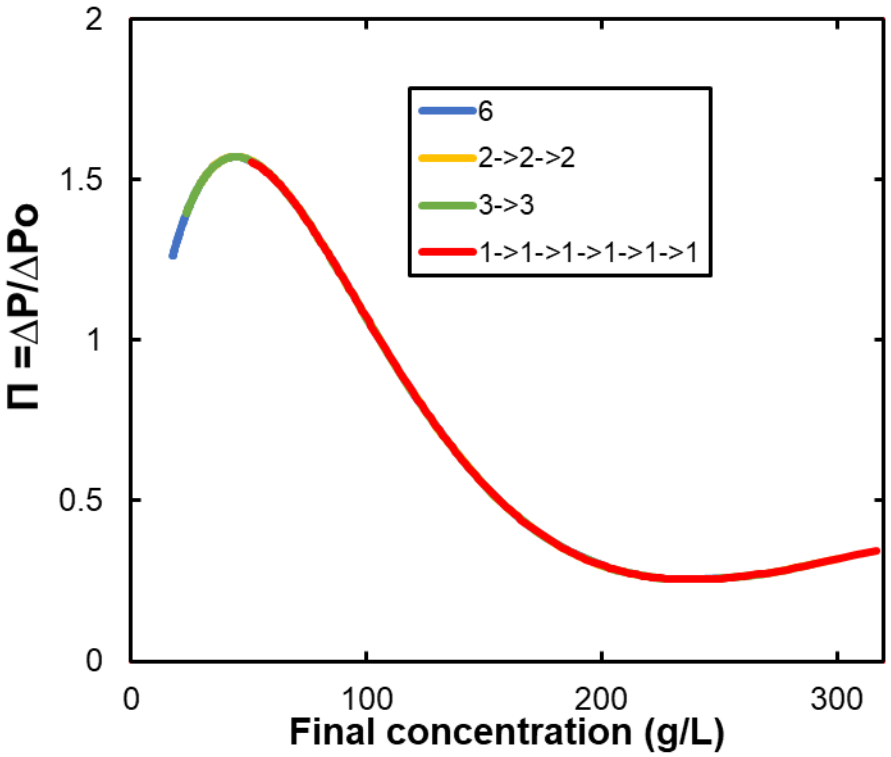

Figure 5.3: Plot of the dimensionless pressure drop versus the final retentate concentration for SPTFF using different module configurations with C_F = 10 g/L over a range of Q_F.

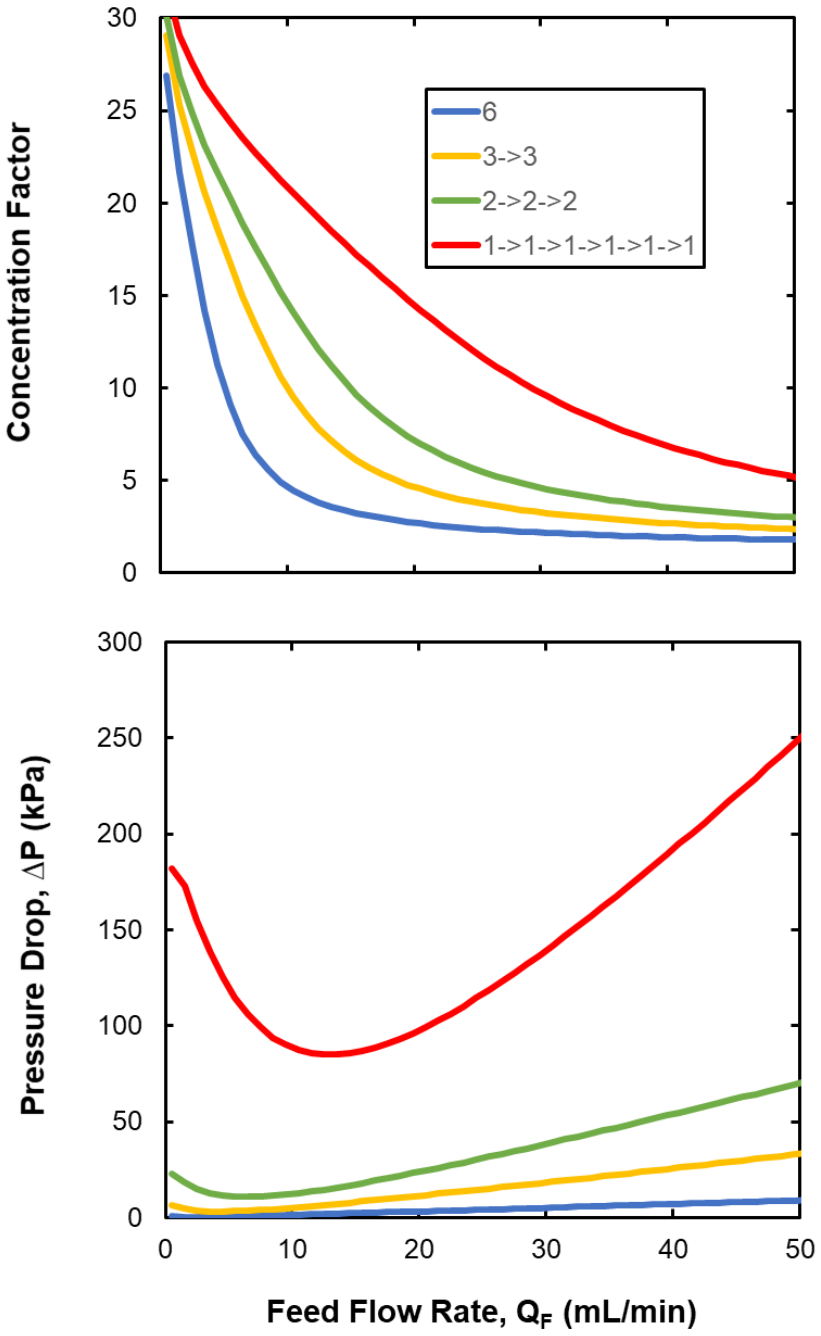

Figure 5.4: Concentration factor and pressure drop vs the feed flow rate at C_F = 10 g/L for different parallel and series configurations of six channels, each with L = 20 cm and w = 2 cm: (a) 6 channels in parallel, (b) 3 parallel followed by 3 parallel, (c) 2-2-2, and (d) 1-1-1-1-1-1 (all channels in series).

In addition to the channel configurations examined in Figure 5.4, it is also possible to arrange the six channels in tapered configurations, e.g., with 3 parallel channels followed by 2 parallel channels and then 1 channel, which we label as the 3-2-1 configuration. The concentration factor and pressure drop for several possible arrangements of the 6 cassettes are summarized in Figure 5.5 for a feed concentration of 10 g/L, a feed flow rate of 20 mL/min, and a feed pressure of 310 kPa. The concentration factor is determined primarily by the total length of the SPTFF module, with the concentration factor decreasing from X = 14.5 for the 1-1-1-1-1-1 configuration (L = 120 cm) to X = 6.9 ± 0.2 for the 3 configurations with L = 60 cm (3-2-1, 2-2-2, and 1-2-3), to X = 4.5 ± 0.1 for the 3 configurations with L = 40 cm, and finally to X = 2.7 for the fully parallel arrangement with L = 20 cm. For configurations with the same total length, the concentration factor is largest for the more uniform arrangement, e.g., 2-2-2 has a slightly greater concentration factor than either the 3-2-1 or 1-2-3 configurations, since the uniform arrangement eliminates having a region with very low Reynolds number. The pressure drop also tends to scale with the total channel length, but in this case there are significant differences between the different configurations with the same total channel length. For example, the pressure drop for the 3-2-1 cascade is only 2.5 kPa; this increases by more than 40% to 3.6 kPa for the 1-2-3 configuration. The lower pressure drop for the 3-2-1 configuration is due to the more uniform flow distribution per module with this arrangement; the high inlet feed flow rate is split among more parallel channels while the lower flow rate near the device exit is handled in a single channel. This effect would be even more pronounced if operating the module at higher feed flow rates or higher feed concentrations, with the latter due to the increase in viscosity of the mAb solution.

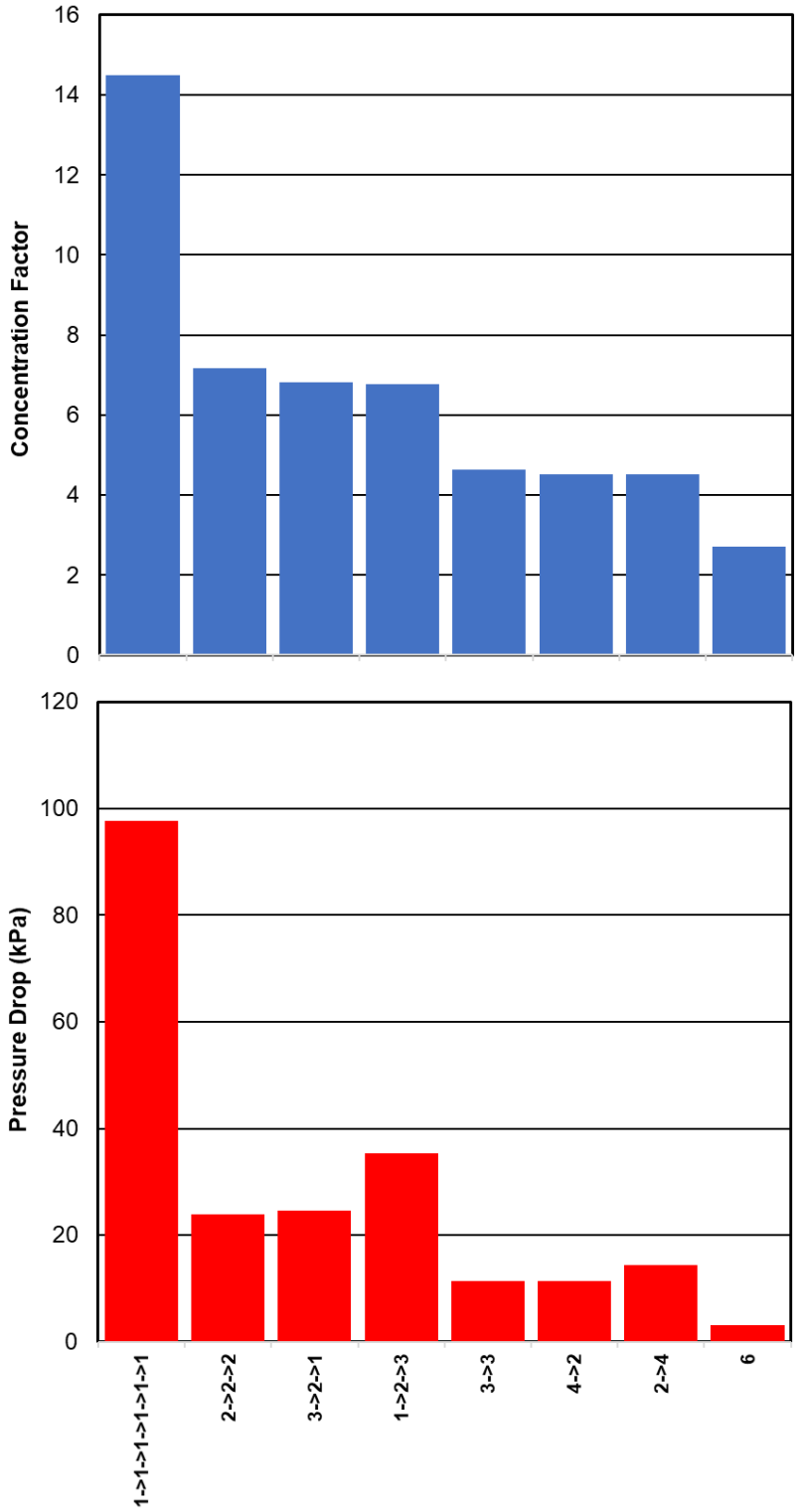

Figure 5.5: Effect of module configuration on the concentration factor and pressure drop for C_F = 10 g/L and Q_F = 20 mL/min.

The analysis in Figure 5.5 examined the performance of the different module configurations at a constant feed flow rate. Since many membranes / modules have a maximum operating pressure, it is also of interest to examine the effect of module configuration at a fixed value of the pressure drop as shown in Figure 5.6. In this case, the concentration factor and average filtrate flux are shown for C_F = 10 g/L with a feed pressure of 310 kPa (45 psi) and a feed-side pressure drop of 50 kPa. This was done iteratively by guessing a value of Q_F, integrating along the membrane length to evaluate ΔP, and then increasing or decreasing the feed flow rate until ΔP = 50 kPa. Note that it was not possible to find a feed flow rate for the 1-1-1-1-1-1 configuration since the minimum ΔP for this long a module was greater than 50 kPa. This was true even at very low feed flow rates since the high conversion under these conditions leads to a very high viscosity, and pressure gradient, near the channel exit. Interestingly, the 1-2-3 cascade had the largest concentration factor but with the lowest average filtrate flux since this cascade had to be operated at the lowest feed flow rate (Q_F = 15 mL/min) to obtain ΔP = 50 kPa. Thus, the 1-2-3 cascade processes the lowest quantity of mAb solution per unit time. By far the greatest flux was obtained with the 6 in parallel configuration since the short path length and large width allows one to operate at Q_F = 250 mL/min, but the concentration factor under these conditions is only 1.2. The configurations with total length of 60 cm have a higher flux but lower concentration factor than those with L = 40 cm since the feed flow rate (at fixed ΔP) varies approximately as $1/L_{total}$. In this case, the more uniform configurations (2-2-2 and 3-3) have the largest average filtrate flux but the smallest concentration factor.

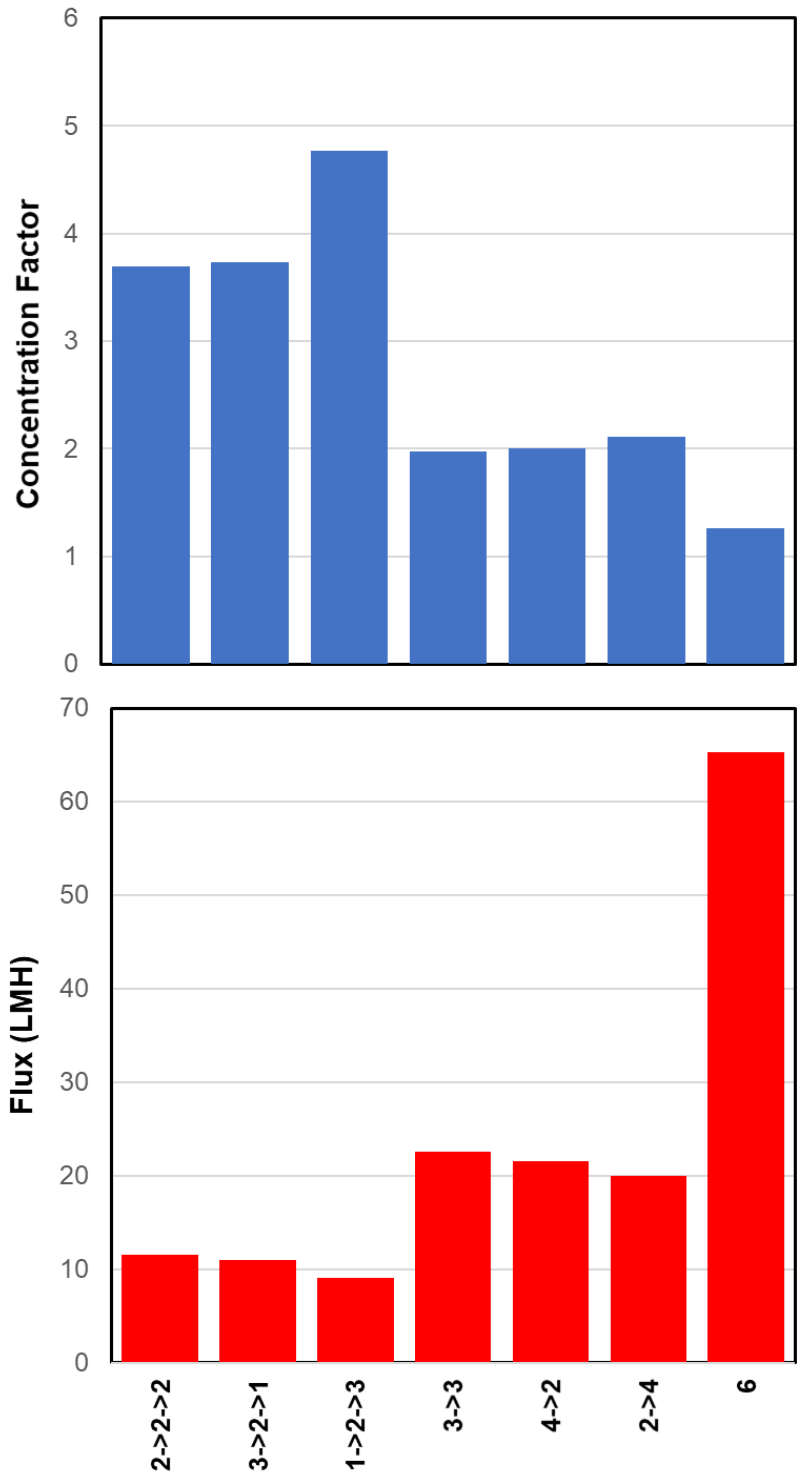

Figure 5.6: Effect of module configuration on the concentration factor and average filtrate flux for simulations with C_F = 10 g/L, ΔP = 50 kPa, and P_F = 310 kPa.

5.3.4 SPTFF design calculations

Most SPTFF processes are designed to achieve a particular concentration factor for a given feed stream, e.g., to concentrate a 10 g/L mAb solution with Q_F = 20 mL/min to a final concentration of 20 g/L (corresponding to a 2-fold reduction in flow rate and volume assuming that the membrane is fully retentive to the mAb). In this case, one would like to minimize the membrane area required for this process, which is equivalent to maximizing the filtrate flux. Simulations were performed with SPTFF modules composed of different numbers and configurations of cassettes, with each cassette in a given module having the same length and width to facilitate module assembly. In this case, the width of the channel was fixed at w = 2 cm based on the results in Chapter 4. Table 5.1 shows the required membrane area and total length, along with the calculated pressure drop, for the different configurations. In each case, the total length and P_F were evaluated iteratively to achieve the desired concentration factor with an exit transmembrane pressure of 14 kPa (2 psi). The lowest membrane area is obtained with the module having 1 long channel, although this module also has the largest pressure drop. Using 3 channels in parallel reduces the pressure drop by more than a factor of 5 due to the reduction in total length in combination with the reduction in flow rate per channel (i.e., fluid velocity), with only a 73% increase in membrane area. Just as significantly, the module with the 3-2-1-1 configuration (which is the geometry of the commercial Cadence™ 4-in-series module) provides a 2-fold reduction in pressure drop relative to the single long channel but with less than a 35% increase in membrane area. The optimal trade-off between the membrane area and pressure drop will be determined by the overall process economics, including the cost per unit area for the membrane module, as well as practical constraints on the pressure drop and the design / assembly of the individual cassettes and then the integrated module.

Table 5.1: Membrane area, total length, and pressure drop to achieve a 2-fold concentration factor for different module configurations with C_F = 10 g/L and Q_F = 20 mL/min.

	Membrane area (cm^2)	Total Length (cm)	Pressure Drop (kPa)
1	180	45	46
2	256	32	16
3	312	26	9
2->1	222	37	27
3->2->1	266	33	19
3->2->1->1	241	34	23
4->3->2->1	286	29	14

The calculations in Table 5.1 are representative of the conditions associated with inline concentration to reduce tankage constraints or to improve the performance of subsequent chromatography steps. SPTFF can also be used for final formulation, but with much higher concentration factors to achieve the desired drug product. Simulations were thus performed for a 20 g/L mAb solution at a feed flow rate of 10 mL/min to achieve a final formulation of 200 g/L, corresponding to a 10-fold concentration as shown in Table 5.2. The membrane width was w = 3 cm and the retentate exit pressure was fixed at 35 kPa (5 psi); simulations at lower exit pressures gave similar results except for the long channel where the model did not converge. The minimum area is again obtained with a single long channel, although in this case the pressure drop is so large that the inlet pressure (766 kPa = 111 psi) is well above the maximum operating pressure for

currently available membranes / modules (which is typically around 400 kPa). The 3 in parallel configuration again reduces the pressure drop by approximately 5-fold with less than a 2-fold increase in membrane area. However, the 3-2-1-1 staged configuration only reduces the pressure drop by 27% with a 36% increase in membrane area since the pressure drop is determined primarily by the flow of the high viscosity mAb solution near the exit of the module.

Table 5.2: Membrane area, total length, and pressure drop to achieve a 10-fold concentration factor for different module configurations with C_F = 20 g/L and Q_F = 10 mL/min.

	Membrane area (cm^2)	**Total Length (cm)**	**Pressure Drop (kPa)**
1	3100	516	766
2	4390	366	271
3	5360	298	147
2->1	3860	429	591
3->2->1	4480	373	450
3->2->1->1	4210	401	556
4->3->2->1	5040	336	360

5.4. Conclusions

The growing interest in implementing continuous biomanufacturing processes has led to increased use of SPTFF for debottlenecking existing processes and for developing interconnected and / or continuous processes. This Chapter presented a detailed examination of the design and optimization of SPTFF modules in terms of the channel geometry and module configuration, focusing on the concentration factor, feed-side pressure drop, and required membrane area for a given process objective. The model predictions were validated using experimental data obtained with the Pellicon® SPTFF system incorporating one or two Pellicon® 3 cassettes in series.

The highest concentration factor (at a given feed flow rate) was always obtained using a single long channel, although this configuration led to the highest pressure drop. The pressure drop could be significantly reduced by adding more channels in parallel, which not only reduces the flow velocity but also reduces the path length (for the same total membrane area). Alternatively, one can use a staged configuration, with the number of parallel channels varying with position within the module. However, the pressure drop in the staged modules depends strongly on the viscosity of the antibody solution. Although one would intuitively expect the greatest pressure losses to occur near the device inlet due to the high feed flow rate at the entrance to the module, the large increase in viscosity with increasing mAb concentration actually causes a greater pressure drop near the retentate exit under most conditions for the antibody examined in this work.

The modeling approach presented in this Chapter provides a framework that can be used for design and optimization of SPTFF modules to achieve specific process objectives, both for inline concentration prior to chromatographic separations and for final formulation (as shown in Tables 5.1 and 5.2, respectively). This should not only reduce the number of experiments required

for development of SPTFF processes, it should also lead to the development of more productive SPTFF modules (e.g., with lower membrane area) for use in bioprocessing.

Chapter 6: pH and Excipient Profiles during Formulation of Highly Concentrated Biotherapeutics using Bufferless Media

The work presented in this chapter is adapted from: Jabra, MG, Tao, Y, Moomaw, JF, Yu, Z, Hovotec, BJ, Geng, SB, Zydney, AL. pH and excipient profiles during formulation of highly concentrated biotherapeutics using bufferless media. Biotechnology and Bioengineering. 117: 3390-3399 (2020). https://doi.org/10.1002/bit.27502. The experimental data for the pH and excipient profiles were obtained at Eli Lilly. Mario Jabra performed all of the modeling work.

Several models have been developed to describe the shifts in pH and excipient concentrations seen during diafiltration of monoclonal antibody (mAb) products accounting for both Donnan equilibrium and electroneutrality constraints. However, these models have assumed that the mAb charge is either constant or only a function of pH, assumptions that will not be valid when formulating highly concentrated mAbs using bufferless or low-buffered media. The objective of the work presented in this Chapter was to incorporate the effects of both pH and ionic strength on the mAb charge, through the use of a charge regulation model based on the amino acid sequence of the mAb, into an appropriate mass balance model to describe the pH and excipient profiles during diafiltration. The model involves no adjustable parameters, with the protein charge evaluated directly from the protonation / deprotonation of the ionizable amino acids accounting for the electrostatic interactions between the charged mAb and the H^+ ions. Model predictions are in excellent agreement with experimental data for the pH and ion concentrations during diafiltration of a mAb and fusion protein with different isoelectric points and different formulation conditions. Model simulations are then used to obtain fundamental insights into the factors controlling the diafiltration behavior as well as guidelines for development of diafiltration processes to achieve target bufferless formulation conditions.

6.1 Introduction

Ultrafiltration (UF) and diafiltration (DF) are used in the final formulation of monoclonal antibodies (mAbs) to achieve the desired pH, buffer composition, and excipient concentrations[18]. However, several studies have shown that the pH and ion concentrations at the end of the diafiltration can be significantly different than those in the diafiltration buffer due to volume exclusion effects[12], ion binding interactions[14], and Donnan equilibrium[13]. A number of models have been developed to describe these phenomena, with a particular focus on the effects of Donnan equilibrium and the need to maintain electroneutrality on the partitioning of ionic species across a semipermeable membrane. For example, Baek et al.[17] evaluated the pH and excipient profiles throughout the diafiltration process by numerical integration of the governing species mass balances, with the mAb charge assumed to be constant, independent of both pH and ionic strength, during the diafiltration. Bolton et al.[55] and Stoner et al.[56] developed models for UF/DF that accounted for the variation of the mAb charge with pH (but not ionic strength), but these models were limited to the evaluation of the pH and excipient concentrations at the end of an extended DF process, without any information on how extensive a diafiltration would be required to achieve these conditions. Miao et al.[57] and Teeters et al.[58] examined pH and ion partitioning by solution of the Poisson-Boltzmann equation, but in both cases the protein surface charge density was assumed to be independent of the solution ionic strength.

Although these models are in good agreement with experimental data obtained during DF into a variety of buffers, it is questionable whether they can be effectively applied to bufferless or low-buffer formulations in which the ionic strength can vary by orders of magnitude over the course of the DF. There is growing interest in formulation of mAb products in bufferless or low-buffer media due to the reduction in pain during subcutaneous or intra-muscular administration of

these products[53]. Gokarn et al.[60] showed that mAbs provide significant "self-buffering" that can be used to control the pH during formulation and storage. Self-buffered solutions of a representative mAb showed less aggregation during accelerated, high temperature, stability studies than was seen with formulations using acetate, glutamate, and succinate buffers. Bahrenburg et al.[61] obtained similar results showing that conventionally buffered solutions had significantly higher opalescence than bufferless formulations.

The objective of the work described in this Chapter was to explore the effects of Donnan equilibrium on the pH and ion concentrations during DF into bufferless or low-buffered solutions. Experiments were performed with a mAb and a fusion protein with different isoelectric points, different initial solution conditions, and different formulation targets. The data were analyzed using an extension of the mass balance model developed by Baek et al.[17] that accounts for the variation in protein charge with both pH and ionic strength due to charge regulation (the change in protonation of ionic amino acids due to electrostatic interactions between the charged mAb and the H^+ ions). The model involves no adjustable parameters; the protein charge at each pH and ionic strength is calculated directly from the known amino acid sequence. Model predictions are in very good agreement with experimental data for the pH and excipient profiles during diafiltration, providing new insights into the underlying phenomena as well as a framework for the development of appropriate DF processes to achieve the target formulation using bufferless media.

6.2 Materials and Methods

Highly purified solutions of one monoclonal antibody (mAb3) and one Fc fusion protein (F1) were generated at Eli Lilly and Company (Indianapolis, IN, USA) for use in the DF experiments. mAb3 (an IgG4 with pI > 7 and ≈6.0 nm radius) and F1 (an acidic protein with pI < 7 and ≈4.5 nm radius) were both produced from fed-batch culture using Chinese hamster ovary (CHO) cells. Both proteins were glycosylated on the fragment crystallizable (Fc) portion, and were at least 45% main product as determined by imaged capillary electrophoresis (for mAb3) or analytical anion exchange chromatography (for F1). The harvested cell culture fluids were purified through protein A chromatography followed by one or two polishing chromatography steps. Protein concentrations were determined from the absorbance at 280 nm using a SoloVPE instrument from C Technologies, Inc. (Bridgewater, NJ USA).

6.2.1 Diafiltration process

DF experiments were performed at ambient temperature in an automated PendoTECH TFF system (Princeton, NJ, USA). Two Masterflex peristaltic pumps (Cole-Parmer, Vernon Hills, IL, USA) were used for retentate circulation and feed / diafiltration solution supply during initial concentration / diafiltration processes. The TFF cassettes used for mAb3 were Ultracel 30 kDa composite regenerated cellulose membranes with 0.22 m^2 effective membrane area (2 x 0.11 m^2) in Pellicon 3 modules with D-screen (MilliporeSigma Corp,, Bedford, MA, USA). For F1, the TFF cassettes used Ultracel 10 kDa membranes with 0.0176 m^2 effective membrane area (2 x 0.0088 m^2) in Pellicon 3 modules with C-screen (MillisporeSigma). The TFF runs were initiated by flushing the modules with purified water to displace any storage solution. The membrane was then equilibrated with the diafiltration solution. Ultrafiltration was initially used to concentrate the

protein solution followed immediately by buffer exchange against the diafiltration solution for a desired diafiltration volume exchange. The feed flow rate was maintained at 5 L/min/m^2 and the transmembrane pressure was set at a target of 100 kPa (15 psi). The permeate flux for the diafiltration process was about 0.5 L/min/m^2. After diafiltration, the retentate solution was further concentrated, the product solution was collected, and the TFF system was cleaned by recirculating defiltration solution followed by 0.1 NaOH. Cleaned modules were stored in 0.1 NaOH solution.

6.2.2 Assays

Samples were taken periodically during the diafiltration process for evaluation of pH and residual ion concentration. The pH was measured using either a Mettler-Toledo (Schwerzenbach, Switzerland) Seven-Excellence pH meter with a Mettler-Toledo InLab® Power Pro electrode (Mettler -Toledo LLC, Columbus, OH, USA) or a Beckman 260 pH/temp meter (Beckman Instruments, Fullerton, CA, USA) with an Accumet AccupHast pH electrode (Thermo Fisher Scientific, Waltham, MA, USA). The chloride and acetate anion concentrations in the retentate samples were analyzed by quantitative chromatography. An 8 minute gradient anion exchange chromatography system with electrolytically suppressed conductivity detection was used to separate and detect the anionic species. A Thermo AS11-HC column (4 x 250 mm) was operated at 1.5 mL/min and ambient temperature with a NaOH gradient using pure water as mobile phase A (MPA) and 400 mM NaOH as mobile phase B (MPB). The gradient was initiated at 3.5% MPB (0 to 0.5 min) and ramps to 13.5% MPB from 0.5 to 3.5 minutes (~14 to ~54 mM NaOH), then held at 13.5% MPB until 6 minutes (3.5 to 6 min), and finally returned to 3.5% MPB at 6.1 to 8 minutes (2 min hold). The electrolytically regenerated suppressor (Thermo AERS 500 or equivalent) was operated at 100-200 mA in recycle mode in order to remove the conductivity

background signal from NaOH before the conductivity detection cell. Sample peak concentrations were determined from a calibration curve constructed using the area versus concentration equation developed using standards ranging from 0.1 -1 mM anion concentration.

6.3 Results and Analysis

6.3.1 Model development

The change in buffer / excipient concentrations during a constant volume diafiltration process are described by a series of mass balances:

$$V\frac{dC_i}{dt} = q_p\left[C_i^{DF} - C_i^p\right] \tag{6.1}$$

where V is the feed (retentate) volume, q_p is the volumetric permeate flow rate, C_i is the concentration of species i in the retentate, and C_i^{DF} and C_i^p are the species concentrations in the diafiltration solution and permeate solution, respectively. Equation (6.1) is easily integrated for a neutral solute since $C_i^p = C_i$ (neglecting any volume exclusion effects). Note that Equation (6.1) can only be applied to fully ionized salts like Na^+ and Cl^-; it cannot be used for buffer species (e.g., acetate = $C_2H_3OO^-$) due to the protonation / deprotonation reactions. Instead, Equation (6.1) is used to describe the change in the total buffer concentration, e.g., the sum of the neutral and ionized forms of acetate or histidine. This is discussed in more detail elsewhere[16].

The concentrations of the charged ions in the permeate will be different than those in the retentate due to Donnan equilibrium across the ultrafiltration membrane[13,16]:

$$X = \left(\frac{C_k}{C_k^p}\right)^{\frac{1}{z_k}} \tag{6.2}$$

where z_k is the ion valence. Equation (6.2) is developed assuming the chemical potential of the ions are equal in the retentate and permeate solutions across the membrane. Equation (6.2) was combined with the electroneutrality constraint:

$$\sum_k z_k C_k + Z_{mAb}\left(\frac{C_{mAb}}{MW_{mAb}}\right) - [OH^-] + [H^+] = 0 \qquad (6.3)$$

where Z_{mAb}, C_{mAb}, and MW_{mAb} are the mAb charge, mass concentration (in g/L), and molecular weight, respectively. Equations (6.1) to (6.3) are identical to the mass balance model presented by Baek et al.[17] although that study assumed that Z_{mAb} was a constant, independent of both pH and ionic strength (evaluated experimentally from zeta potential measurements).

It is well known that the protein charge is a function of pH due to the protonation / deprotonation of the various charged amino acids. However, experimental studies of numerous proteins indicate that the protein charge measured by both electrophoretic mobility[56,57] and titration[58] is also a function of the solution ionic strength. This is typically attributed to the change in the local H^+ concentration at the protein surface due to shielding of the electrostatic interactions between H^+ and the charged protein due to other ionic species. This is discussed in more detail in Section 6.3.2.

In this work, the mAb charge was calculated directly from the number (n_i) and $pK_{a,i}$ of the ionizable amino acids:

$$Z_{mAb} = Z^+_{max} - \sum_i n_i r_i \qquad (6.4)$$

where Z^+_{max} is the maximum protein charge (evaluated with all of the ionizable amino acids in their fully protonated form) and r_i is the fractional charge of each amino acid at any given pH and ionic strength. The latter can be evaluated as [59]:

$$r_i = \frac{1}{1 + H^+_{bulk} \exp\left(-\frac{e\,\psi_s}{k_B T}\right) 10^{pK_{a,i}}} \tag{6.5}$$

where e is the electronic charge (e = 1.602 x 10^{-19} C), k_B is Boltzmann's constant, T is the absolute temperature, and H^+_{bulk} is the hydrogen ion concentration in the bulk solution (equal to 10^{-pH}). The $pK_{a,i}$ values for the different amino acids were taken from Voet and Voet[60] and are shown in Table 6.1. Note that these are average values, ignoring the effects of the local environment and protein conformation on the amino acids. The presence of acidic and basic variants of the mAbs was not included in the analysis; the average mAb charge was assumed to be equal to that of the main product.

Table 6.1: pK_a values for various amino acids used in simulations

Amino Acid	pK_a
Aspartic Acid	3.9
Glutamic Acid	4.3
Histidine	6
Cysteine	9.1
Tyrosine	10.1
Lysine	10.8
Arginine	12.5

Equation (6.5) is often referred to as a charge regulation model[62] since the extent of protonation of the various ionizable amino acids is determined by the local pH at the protein surface, which is in turn a function of the protein charge via the protein surface potential (ψ_s). The simplest model for the surface potential is to treat the mAb as a uniformly charged sphere of radius *a* giving[61]

$$\psi_s = \frac{e\, Z_{mAb}}{4\pi\varepsilon a(1+\kappa a)} \tag{6.6}$$

where ε is the permittivity of the suspending medium ($\varepsilon = 6.93 \times 10^{-10}$ C/V/m) and κ is the inverse of the Debye's length:

$$\kappa^{-1} = \left[\frac{N_A e^2}{\varepsilon k_B T}\sum z_i^2 C_i\right]^{1/2} \tag{6.7}$$

where N_A is Avogadro's number. Equations (6.4) - (6.7) have been shown to be in good agreement with the measured charge for a number of proteins, including ovotransferrin[62] and bovine serum albumin[57]; an example showing the charge of ribonuclease A as a function of solution pH at different ionic strength[58] is shown in Section 6.3.2. The calculated charges for the different proteins examined in this work are shown in Section 6.3.2 using the known amino acid sequences for these proteins. The calculated values of the mAb isoelectric point were in good agreement with the experimentally determined values for both proteins, providing further confirmation of the charge regulation model.

The bulk pH was evaluated from the calculated concentrations of the various buffer species using the known pK_a values for the buffers. For example, the pH is related to the relative amounts of the ionized and neutral forms of acetate as:

$$pK_{Acet} = pH + log_{10}\left(\frac{Acetate^{-1}}{Acetate^{0}}\right) = 4.76 - \frac{0.5\sqrt{I}}{1+\sqrt{I}} \tag{6.8}$$

where *I* is the total ionic strength of the solution accounting for the contributions from all charged species (both buffer components and salt). The last expression on the right-hand side of Equation (6.8) accounts for non-idealities in the ion activity coefficients using Debye-Huckel theory[63]. Corresponding equations were used for other buffers, with appropriate expressions for the pK_a.

The pH, salt, and buffer concentrations during the diafiltration process were evaluated as follows. First, the concentrations of all species in the retentate were evaluated based on the initial pH and total salt and buffer concentrations in the feed using Equations (6.3) to (6.8). The corresponding concentrations in the permeate were evaluated using Equations (6.2), (6.3), and (6.8) accounting for the Donnan equilibrium. The total buffer and salt concentrations in the retentate at time $t + \Delta t$ were then determined from Equation (6.1) using a simple first order Euler integration. The entire procedure was then repeated, with the protein charge re-evaluated at each time step based on the pH and ionic strength using Equations (6.4) to (6.7). All calculations were implemented in Mathematica.

6.3.2 Charge Regulation Model

The net protein charge is determined by the relative protonation / deprotonation of the ionizable amino acids. A number of experimental studies have demonstrated that the protein charge is a function of both pH and ionic strength[56,64] with the ionic strength dependence arising from shielding of the electrostatic interactions between H^+ and the charged protein due to other ionic species.

Figure 6.1 shows literature data for the charge of ribonuclease A as a function of solution pH at ionic strengths of 0.01 and 0.15 M as determined by potentiometric titration[58]. The solid

curves are calculations using the charge regulation model with the pK_a values for the ionizable amino acids given in Tanford and Hauenstein[58]. The model calculations are in very good agreement with the data over the full range of conditions, providing strong validation of the charge regulation model. The ribonuclease A charge decreases with increasing pH as expected, with the isoelectric point essentially independent of solution ionic strength. The absolute value of the charge is greater in the 0.15 M solution due to the shift in local pH (i.e., H^+ concentration) at the protein surface associated with electrostatic interactions between the H^+ ions and the charged ribonuclease A.

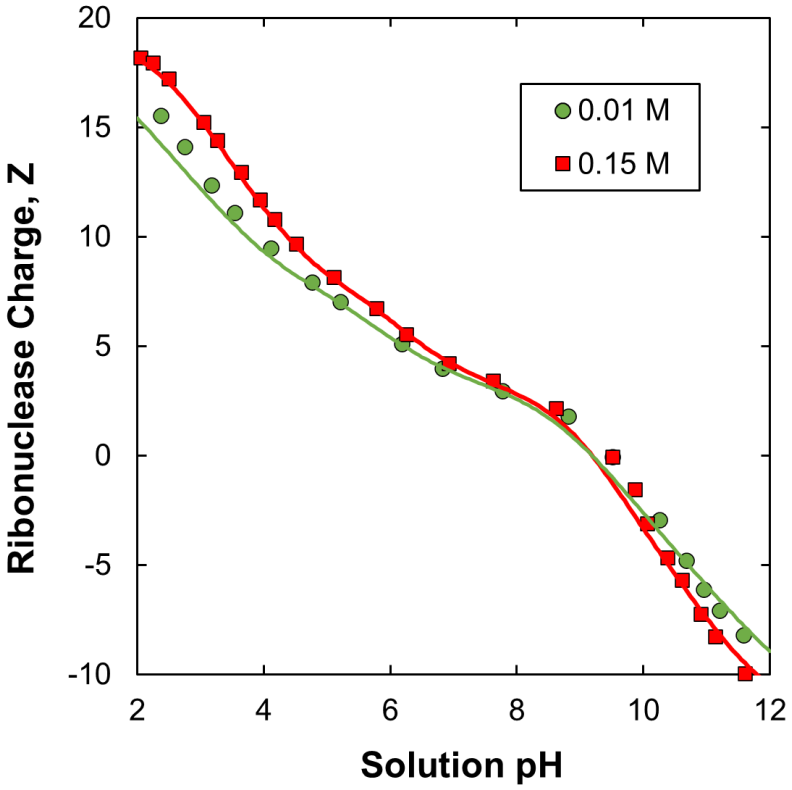

Figure 6.1: Ribonuclease A charge as a function of solution pH at ionic strengths of 0.01 M and 0.15 M. Solid curves are based on the charge regulation model using the pK_a values reported in Tanford and Hauenstein[60]. Symbols are experimental data from the same source.

The calculated charge for mAb3 and F1 are shown in Figures 6.2 and 6.3, respectively, as a function of the solution ionic strength for three values of the pH. The charge for both proteins decrease with increasing pH due to the protonation of the aspartic and glutamic acids (at very low pH) followed by the protonation of histidine (which has a $pK_a = 6.0$). The calculated charge for mAb3 increases with increasing ionic strength due to the charge regulation effects. In this case, the positively charged mAb3 repels the H^+ ions, leading to a greater increase in local pH at the surface of the protein in the low ionic strength solution. The net result is that the calculated charge on mAb3 at pH 5 decreases from $Z_{mAb} = 29.7$ in the 100 mM solution to only $Z_{mAb} = 18.6$ in the 1 mM solution. The effect of charge regulation decreases as the pH approaches the protein isoelectric point since the magnitude of the electrostatic repulsion between mAb3 and the H^+ ions is reduced.

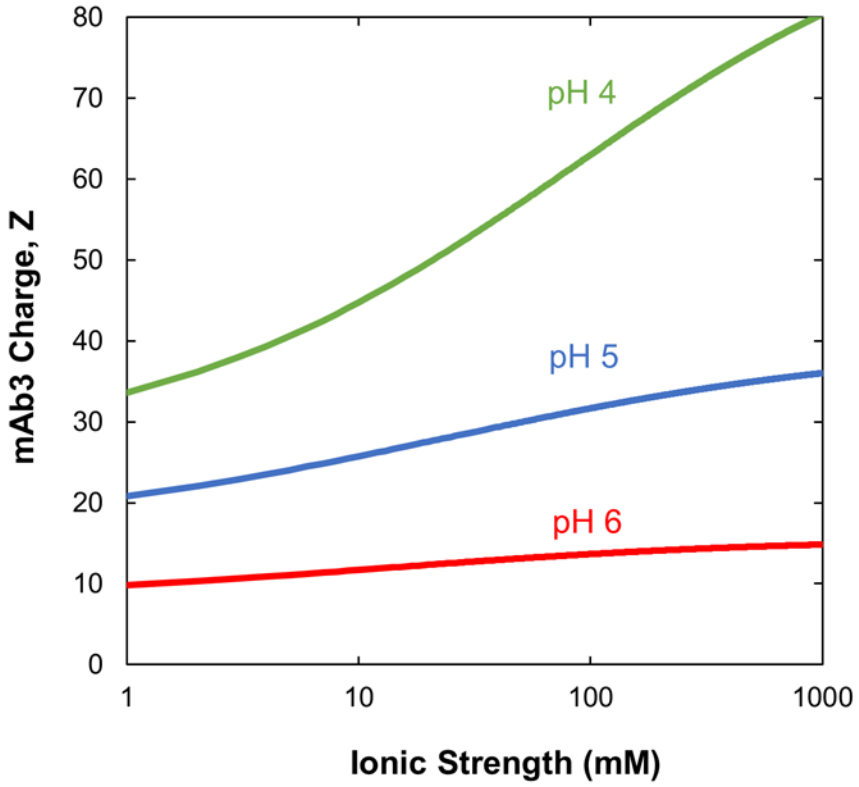

Figure 6.2: Calculated charge of mAb3 as a function of ionic strength at pH of 4, 5, and 6 based on the charge regulation model.

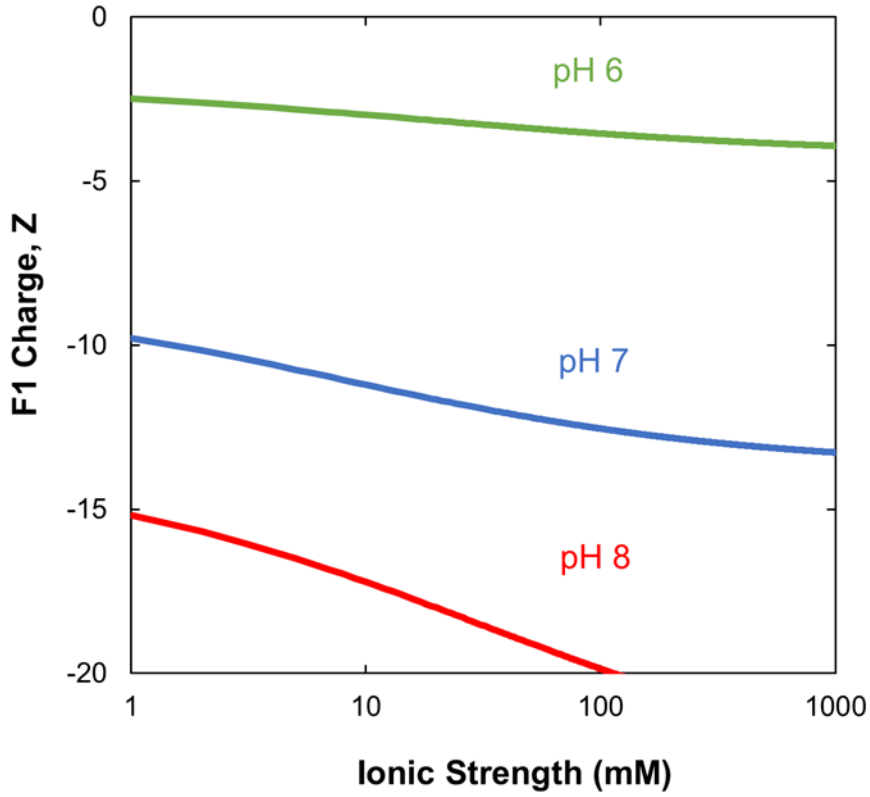

Figure 6.3: Calculated charge of F1 as a function of ionic strength at pH of 6, 7, and 8 based on the charge regulation model.

In contrast to mAb3, the net charge on the negatively charged fusion protein is predicted to be less dependent on the solution ionic strength since the local pH at the protein surface and the bulk pH are equal when the protein charge is very small. The effects of charge regulation reduce the magnitude (absolute value) of the calculated values of the protein charge, which leads to a smaller positive charge at low pH and a smaller negative charge at high pH as the solution ionic strength is reduced. The results in Figures 6.2 and 6.3 were used in the mass balance / Donnan equilibrium model to evaluate the protein charge throughout the diafiltration process.

6.3.3 Model Validation

Experimental data for the pH profile (top panel) and the acetate and chloride concentrations (bottom panel) during diafiltration of mAb3 are shown in Figure 6.4. The antibody was originally in a solution of 45.5 mM acetate buffer with 185 mM NaCl at pH 5.2 at an antibody concentration of 60 g/L. The diafiltration was performed using deionized water at pH 7 as the diafiltration solution (with no added buffer or salt). The solid curves in Figure 6.4 are the model predictions determined from numerical integration of Eq. (6.1); the ion concentrations in the permeate at each time step were evaluated using Eqs. (6.2) and (6.3) with the charge on mAb3 determined from Eqs. (6.4) to (6.7). The radius of mAb3, a = 6.0 nm, was determined by dynamic light scattering. The model involves no adjustable parameters since the mAb3 charge is calculated directly from the known amino acid sequence.

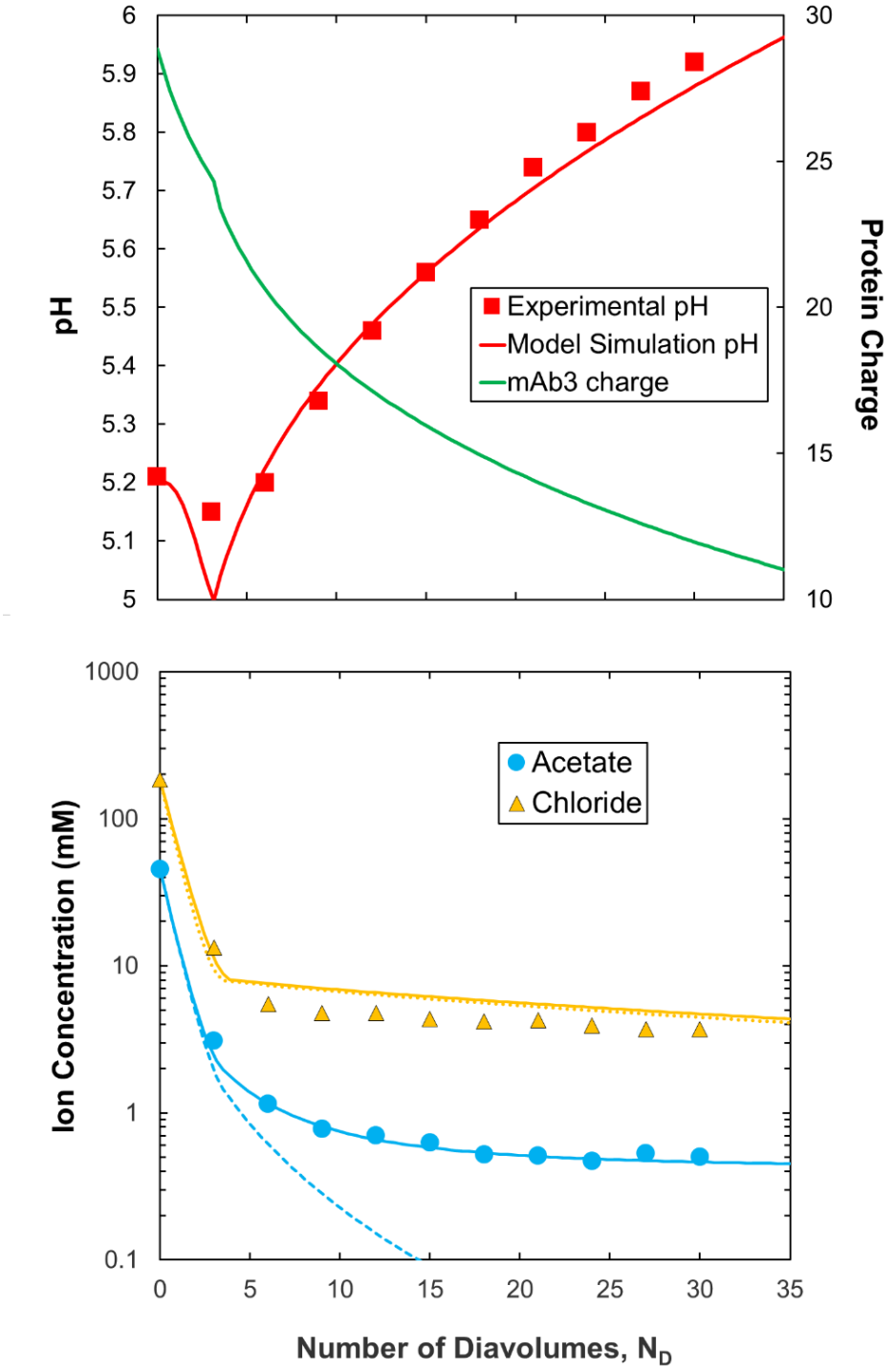

Figure 6.4: Diafiltration of a 60 g/L solution of mAb3 initially in a 45.5 mM acetate buffer with 185 mM NaCl into DI water. Top panel – pH and mAb charge profiles. Bottom panel – acetate and chloride concentrations. Solid curves are model calculations accounting for acetate binding; dashed curve for acetate is prediction without acetate binding.

The model calculations are in very good agreement with the experimental data for both the pH and the acetate / chloride ion concentrations. The initial drop in pH is a direct result of the decrease in mAb3 charge associated with the rapid reduction in the ionic strength of the protein solution as chloride and acetate are removed; this drop in net positive charge causes a release of H^+ ions into the solution due to the deprotonation of some of the basic ($-NH_3^+ \rightarrow -NH_2 + H^+$) and acidic ($-COOH \rightarrow -COO^- + H^+$) side groups on the amino acids. The pH then increases for $N_D >$ 3, attaining a value slightly above 5.9 after 30 diavolumes. This increase in pH is due to the removal of the acetate buffer coupled with the self-buffering provided by mAb3 (since there is no buffer in the diafiltration solution). The pH is predicted to continue to increase well beyond the 30 diavolumes shown in Figure 6.4, eventually approaching a pH just slightly below the isoelectric point of mAb3. This is discussed in more detail in the next section.

The model calculations are also in good agreement with experimental data for the acetate and chloride concentrations (bottom panel of Figure 6.4). The dashed curve for the acetate concentration is the model prediction given by numerical solution of Equations (6.1) to (6.8), while the solid curves were evaluated assuming that mAb3 binds one acetate ion per antibody. In this case, the total concentration of acetate was equal to the concentration of free acetate plus the concentration of bound acetate, with the latter evaluated from the molar antibody concentration times the number of bound acetate per mAb. Acetate binding was also assumed to reduce the net charge on the antibody by one. The extent of acetate binding was determined by simply fitting the model calculations to the experimental results. The model calculations in the absence of any acetate binding significantly under-predict the measured acetate concentration for $N_D > 5$. The acetate and chloride concentration decrease sharply over the first several diavolumes due to the rapid ion removal since the ion concentrations in the permeate are very similar to those in the

retentate at relatively high ionic strength. At $N_D = 5$, the chloride concentration has decreased to 7.5 mM, which is just sufficient to balance the calculated charge for mAb3 of Z = 20 (with $C_{mAb}/MW_{mAb} = 0.4$ mM). As the diafiltration continues, the chloride and acetate concentrations continue to decrease very slowly, with the calculated charge also decreasing slowly as the pH increases (top panel). The very slow change in ion concentrations is due to the Donnan effect. For example, at $N_D = 5$, the calculated concentration of acetate in the permeate solution is only 0.29 mM, which is 26-fold smaller than that in the retentate due to the strong ion partitioning (Eq. 6.2); this is what causes the very slow rate of acetate removal (Eq. 6.1).

Figure 6.5 shows experimental data for diafiltration of a fusion protein (F1) with a calculated isoelectric point around 5.7. The fusion protein was initially in a 20 mM Tris buffer with 120 mM Na_2SO_4 and around 10 mM chloride from initial pH adjustments at a concentration of 50 g/L with pH values of 6.29, 6.43, and 6.69 obtained by appropriate addition of 1 N HCl. In contrast to the behavior seen with mAb3, the pH during the diafiltration of the negatively charged F1 increases over the first 5 diavolumes due to the reduction in the solution ionic strength and the corresponding reduction in the magnitude (absolute value) of the calculated protein charge. The presence of an inflection point during the exponential decrease of the ionic strength vs diavolume, led to a sharp change in the pH at N_D around 5. The predicted pH profile then goes through a maximum between 4 and 5 diavolumes before slowly decreasing towards the protein isoelectric point as the DF continues. This slow decline in pH is associated with the strong ion partitioning at low salt concentrations due to the Donnan equilibrium across the ultrafiltration membrane. The model predictions, which again involve no adjustable parameters, are in very good agreement with

the experimental data for all 3 diafiltration experiments, properly capturing both the initial increase in pH followed by the slower decline for $N_D > 5$.

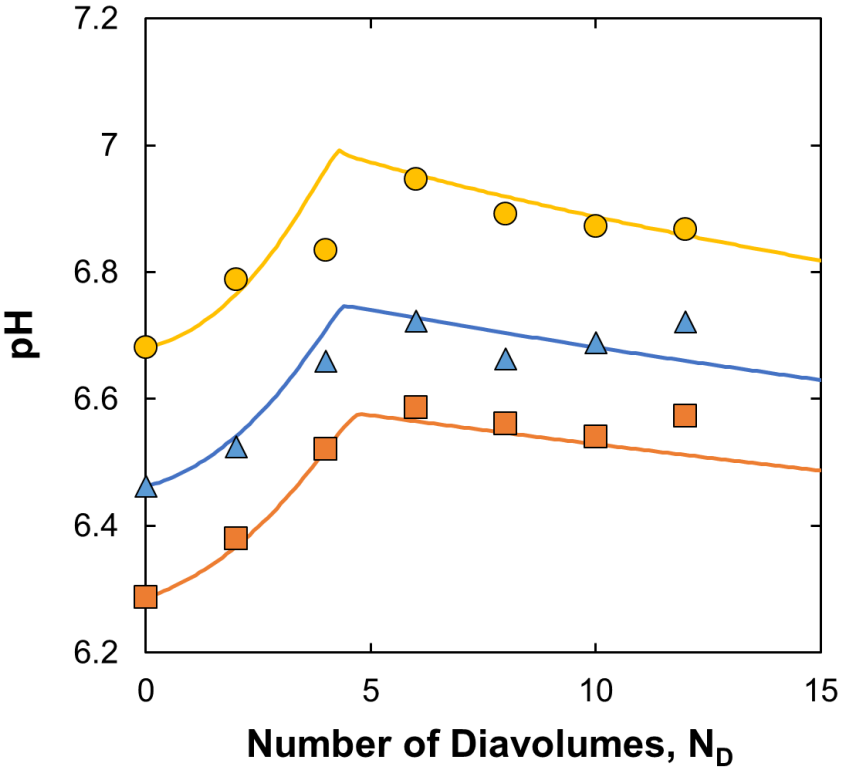

Figure 6.5: Diafiltration of a 50 g/L solution of a fusion protein (F1) initially in a 20 mM Tris buffer with 120 mM Na_2SO_4 and 10 mM NaCl into DI water. Initial pH adjusted to 6.29, 6.43, or 6.69 using 1 N HCl. Solid curves are model predictions.

The model validation was also done with another antibody (mAb1) which has a different number of amino acids than mAb3 but is also positively charged at pH<7. Several runs with different starting pH and buffer concentrations are shown in Figure 6.6. The diafiltration buffer was DI water at pH 7. Again, the model predictions are in good agreement with the experimental data for the various diafiltration experiments, providing further confirmation of the diafiltration model. The extent of the pH shift is slightly greater when the initial pH is further away from the isoelectric point of the protein. For instance, the pH in Run 1 goes from 5.0 to 5.5 while the pH in

Run 4 only goes from 5.6 to 5.95; the smaller pH shift in Run 3 is due to the smaller net charge on the mAb as the pH approaches the protein pI.

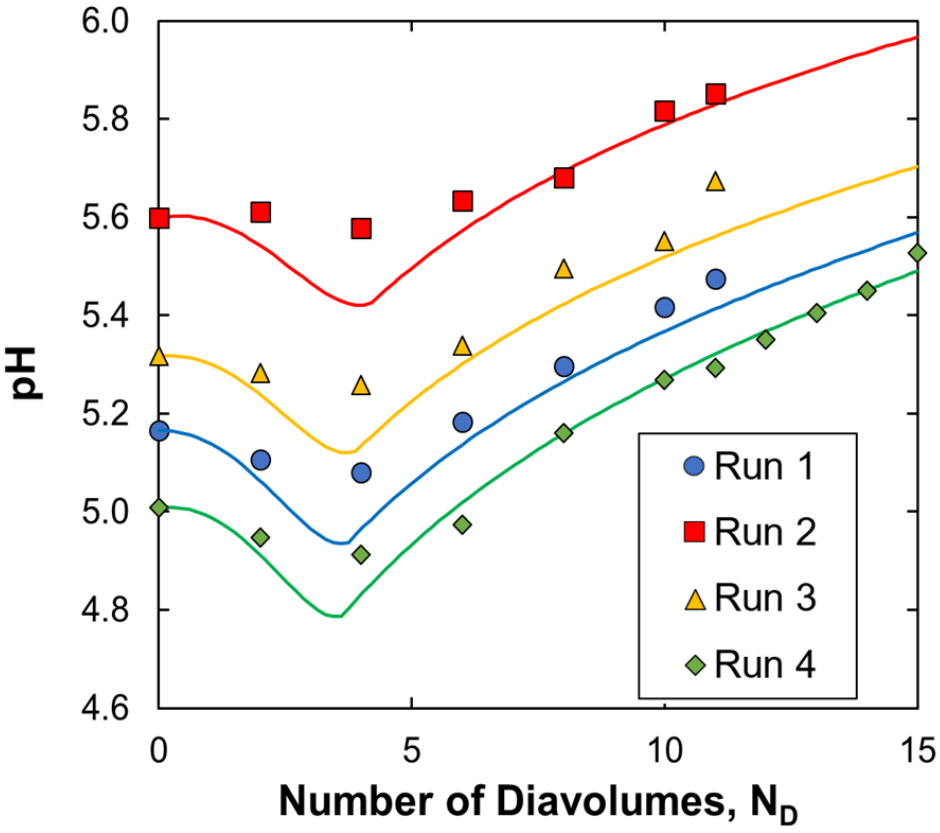

Figure 6.6: Diafiltration of a 35 g/L solution of mAb1 initially in an Acetate/NaCl buffer with concentrations of 22 mM/99 mM in Run 1, 57 mM/87 mM in Run 2, 30 mM/96 mM in Run 3 and 20 mM/100 mM in Run 4, each with a different starting pH.

6.3.4 Model Simulations

In order to obtain additional insights into the factors controlling the diafiltration behavior when using bufferless media, a series of model simulations were performed to explore the key physical phenomena during the diafiltration process. Figure 6.7 shows the calculated pH profiles over an extended diafiltration (out to 1000 diavolumes) for three separate conditions: (1) mAb3

(with the protein charge evaluated as a function of pH and ionic strength from Eqs. (6.4) to (6.7) using the known amino acid sequence), (2) an antibody with the same size and molecular weight as mAb3 but with $Z_{mAb} = 2$ independent of both pH and ionic strength, and (3) an antibody with $Z_{mAb} = 10$. The very large number of diavolumes examined in Figure 6.7 is used to show the very slow approach to steady-state in this system; actual DF processes would typically be limited to a maximum of 20 diavolumes. The initial buffer conditions were fixed at 45.5 mM acetate buffer at pH 5.2 with 185 mM NaCl (equivalent to the conditions examined previously in Figure 6.4). The simulations with constant mAb charge show no decrease in pH at the start of the diafiltration, in contrast to the results with mAb3, providing further confirmation that this initial decline is directly related to the change in calculated mAb charge with a reduction in ionic strength.

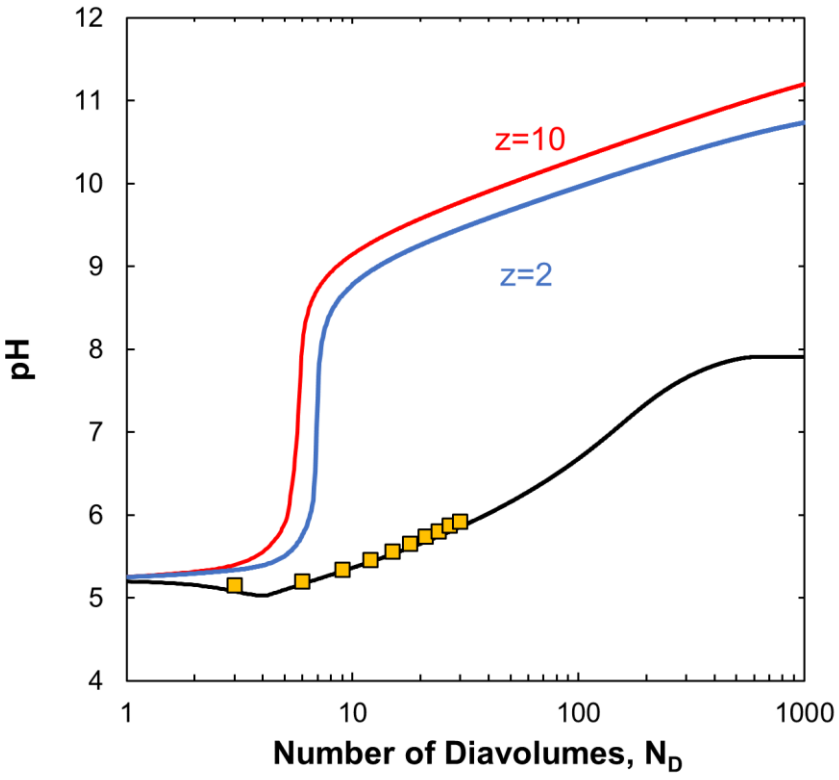

Figure 6.7: Model simulations for diafiltration of mAb3, a protein with Z_{mAb} = 2, and a protein with Z_{mAb} = 10 into DI water at pH 7. In each case, the mAb concentration was 60 g/L with an initial buffer of 45.5 mM acetate and 185 mM NaCl. Symbols represent experimental data for mAb3 (taken from Figure 6.4).

The pH profiles for the runs with Z_{mAb} = 2 and 10 show a slow increase in pH over the first few diavolumes, followed by a very rapid pH increase around N_D = 6, with the pH then continuing to increase slowly even out to more than 1000 diavolumes. This slow increase in pH at the end of the diafiltration is due to the gradual removal of the chloride and acetate ions, similar to the behavior seen in the lower panel of Figure 6.4. When N_D = 1000, the chloride ion concentration for the simulation with Z_{mAb} = 10 is 2 mM, which means that the chloride ion still plays a significant role in balancing the positive charge on mAb3 (the OH^- concentration at this point in

the diafiltration is only 1.59 mM). Note that the exponential decay given by the classical diafiltration equation[65]:

$$C_i = C_{i,o} exp(-N_D) \tag{6.9}$$

would yield a chloride ion concentration of less than 10^{-400} mM (corresponding to less than a single chloride ion in a 2000 L feed).

At true steady-state, the concentration of all ions other than H^+ and OH^- will be equal to zero when using a diafiltration solution that has no buffer or salt (based on Eq. 6.1 with the time derivative set equal to zero). The final value of the pH will thus be determined by the electroneutrality constraint (Eq. 6.3), but with the protein charge balanced by the H^+ and OH^-:

$$Z_{mAb}\left(\frac{C_{mAb}}{MW_{mAb}}\right) + [H^+] - \frac{K_W}{[H^+]} = 0 \tag{6.10}$$

where $K_w = 10^{-14}$ is the equilibrium constant for the dissociation of water. Eq. (6.10) is a quadratic equation for the H^+ concentration. However, the term involving K_w will dominate for the positively-charged mAb3, with the steady-state pH given as:

$$pH = 14 + log_{10}\left[Z_{mAb}\left(\frac{C_{mAb}}{MW_{mAb}}\right)\right] \tag{6.11}$$

Equation (6.11) yields pH = 10.9 for $Z_{mAb} = 2$ and pH = 11.6 for $Z_{mAb} = 10$; the solution of the quadratic equation gives the same values out to one decimal point. Both of these are consistent with the simulations in Figure 6.6 but are still slightly above the values even at $N_D = 1000$.

The behavior for mAb3 with the calculated charge a function of both pH and ionic strength is more complex. First, the solution shows an initial decrease in pH over the first 4 diavolumes followed by a more gradual increase in pH due to the gradual reduction in the mAb3 charge as the pH approaches the isoelectric point of the protein. The pH then approaches its steady-state value, determined by solution of Eq. (6.10) using the charge regulation model to calculate the protein

charge (Eqs. 6.4 to 6.6) giving pH = 7.89 assuming that the protein remains stable at a value slightly below the pI of the positively-charged mAb3. In this case, the small positive charge on mAb3 (Z_{mAb} = 0.45) is balanced by the slight excess in OH^- (compared to H^+) to satisfy the overall electroneutrality constraint (Eq. 6.10).

The effects of adding small amounts of NaCl to the bufferless diafiltration solution are examined in Figure 6.8. Model simulations were performed using mAb3 but without any acetate binding to simplify the analysis. The addition of only small amounts of NaCl significantly reduces the magnitude of the pH increase over the latter portion of the DF. This is particularly true at large numbers of diavolumes, where the pH for the run with 1 mM NaCl attains a value of 6.08 at N_D = 400 compared to pH = 7.83 for the run with 0 mM NaCl. This effect is even more pronounced for the run with 20 mM NaCl where pH = 5.50 at N_D = 400. This large difference in behavior is a direct result of the "retention" of Cl^- by the semipermeable membrane in the presence of the positively-charged mAb3, with the chloride ion concentration in the retentate equal to 4.2 mM at N_D = 400 for the run with 1 mM NaCl in the diafiltration solution. Thus, under these conditions, the electroneutrality constraint is determined largely by the presence of the chloride ion and not the OH^-, leading to the very different diafiltration behavior seen in Figure 6.8.

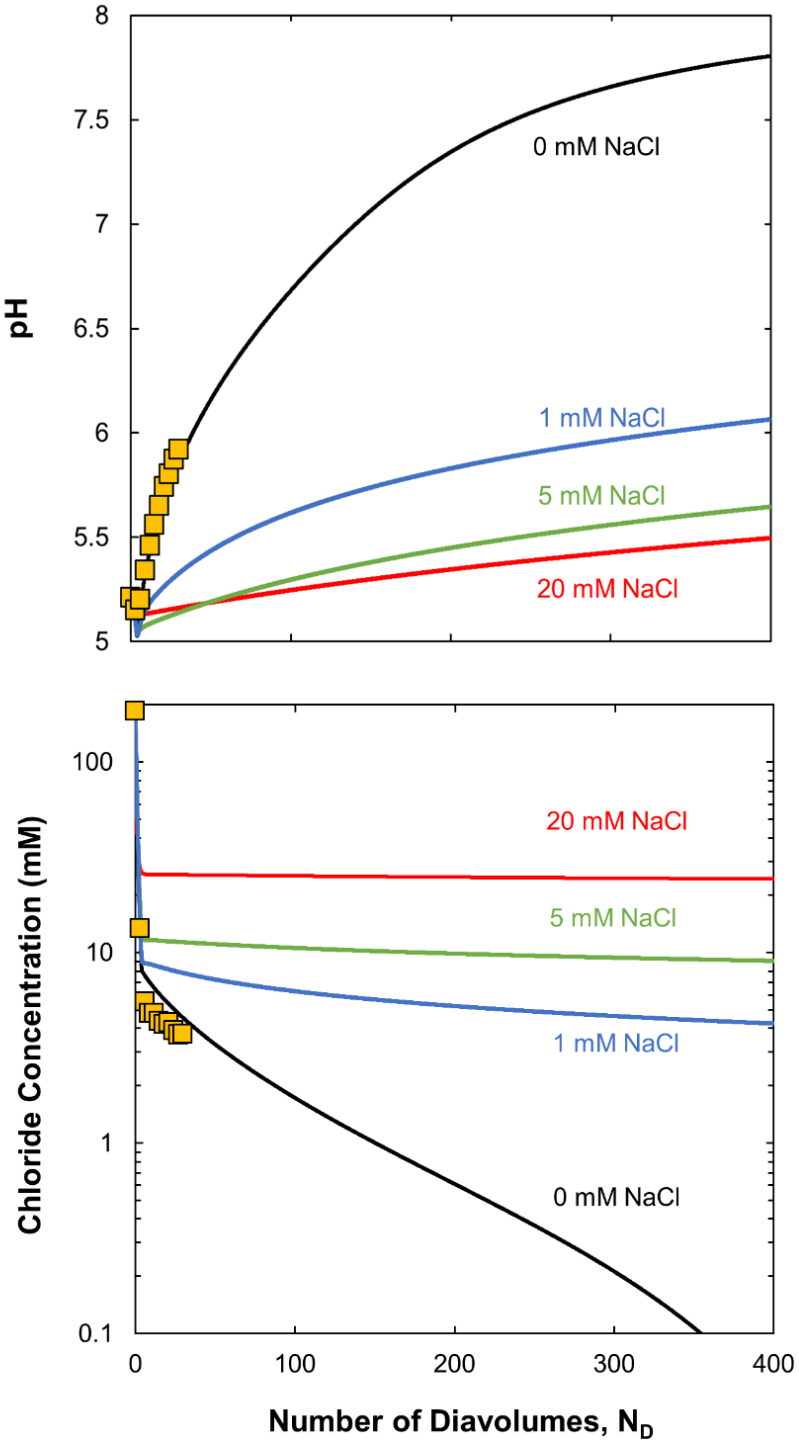

Figure 6.8: Model simulations for diafiltration of 60 g/L solutions of mAb3, in an initial buffer with 45.5 mM acetate and 185 mM NaCl at pH 5.2, using bufferless solutions at pH 7 with different NaCl concentrations. Symbols represent experimental data for mAb3 (taken from Figure 6.4).

All of the model calculations in Figures 6.4 to 6.8 were performed with the pH of the diafiltration solution set to pH 7. Figure 6.9 shows a series of simulations in which the pH of the bufferless diafiltration solution was reduced by adding very small quantities of HCl (with sufficient Cl^- to balance the positive charge on the added H^+). Reducing the pH of the diafiltration solution from 7 to 5 (i.e., increasing the H^+ concentration in solution by a factor of 100) caused only a very small shift in the pH profiles, with the pH at $N_D = 35$ reduced from 5.96 to 5.92. The very small effect of pH between pH 5 and 7 reflects the much lower H^+ concentration (0.01 mM at pH 5) compared to that of the residual salt (Cl^- concentration of 0.5 mM at $N_D = 35$) and the buffering capacity of the mAb. Further reductions in the pH of the bufferless diafiltration solution do result in a corresponding reduction in the pH during diafiltration, with the pH at $N_D = 35$ reduced to 5.57 for the run with a DF solution at pH 4 and to 4.2 for the run with a DF solution at pH 3. Under these conditions, the concentration of positively-charged H^+ entering the system with the DF solution is of the same order of magnitude as the total charge on mAb3. For example, when using a DF solution at pH 3, the H^+ concentration entering the system is 1 mM compared to a mAb3 concentration of 0.4 mM and a total mAb3 charge of around 4 mM. Thus, the H^+ concentration in the diafiltration solution is beyond the intrinsic buffering capacity of mAb3, leading to the much lower values of the pH seen in Figure 6.9.

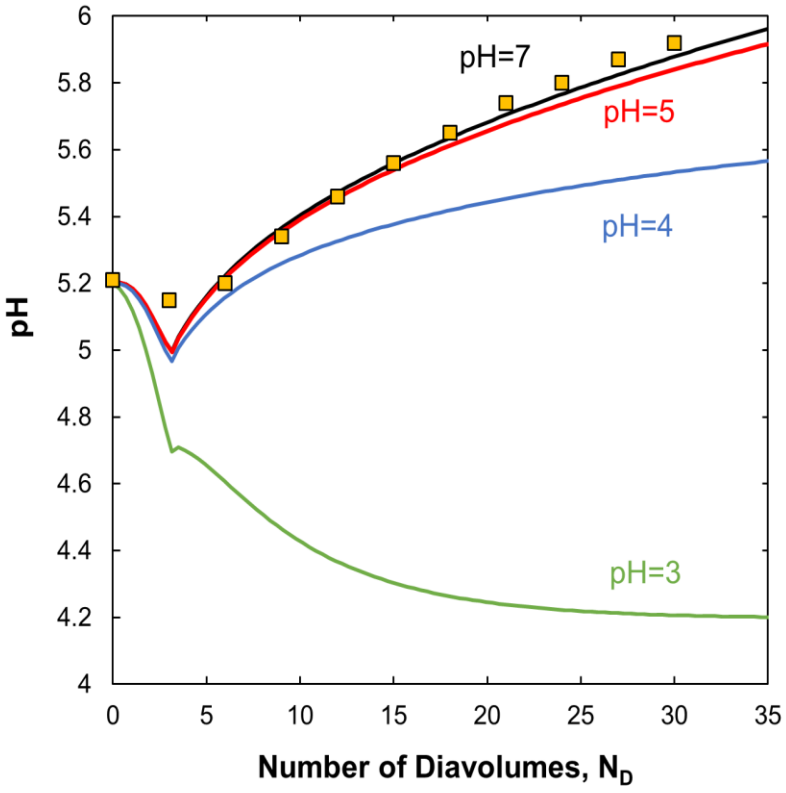

Figure 6.9: Model simulations for diafiltration of 60 g/L solutions of mAb3, with an initial buffer of 45.5 mM acetate and 185 mM NaCl at pH 5.2, using bufferless solutions with pH of 3, 4, 5 and 7 (adjusted with HCl). Symbols represent experimental data for mAb3 using a pH 7 diafiltration solution (taken from Figure 6.4).

6.3.5 Diafiltration Design

The diafiltration model developed in this Chapter can also be used to design a diafiltration process that can achieve a specific target pH value (and buffer conditions) after a desired number of diavolumes by iterating on either the initial conditions or the properties of the diafiltration buffer solution. In the top panel, simulations were performed for the diafiltration of mAb3 (initially in a 45.5 mM acetate buffer with 185 mM NaCl at pH 5.2) targeting a pH of 6 after 10 diavolumes. In this case, it was not possible to achieve the target pH of 6 using a bufferless formulation (at any

pH) due to the strong buffering provided by the antibody; this is shown by the black curve in Figure 6.10. Therefore, four different options were explored with different buffer properties and / or with an adjustment in the initial pH of the feed. The design adjustments are summarized in Table 6.2. In all 4 cases, the pH achieves a final value of 6.0 (within 0.02 pH units) after 10 diavolumes as desired, although the pH trajectories during the diafiltration were very different. Note that none of the simulations attained steady-state after 10 diavolumes, although the rate of change in pH at the end of the DF was relatively slow.

Table 6.2: Feed and buffer adjustments for the diafiltration design for cases in Figure 6.10

Case	Initial pH	Buffer pH	Buffer Composition
A	6.1	pH 7	DI water
B	5.2	pH 7	10 mM Histidine with 20 mM NaCl for $N_D<5$, DI water for $N_D>5$
C	5.2	pH 6 for $N_D<5$, pH 7 for $N_D>5$	5.5 mM Histidine for $N_D<5$, DI water for $N_D>5$
D	5.2	pH 5.8	5 mM Histidine
E	6.7	pH 3.72	DI water
F	6.7	pH 6.52 for $N_D<5$, pH 7 for $N_D>5$	5 mM Phosphate for $N_D<5$, DI water for $N_D>5$
G	6.7	pH 6 for $N_D<3$, pH 7 for $N_D>3$	20 mM Acetate for $N_D<3$, DI water for $N_D>3$
H	6.3	pH 7	DI water

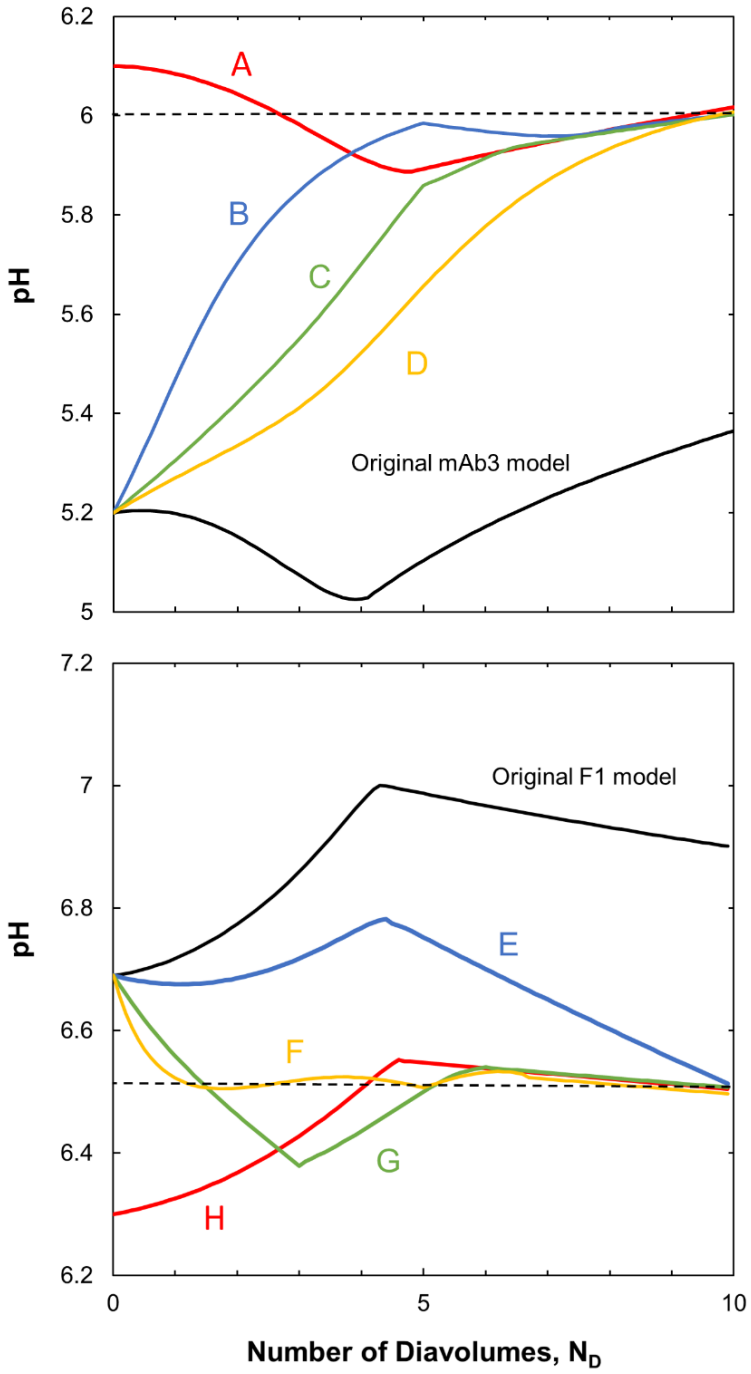

Figure 6.10: Design calculations for diafiltration of mAb3 to achieve a target pH of 6 after 10 diavolumes (top panel) and for diafiltration of F1 to achieve a target pH of 6.5 after 10 diavolumes (bottom panel). Conditions for Curves A through H are described in the text.

The performance of the different DF processes for mAb 3 are compared in Table 6.3, which shows the predicted concentrations of chloride, acetate, and histidine at the end of the DF. The process using diafiltration into DI water at pH 7 (Case A) still has significant concentrations of residual acetate and chloride after 10 diavolumes because of the very slow removal of these species due to Donnan partitioning; the positive charge on mAb3 is balanced by the Cl^- and $C_2H_3OO^-$ to maintain electroneutrality. The use of a histidine buffer throughout the DF (Case D) resulted in an even greater final Cl^- concentration due to the positive charge on the histidine. The histidine buffer was very rapidly removed when the diafiltration was performed using DI water for the final 5 diavolumes (Cases B and C) since the positively-charged histidine is effectively "pushed" into the permeate due to the Donnan effect. Thus, the DF performed with 15 mM histidine and 17 mM NaCl as the diafiltration solution for the first 5 diavolumes (Case B) provides a final product with significantly lower acetate concentration than that obtained when using DI water throughout the diafiltration. In this case, the presence of the NaCl during the first 5 diavolumes reduces the Donnan effect and enhances the removal of acetate. This type of mixed diafiltration, using two different diafiltration solutions during the DF process, not only provides the target pH in an essentially bufferless formulation, it also does so under conditions where the pH gradient at the end of the process is close to zero, leading to a highly robust process with respect to small variations in the extent of diafiltration.

Table 6.3: Concentration of different ionic species at the end of 10 diavolume diafiltrations process to achieve a target pH of 6 for cases A, B, C and D (from Figure 6.10).

Case	Chloride Concentration	Acetate Concentration	Histidine Concentration
A	3.5 mM	0.6 mM	--
B	4.1 mM	0.04 mM	<0.01 mM
C	3.8 mM	0.3 mM	<0.01 mM
D	6.3 mM	0.03 mM	3.9 mM

The bottom panel of Figure 6.10 shows a corresponding set of simulations for F1 (initially in a 20 mM Tris buffer with 120 mM Na_2SO_4 and 10 mM NaCl at a concentration of 50 g/L and pH 6.69) with the final formulation having a target pH of 6.5 after 10 diavolumes. Again, it was not possible to achieve a pH of 6.5 using a bufferless formulation with a starting pH of 6.7. Four different options were considered by either altering the feed or buffer conditions. In all four options, the DF yielded final concentrations of Na^+ = 3.4 ± 0.1 mM and Tris = 0.15 ± 0.07 mM with negligible amounts of the negatively-charged phosphate, acetate, and sulfate (<0.01 mM) due to the strong ion partitioning associated with the negatively-charged fusion protein. The simulations for options F, G, and H show minimal changes in pH over the last few diavolumes, leading to robust diafiltration processes.

6.4 Conclusions

The growing interest in the use of "self-buffered" or nearly bufferless formulations for monoclonal antibody products has created significant challenges due to the very large shifts in pH that can occur during the diafiltration process. This was demonstrated experimentally for both a monoclonal antibody and a fusion protein during diafiltration into water. Note that the resulting drug substance would likely need to be adjusted to achieve an appropriate drug product formulation. For example, the work by Usach et al.[59] suggests that isotonic solutions can result in less injection pain, which could be achieved by addition of a non-ionic species like polysorbate or sorbitol to the protein solution after the diafiltration.

In order to properly describe these pH variations, it is necessary to account for the change in antibody charge with both pH and ionic strength during the DF. In this Chapter, a charge regulation model has been developed to evaluate the protein charge directly from the amino acid sequence, allowing *a priori* evaluation of the protein charge and in turn the pH, buffer composition, and excipient concentrations throughout the diafiltration process based on the numerical integration of the mass balance equations. Model predictions were shown to be in very good agreement with experimental data for the diafiltration of a monoclonal antibody and a fusion protein with very different isoelectric points and formulation conditions. The initial decrease in pH seen when using a positively-charged mAb was directly due to the reduction in mAb charge caused by the rapid reduction in ionic strength at the beginning of the DF, an effect that cannot be predicted by any of the previously published DF models. In addition, model simulations demonstrated that incredibly large numbers of diavolumes are required to achieve steady-state conditions during the diafiltration, with the pH after 1000 diavolumes still varying slowly during

the DF process due to very slow removal of acetate and chloride ions because of Donnan partitioning across the semipermeable membrane.

The diafiltration model also provides a tool for the design and optimization of the diafiltration process to achieve specific formulation pH after a targeted number of diavolumes. In particular, the addition of a small amount of NaCl to the bufferless diafiltration solution causes a large reduction in the pH profile during the DF process as the positive charge on the mAb is balanced by the negatively-charged chloride ions instead of the OH^- in the salt-free solution. Model simulations were used to identify a variety of diafiltration strategies to achieve the target pH when using a bufferless or low-buffered diafiltration solution, including pre-adjustment of the feed pH or the addition of small amounts of buffer or NaCl to the diafiltration solution. Mixed diafiltration processes, using weakly buffered salt solutions for the first several diavolumes followed by DI water for the remaining diavolumes, could not only achieve the desired pH in a nearly bufferless formulation, it also yielded highly robust DF processes. This new diafiltration model, accounting for the effects of charge regulation on the protein charge, provides a framework for designing highly effective diafiltration processes using both buffered or bufferless diafiltration solutions based solely on the amino acid sequence of the protein. The final design for such processes would ultimately be determined based on a variety of practical and economic constraints on the DF process.

Chapter 7 pH and Excipient shifts during Batch Ultrafiltration and SPTFF

pH shifts and excipient partitioning occur in all membrane processes involving electrically charged proteins due to the Donnan effect. A number of previous studies have reported pH shifts during batch ultrafiltration, although available models for describing the magnitude of these pH shifts have significant limitations. In addition, there have been no previously published studies examining the pH shifts during SPTFF. The objective of the work described in this Chapter was to extend the analysis presented previously in Chapters 4 and 6 to describe the pH shifts that occur in both batch ultrafiltration, where the pH changes as a function of time, and SPTFF, in which the pH shift occurs along the length of the module and depends on the conversion (ratio of cumulative permeate flow rate compared to the inlet feed flow rate). The model involves solution of the Nernst-Planck equations accounting for convection, diffusion, and electromigration of charged species across the semipermeable membrane. Model calculations for batch UF are in good agreement with experimental results; additional experimental data will be required for validation of the SPTFF model as well as its application to the analysis of pH shifts during countercurrent staged diafiltration processes. The model provides important insights into the factors controlling the pH shift and excipient partitioning during both UF and SPTFF as well as a framework that can be used to guide future experimental studies of these phenomena.

7.1 Introduction

pH shifts and excipient partitioning have been well studied experimentally and theoretically during batch UF, with the goal of predicting the final pH and buffer composition as a function of time as the charged protein is concentrated. For example, Bolton et al.[13] developed a model for the pH shift and excipient partitioning during protein ultrafiltration incorporating Donnan equilibrium. However, the model ignores the effects of buffer non-idealities, and more significantly it assumes that the electrochemical potentials of the ionic species in the retentate are equal to those in the entire pool of permeate even though the permeate in a batch ultrafiltration process is typically taken directly to waste or collected in a physically distinct holding tank. Ladwig et al.[66] used a different approach based on the solution of the Poisson-Boltzmann equation accounting for electrostatic interactions between charged ions and the charged protein, with only the ions in the region outside of the electrical double layer assumed to be exchangeable between the retentate and permeate. No independent validation of this assumption was provided. Hebbi et al.[67] developed a model for batch UF based on solution of the Nernst-Planck transport equations, but the final pH at the end of the UF was evaluated using a "state-time model, rather than a mechanistic model." No evidence was provided to support the use of this largely heuristic expression for the final pH.

In contrast to batch UF, in which the mAb concentration, pH, and excipient / buffer concentration vary with time, these parameters all vary along the length of the module during SPTFF. This has significant implications for the development of a mathematical model to describe this length dependence since the composition of the permeate solution at the end of the SPTFF channel will be influenced by the extent of ion / buffer transport that occurs near the channel inlet. If the permeate flow channel within the SPTFF module is assumed to be well-mixed, then the

driving force for mass transfer at any point in the SPTFF device will be a function of the rate of mass transfer at all other positions. This is in sharp contrast to the behavior in batch UF where the permeate that is collected near the start of the protein concentration is removed from the system and should thus have no effect on ion / buffer transport at later times during the UF process (even if this phenomenon has been ignored in many previous models of batch UF).

The work presented in this Chapter describes a new model for the pH and excipient concentrations as a function of time during batch UF, specifically accounting for the removal of the collected permeate, and along the length of an SPTFF module, specifically accounting for the variation in ion / solute transport with axial position. The local filtrate flux is described using the concentration polarization model developed in Chapter 4, with the local solute (ion) flux evaluated by solution of the Nernst-Planck equations including contributions from convection, diffusion, and electromigration. Different mixing models were used for the permeate flow channel in SPTFF to explore the effects of mixing on the driving force for solute transport. The model enables *a priori* prediction of the pH shifts and excipient concentrations during both UF and SPTFF processes, and it also provides a framework for the analysis of these phenomena in countercurrent staged diafiltration processes incorporating SPTFF modules with high single-pass conversion.

7.2 Model Development

7.2.1. Batch ultrafiltration

The change in mAb and solute (ion) concentration with time during a batch ultrafiltration process is described by a simple overall and species mass balances:

$$\frac{dV}{dt} = -q_p \tag{7.1}$$

$$\frac{dC_pV}{dt} = 0 \tag{7.2}$$

$$\frac{dC_iV}{dt} = -N_iA \tag{7.3}$$

Equation (7.2) is valid for a fully-retentive membrane where C_p is the protein concentration at time t. The solute flux (N_i) is evaluated using the Nernst Planck equation[68]:

$$N_i = J_vC_i - D_i\left(\frac{dC_i}{dx}\right) - z_iC_i\left(\frac{D_iF}{RT}\right)\frac{d\Phi}{dx} \tag{7.4}$$

where the solute flux is given by the sum of the convective, diffusive and electrophoretic transport. z_i is the valence of ionic species i, F is Faraday's constant, D_i is the species diffusivity, and Φ is the electrostatic potential.

Equation (7.4) is integrated over the membrane thickness (L_m) assuming that N_i, J_v, and dΦ/dx are all constants (independent of position x) giving,

$$\ln\left[\frac{N_i - J_vC_{i,R} + z_iC_{i,R}\left(\frac{D_iF}{RT}\right)\frac{d\Phi}{dx}}{N_i - J_vC_{i,P} + z_iC_{i,P}\left(\frac{D_iF}{RT}\right)\frac{d\Phi}{dx}}\right] = -\frac{L_m}{D_i}\left[J_v - \left(\frac{z_iD_iF}{RT}\right)\right] \tag{7.5}$$

where $C_{i,R}$ and $C_{i,P}$ are the ion concentrations in the retentate and permeate solutions, respectively. Equation (7.5) is rearranged to calculate the solute flux (N_i):

$$N_i = \left[J_v - z_i\left(\frac{D_iF}{RT}\right)\frac{d\Phi}{dx}\right]\left[\frac{C_{i,R} - C_{i,P}\,e^{\beta}}{1 - e^{\beta}}\right] \tag{7.6}$$

where the parameter β is given as:

$$\beta = -\left(\frac{L_m}{D_i}\right)\left[J_v - z_i\left(\frac{D_iF}{RT}\right)\frac{d\Phi}{dx}\right] \tag{7.7}$$

Equation (7.6) is the integrated form of the Nernst-Plank equation.

Note that for a really thin membrane, the derivative terms in Equation (7.4) will dominate so that:

$$D_i\left(\frac{dC_i}{dx}\right) + z_i C_i\left(\frac{D_i F}{RT}\right)\frac{d\Phi}{dx} \approx 0 \qquad (7.8)$$

Under these conditions, a relationship between the ion concentrations in the retentate and permeate solutions can be obtained by integrating Equation (7.8) across the membrane giving:

$$\ln\left(\frac{C_{i,R}}{C_{i,P}}\right)^{\frac{1}{z_i}} = \frac{F\Delta\Phi}{RT} \qquad (7.9)$$

Since the electric potential difference ($\Delta\Phi$) is the same for all species, Equation (7.9) is equivalent to the Donnan equilibrium expression used in Chapter 6 to describe ion partitioning in diafiltration processes:

$$\left(\frac{C_{i,R}}{C_{i,P}}\right)^{\frac{1}{z_i}} = X \qquad (7.10)$$

Equation (7.10) assumes local equilibrium across the membrane, which may not be valid during UF and SPTFF.

The filtrate flux in Equation (7.4) was evaluated as a function of the protein concentration using the concentration polarization model given by Equation (4.8) assuming that the flux is in the mass transfer-limited regime. Equations (7.6) and (7.7) are both expressed in terms of the (unknown) gradient in the electrical potential across the membrane, $d\Phi/dx$. The potential gradient was thus evaluated by imposing the constraint of no net current flow through the membrane as given by Equation (7.11)

$$\sum_i z_i N_i = 0 \qquad (7.11)$$

along with the condition that both the retentate and permeate solutions are electrically neutral, i.e.,

$$\sum_i z_i C_i + Z_{mAb}\left(\frac{C_{mAb}}{MW_{mAb}}\right) - [OH^-] + [H^+] = 0 \qquad (7.12)$$

where Z_{mAb}, C_{mAb}, and MW_{mAb} are the mAb charge, mass concentration (in g/L), and molecular weight, respectively. The mAb concentration in the permeate solution is equal to zero since the membrane is assumed to be fully retentive to the mAb.

Equations (7.1), (7.2), (7.3), (7.6), (7.7), (7.11) and (7.12) were solved as follows. First, the solute flux (N_i) and the electric potential gradient ($d\Phi/dx$) for each species were evaluated from the known concentrations at time t (beginning at t = 0) using Equations (7.6), (7.7), (7.11) and (7.12). Then Equations (7.1) to (7.3) were used to evaluate the feed volume, the mAb concentration, and the species concentrations at $t+\Delta t$ using a simple Euler integration All calculations were performed using Wolfram Mathematica. The Euler integration method allows for the local calculation of each of the parameters inside a Do loop function.

7.2.2 SPTFF model

The change of local flow rate and species concentration along the length of the membrane was described using differential material balances described by Equations (7.13) to (7.16) for both the retentate and permeate streams:

$$\frac{dq_R}{dz} = -2wJ_v \qquad (7.13)$$

$$\frac{dq_p}{dz} = 2wJ_v \qquad (7.14)$$

$$\frac{dq_R C_{i,R}}{dz} = -2wN_i \qquad (7.15)$$

$$\frac{dq_P C_{i,P}}{dz} = 2wN_i \qquad (7.16)$$

where q_r and q_p are the local retentate and permeate flow rates and w is the channel width. The solute flux (N_i) was evaluated using Equations (7.6) and (7.7) at each point in the module, with the local filtrate flux (J_v) evaluated using the model presented in Chapter 4:

$$\frac{1}{J_v} = \frac{1}{J_{lim}} + \frac{1}{J_{mem}} \tag{7.17}$$

$$J_{lim} = k_0 \left(\frac{\eta_b}{\eta_0}\right)^{\frac{1}{3}} \int_{C_b}^{C_w} \left(\frac{M_p}{RT}\right) \left(\frac{\eta_0}{\eta}\right) \left(\frac{d\Pi}{dC}\right) \frac{dC}{C} \tag{7.18}$$

$$J_{mem,} = \frac{L_p}{\eta_0} \left(\Delta P_{TM} - \Delta\Pi\right) \tag{7.19}$$

Equations (7.13) to (7.16) are readily modified to account for systems with multiple flow channels in parallel by replacing w with $N_c w$ where N_c is the number of cassettes in each region of the module.

The above equations were solved simultaneously along with the constraints of no net current flow (Equation 7.11) and electroneutrality (Equation 7.12). The pH at each point in the module was evaluated using the Henderson-Hasselbalch equation for the different buffers:

$$pH = pK_a + \log_{10}\left(\frac{[Base]}{[Acid]}\right) \tag{7.20}$$

The net protein charge was evaluated from the local pH and ionic strength using the charge regulation model developed in Chapter 6.

7.3 Results and Discussion

7.3.1 pH shifts during batch ultrafiltration

Typical experimental data for the pH as a function of mAb concentration during a batch ultrafiltration are shown in Figure 7.1. The data were obtained with mAb1 in a 5 mM acetate buffer at an initial mAb concentration of 22 g/L. The pH increased from 5.23 to more than 5.6 as the mAb was concentrated from 22 to 180 g/L. This increase in pH is due to the preferential transport of positively-charged H^+ ions across the membrane due to electromigration driven by the presence of the positively-charged mAb in the retentate solution.

The solid curve in Figure 7.1 shows the predicted pH profile given by solution of the governing mass balances with the ion flux evaluated using the integrated Nernst-Planck equation and the mAb charge evaluated as a function of pH and ionic strength using the charge regulation model described in Chapter 6. The model is in very good agreement with the experimental data, properly capturing the nearly 2.5-fold reduction in the H^+ concentration. The model predicts that the acetate concentration will increase from 5.0 to 5.66 mM while the chloride concentration increases from 5 to 22 mM over the course of the ultrafiltration, with the increase in $C_2H_3O_2^-$ and Cl^- counterbalancing the positively charged mAb to maintain electroneutrality in the retentate solution. The smaller increase in the acetate concentration arises because only a fraction of the total acetate is present in the ionized (negatively-charged) form while all of the Cl^- is charged.

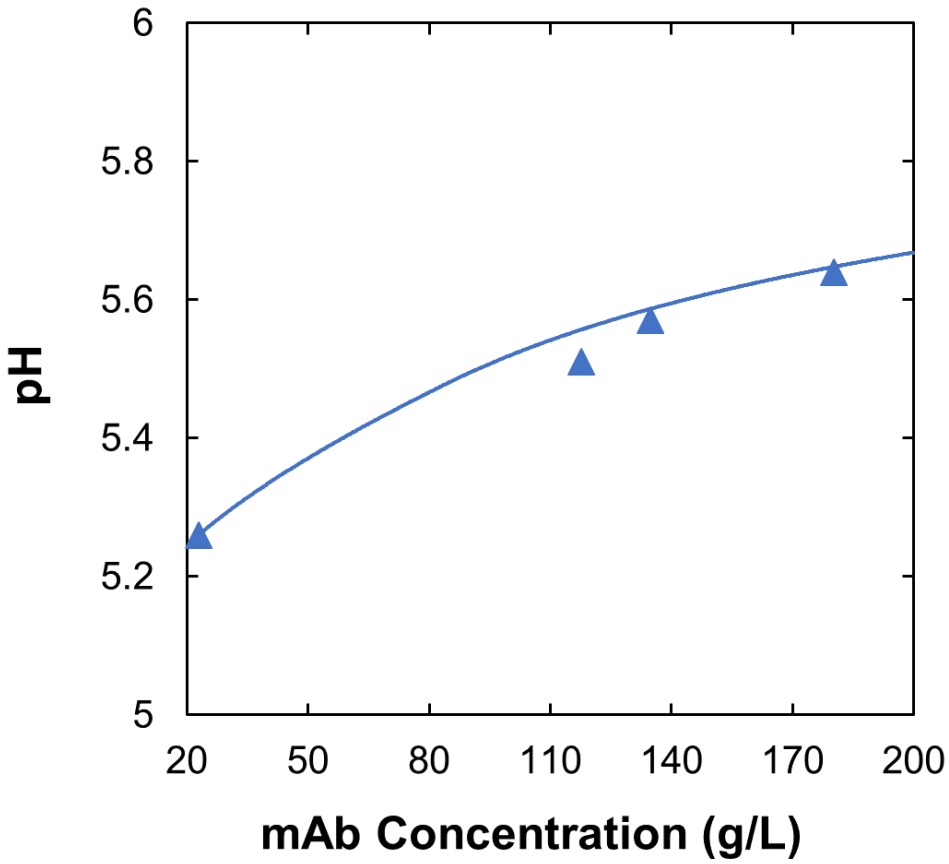

Figure 7.1: pH as a function of mAb concentration during batch ultrafiltration beginning with a 22 g/L solution of mAb1 in 5 mM Acetate buffer and 5 mM NaCl. Solid curve is model calculation.

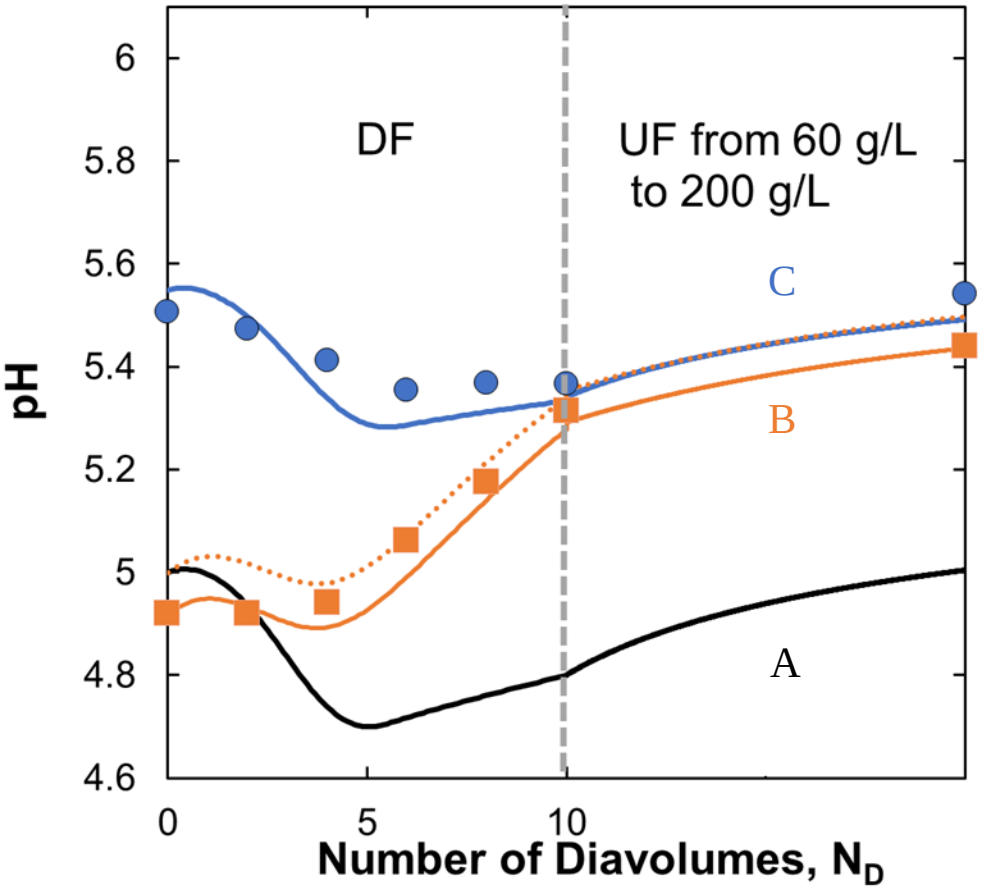

Figure 7.2: Diafiltration and ultrafiltration processes to achieve a mAb3 formulation at a final concentration of 200 g/L at pH 5.5

Figure 7.2 shows results from two experimental runs for a sequential diafiltration / ultrafiltration process designed to achieve a final formulation of 200 g/L at pH 5.5 after 10 diavolumes starting with a 60 g/L solution of mAb3 in a 20 mM acetate, 200 mM sodium sulfate buffer and chloride as the antibody's counterion. In both cases the diafiltration was performed using DI water as the diafiltration buffer for 10 diavolumes, with the ultrafiltration then used to increase the concentration to 200 g/L. The solid curves are the model calculations for 3 conditions as summarized in Table 7.1. Case A uses DI water at pH 7 for the DF buffer. Case B uses 5 mM

histidine at pH of 5.34 as the DF buffer. Case C uses DI water at pH 7 for the diafiltration but with the initial pH of the mAb increased to 5.55. The model results are in very good agreement with the experimental data for both Cases B and C – no data were provided for Case A. Table 7.1 summarizes the final sulfate, chloride, and histidine concentrations at the end of the diafiltration / ultrafiltration process. The sulfate concentration was lowest for Case C with a final concentration of 13.5 mM compared to 19.2 mM in Case B and 20 mM in Case A.

Table 7.1: Starting and final ultrafiltration conditions for cases in Figure 7.2

Case	Starting pH	Buffer pH	Buffer Histidine Concentration	Sulfate Concentration after UF	Chloride Concentration after UF	Histidine Concentration after UF
A	5	7	0	20.0 mM	0.014 mM	--
B	5	5.34	5 mM	19.2 mM	3.3 mM	0.05 mM
C	5.55	7	0	13.5 mM	<0.01 mM	--

7.3.2 Mixing behavior

Additional validation of the model equations was obtained by evaluating the pH after simple dilution of a Phosphate Buffer with a 20 mM Histidine buffer at pH 7. The total phosphate and histidine concentration after dilution was evaluated as:

$$C_{i,M} = \frac{1}{D_f} C_{i,F} + \left(1 - \frac{1}{D_f}\right) C_{i,DF} \tag{7.21}$$

where $C_{i,M}$, $C_{i,F}$ and $C_{i,DF}$ are the total phosphate / histidine concentrations of the mixture, initial feed solution, and dilution (diafiltration) buffer, respectively, and D_f is the dilution factor, equal to the ratio of the volume of dilution fluid to the volume of the feed.

The pH after dilution is shown as a function of the dilution factor in Figure 7.2. In both cases, the pH initially increases with increasing dilution factor due to increase in the pK_a value of the phosphate buffer at low ionic strength[63]:

$$pK_{phos} = 7.2 - \frac{1.8\sqrt{I}}{1+\sqrt{I}} \qquad (7.22)$$

where Equation (7.22) accounts for the ionic strength dependence of the phosphate activity coefficient as given by a modified form of Debye-Huckel theory. The pH increase is much more pronounced for the 100 mM phosphate solution due to the much greater change in the ionic strength, and thus the pK_a value. The pH decreases at very high dilutions due to the buffering provided by the histidine having a pK_a value of 6.0.

The solid curves in Figure 7.3 are the model calculations, which again involve no adjustable parameters. In this case, there is no solute or filtrate flux since there is no membrane in the dilution process. Instead, the final volume and the total concentration of phosphate and histidine are evaluated based on the dilution factor. The pH is then determined by iterative solution of Equations (7.20) and (7.21) while accounting for the buffer non-idealities. The model is in very good agreement with the experimental data, properly capturing both the increase in pH at small dilution factors and the decrease in pH at high dilution factors as well as the shift in the location of the maximum to higher dilution factors for the 100 mM phosphate buffer compared to the 20 mM phosphate.

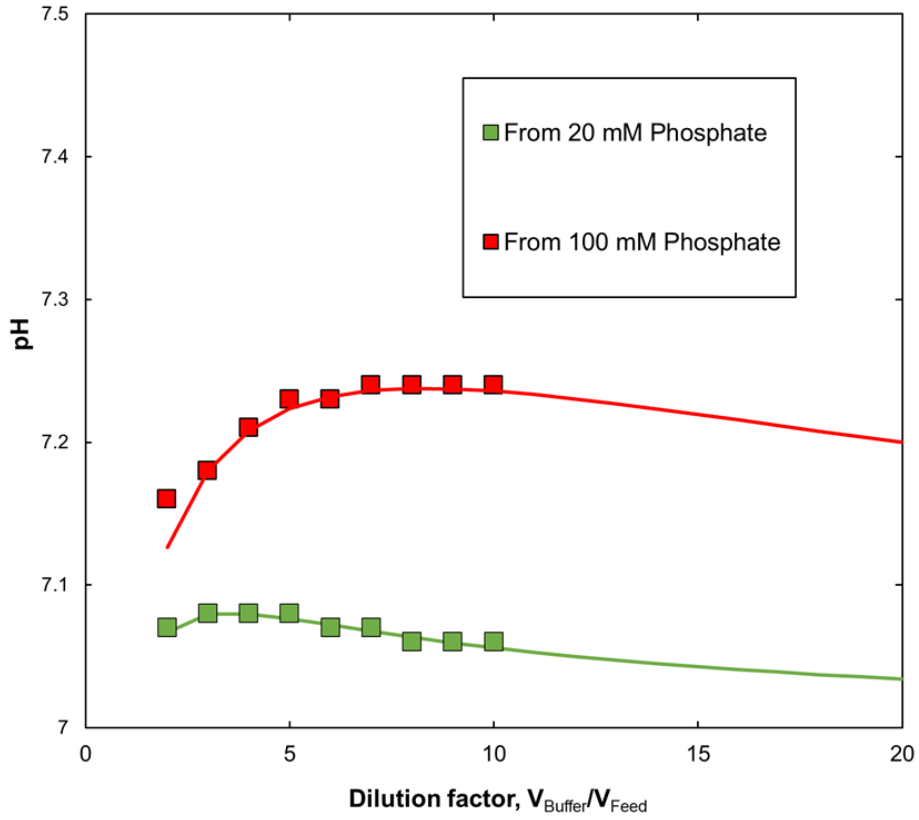

Figure 7.3: pH as a function of dilution factor for a 20 or 100 mM phosphate buffer diluted with 20 mM Histidine buffer at pH 7. Solid curves are model calculations.

.

7.3.3 pH shifts in SPTFF

Typical model simulations for the pH as a function of position in the SPTFF module in both the retentate and permeate solutions are shown in Figure 7.4. The simulations were performed for the Pall Cadence SPTFF module during ultrafiltration of a 12 g/L solution of mAb3 (discussed in Chapter 6) in a 5 mM acetate buffer. The feed flow rate was 150 mL/min, and the module is predicted to provide a 5-fold increase in the mAb concentration. The pH in the retentate solution increases with increasing axial position, similar to the increase in pH seen during batch

ultrafiltration in Figure 7.1. As discussed previously, this is due primarily to the preferential transport of H^+ ions into the permeate and away from the positively-charged mAb. In contrast to the behavior in a typical batch ultrafiltration module, which has relatively low conversion in a single pass (<10%), the pH in the permeate solution decreases fairly sharply in the first half of the module with a somewhat more gradual decrease in pH seen in the region closer to the module exit. The reduction in permeate pH arises from the enhanced H^+ transport, with relatedly little acetate transported into the permeate due to preferential partitioning of the acetate in the retentate solution because of the attractive electrostatic interactions with positively-charged mAb. The lower gradient in permeate pH near the module exit reflects the back diffusive transport associated with the H^+ gradient between the permeate and retentate solutions.

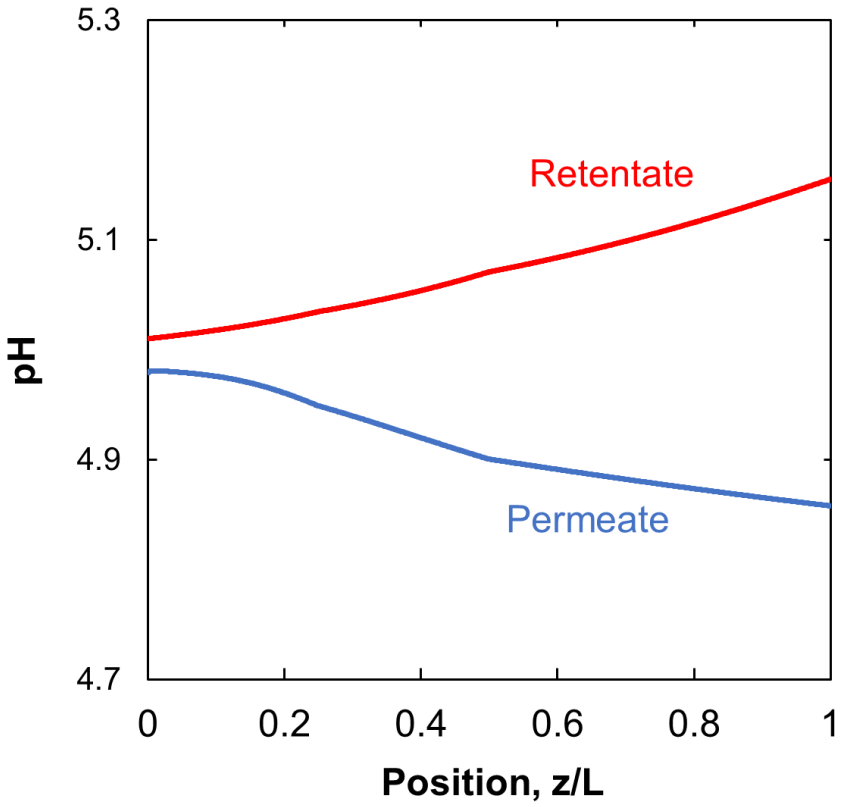

Figure 7.4: pH as a function of position in Pall SPTFF module for mAb starting at 12 g/L in 5 mM Acetate

Figure 7.5 shows a direct comparison of the predicted pH profiles in a batch ultrafiltration and SPTFF module as a function of the local mAb concentration, which is a function of time in batch UF and a function of pH in SPTFF. The simulations were performed for a 5 g/L solution of mAb3 initially in a 5 mM acetate buffer with 5 mM NaCl at pH 5. In both cases, the pH increases to more than 5.1 due to the preferential transport of H^+ into the permeate. The pH profiles in the batch UF and SPTFF systems are very similar, with the final pH differing by less than 0.02 pH units.

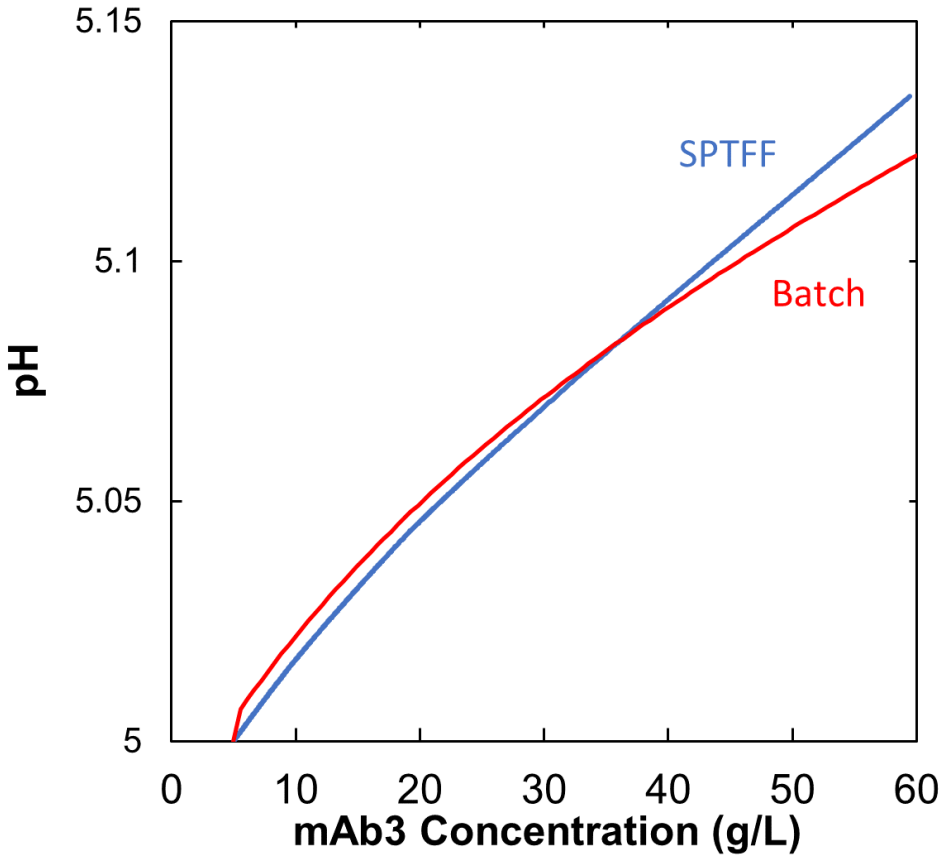

Figure 7.5: Simulations for pH in batch UF and SPTFF for a 5 g/L mAb feed in 5 mM acetate buffer with 5 mM NaCl at pH 5.

In contrast to models that assume equilibrium between the retentate and permeate solutions, the UF / SPTFF model developed in this Chapter explicitly accounts for the solute flux across the membrane using the Nernst-Planck equation, which is an explicit function of the membrane thickness. Figure 7.6 shows the predicted variation of the solute flux on the filtrate flux for different values of the membrane thickness for a mAb at the same feed conditions as in Figure 7.4. When the membrane thickness is 100 μm, (top panel), the solute flux is dominated by convection for J_v > 10 μm/s and thus increases nearly linearly with increasing filtrate flux under these conditions. In contrast, the solute flux through a membrane that is 1 μm thick is dominated by diffusion, with the magnitude of the solute flux being nearly independent of the filtrate flux even up to J_v = 100 μm/s. The total acetate flux is significantly lower than the chloride flux, even though the acetate and chloride concentrations are both 5 mM, since acetate has a smaller diffusion coefficient and has less electrophoretic flux since only a fraction of the acetate is negatively-charged.

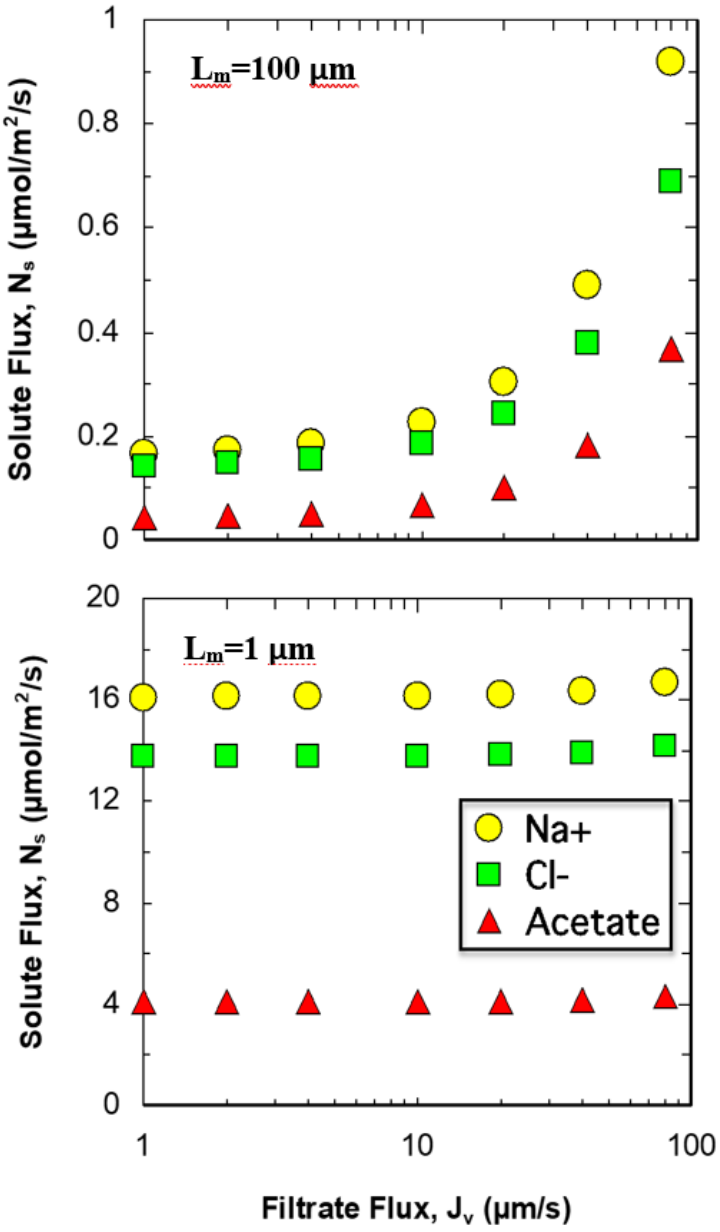

Figure 7.6: Solute flux for Sodium, Chloride and Acetate as a function of the filtrate flux for membranes that are 100 µm (top panel) or 1 µm (bottom panel) thick

The effect of charge regulation on the pH profile during an SPTFF process used to concentrate a 5 g/L solution of mAb3 in 5 mM Acetate and 5 mM NaCl is examined in Figure 7.7.

The blue curve represents the model predictions using the charge regulation model from Chapter 6 to evaluate the mAb charge as a function of pH and ionic strength. The red and green curves represent the simulations for a mAb with constant charge of Z_{mAb} = 26 and 10 electron charges, respectively. The mAb3 charge decreases from Z_{mAb} = 26 at 5 g/L to 23 at 60 g/L due primarily to the increase in pH in the SPTFF module. This reduction in mAb charge leads to a smaller increase in pH during SPTFF. In contrast, the pH shift for the simulation with Z_{mAb} = 10 shows a smaller pH shift due to the more equal partitioning of the charged ions between the retentate and permeate solutions under these conditions.

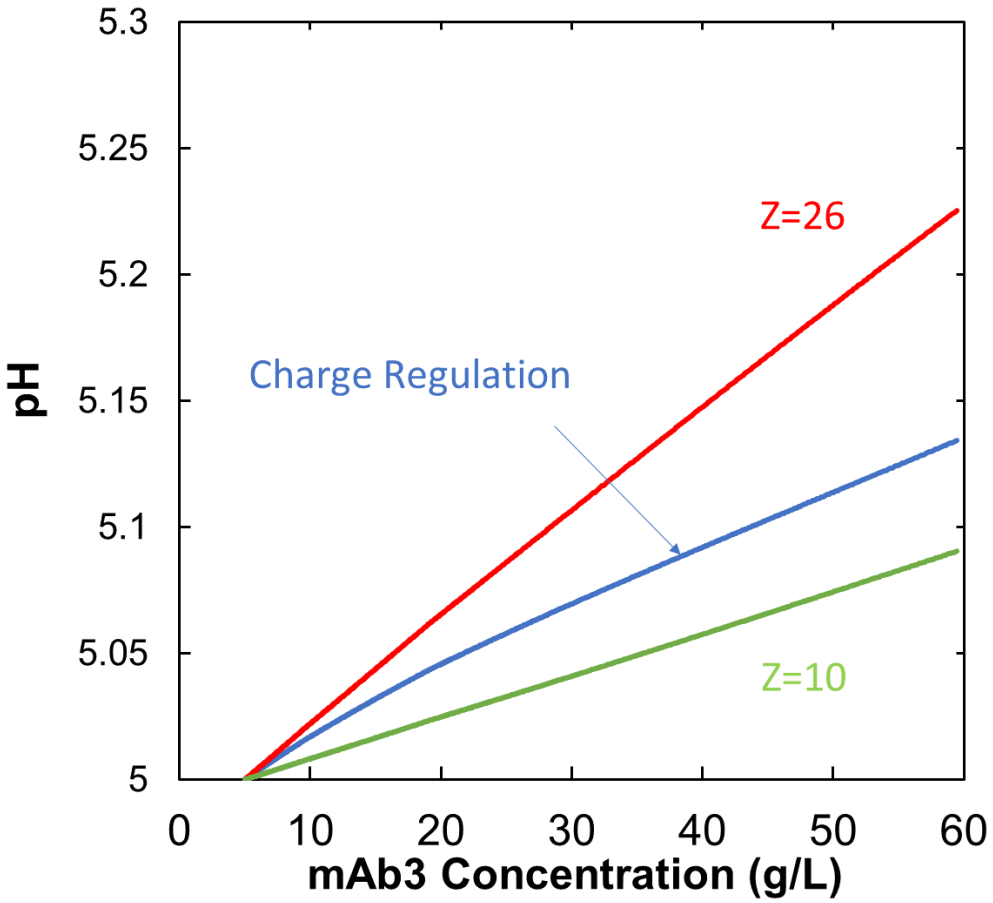

Figure 7.7: pH shifts during SPTFF of a 5 g/L solution on mAb3 in 5 mM acetate buffer and 5 mM NaCl for the charge regulation model and at different constant mAb charges.

7.4 Conclusions

Although pH and excipient shifts during ultrafiltration are less pronounced than those during diafiltration (in which the properties of the diafiltration buffer drive the change in pH), a proper understanding of the UF behavior is needed to obtain accurate predictions of the pH and excipient concentration at the end of either batch UFDF or SPTFF processes. In this Chapter, a new mathematical model was developed for the pH and ion concentrations in both UF and SPTFF,

with the solute flux across the membrane evaluated using the Nernst-Planck equation to account for the convective, diffusive, and electrophoretic contributions to ion / solute transport.

Model predictions were in very good agreement with experimental data obtained in batch ultrafiltration of a monoclonal antibody product as well as in a combined diafiltration-ultrafiltration process used for final formulation of the antibody. In addition, the same model framework was used to describe the pH change after buffer mixing, accurately describing the change in pH for mixing phosphate and histidine buffers with different dilution ratios. This model was then extended to evaluate the pH profiles in both the retentate and permeate solutions along the length of an SPTFF module. The magnitude of the pH shift in SPTFF was very similar to that in a batch UF process when plotted as a function of the local mAb concentration, which varies with time in batch UF and with position in SPTFF. This model was then used to explore the effects of excipient concentration, filtrate flux, and membrane thickness on the solute flux, as well as the effect of charge regulation on the pH profile. Experimental studies will be required to validate the SPTFF model predictions, but this model should provide an effective framework to estimate the magnitude of pH shifts in SPTFF and to design SPTFF processes to achieve a final formulated antibody product at a target pH and excipient concentration, similar to the DF model examined previously in Chapter 6.

Chapter 8 Conclusions and Future work

8.1 Conclusions

The work presented in this thesis provides a detailed investigation of the phenomena governing the behavior of membrane systems for the concentration and formulation (buffer exchange) of monoclonal antibodies and other recombinant protein products. This includes experimental and theoretical studies of single pass tangential flow filtration (SPTFF) modules, opportunities for using hollow fiber dialyzers as a novel alternative for buffer exchange, the development of countercurrent staged SPTFF modules for continuous diafiltration, and the effects of charge regulation on the performance of diafiltration processes employing low-buffered or even bufferless formulations.

The results in Chapters 2 and 3 demonstrate the effectiveness of performing continuous buffer exchange using either a multi-stage countercurrent diafiltration process employing multiple SPTFF modules or countercurrent hollow fiber membrane dialyzers. Both systems were able to achieve more than 99.9% buffer exchange, corresponding to a 1000-fold removal of the penultimate buffer and any trace impurities (the target in most buffer exchange processes). Preliminary economic analysis of the countercurrent staged diafiltration showed that a 3-stage system typically provided the lowest overall cost accounting for the costs of both the modules and buffer requirements. The countercurrent hollow fiber dialyzers used less buffer than either the countercurrent or batch diafiltration systems, with the dialyzers costing only $20 for a module that can process nearly 1 kg of antibody per day. Both systems were able to run continuously for more than 24 hr at high protein concentrations, making them very attractive for use in continuous

bioprocessing both for inline adjustment of buffer conditions and for final product formulation. In particular, the countercurrent hollow fiber dialysis system showed no evidence of any membrane fouling over 5 days of continuous operation, which is likely due to the absence of any pressure-driven filtration.

Chapters 4 and 5 present a model for the filtrate flux and pressure drop in SPTFF modules that accounts for the change in flow rate and mAb concentration within the module as well as the effects of protein-protein interactions on concentration polarization through the concentration dependence of the mAb viscosity and osmotic pressure. The model was validated using experimental data for a highly purified monoclonal antibody provided by Biogen. All of the model parameters were evaluated from independent experimental measurements for the properties of the antibody and for the geometry and pressure losses within the SPTFF module. This model was then used to explore the design and optimization of SPTFF modules for specific performance criteria. Simulations demonstrated that the optimal channel width was around 2 cm due to the large loss of available filtering area for narrower channels associated with sealing the membranes in the cassette. Very long thin channel modules provided the greatest concentration factors (or conversions) but at the cost of a high feed-side pressure drop. This pressure drop could be reduced using multiple modules in a staged parallel configuration.

Chapter 6 presents a new model for the pH shifts and excipient partitioning during diafiltration of highly concentrated mAbs into a bufferless media specifically accounting for the change in mAb charge with solution pH and ionic strength using a charge regulation model. The model involves no adjustable parameters, with the mAb charge calculated based on the known amino acid composition accounting for the protonation / deprotonation of the acidic and basic amino acids. Model calculations were shown to be in excellent agreement with experimental data

for the solution pH as well as the acetate and chloride concentrations throughout the diafiltration of a highly purified monoclonal antibody and Fc fusion protein over a range of buffer conditions and product concentrations. The results demonstrated that very large numbers of diavolumes, in some cases in excess of 1000 diavolumes, are required to obtain the steady-state pH and buffer composition when using bufferless media due to the difficulty in removing counterions that are required to balance the protein charge, e.g., Cl^- ions during diafiltration of a positively-charged mAb. The model also provides a framework for the identification of the appropriate diafiltration conditions needed to achieve a final pH and buffer composition after a fixed number of diavolumes. Several novel diafiltration scenarios were identified in which the diafiltration buffer was changed mid-way through the process, enabling the desired final formulation to be achieved with much smaller pH excursions during the process.

The flux and pH / excipient partitioning models were then combined in Chapter 7 to study the pH shifts during batch ultrafiltration and SPTFF, with the ion flux across the membrane evaluated using the integrated form of the Nernst-Planck equation. In this case, the increase in concentration of the positively-charged mAb (with either time or position) causes a change in pH based on the need to maintain electroneutrality in the retentate solution. The SPTFF model provides a framework for evaluating the variation in pH and excipient concentration with position, including the changes in mAb concentration and charge along the length of the module.

In total, the experimental results and mathematical models developed in this dissertation provide important insights and valuable tools for the implementation of membrane processes for concentration and buffer exchange / desalting in the development of both batch and continuous downstream processes. Several biopharmaceutical companies have already begun using these results in their process development programs. For example, Eli Lilly has implemented the batch

diafiltration model presented in Chapter 6 to estimate the anticipated pH shifts in their mAb formulation processes, and they have used this model to identify appropriate diafiltration buffer conditions needed to achieve the targeted formulation. Lilly's process development group has also constructed a 3-stage countercurrent diafiltration system based on the work presented in Chapter 2 of this thesis, with the modeling results from Chapter 7 used to estimate the pH of the formulated product. The National Institute for Innovation in Manufacturing of Biopharmaceuticals (NIIMBL) recently presented a framework for Integrated Continuous Biomanufacturing (ICB), written by authors from Astrazeneca, Merck, Just Biotherapeutics, Eli Lilly, Janssen, and Novartis, that specifically includes countercurrent staged diafiltration as a key unit operation for buffer exchange[69], while a companion article by the same authors highlighted the potential advantages of using hollow fiber dialyzers for final formulation[70].

8.2 Future Work

Although the 3-staged countercurrent diafiltration system was successfully operated for 24 hours at an IgG concentration of 140 g/L, current mAb products are commonly formulated at mAb concentrations of 200 g/L or higher. It would be very worthwhile to perform experimental studies at these high concentrations using a purified monoclonal antibody (instead of the polyclonal IgG), although this would require very significant quantities of mAb. Note that the use of higher feed concentrations will also result in lower buffer usage per unit mass of formulated mAb, which would reduce the overall cost of the formulation step. These experiments would likely need to use PID controllers with accurate measurement of the feed and retentate flow rates to ensure constant volume diafiltration; the data presented in Chapter 2 showed a small dilution effect due to the

difficulty in obtained the desired high conversion throughout the diafiltration process. It would be very desirable to perform similar experiments using the countercurrent hollow fiber dialysis system, with the side-by-side operation of these two systems using the same feed providing the basis for a more rigorous comparison of the economics and performance of these alternative platforms.

Although the results in Chapters 4 and 5 showed very good agreement between the flux model and experimental data in both the Pellicon® 3 and Pall Cadence® SPTFF modules, the results were limited to a single monoclonal antibody product. Future work in this area should examine the behavior of other antibodies or recombinant proteins with different physical properties, e.g., osmotic pressure and solution viscosity. It would also be interesting to explore the use of excipients like arginine and hydantoin that are known to reduce the viscosity of antibody solutions[71]. This would not only provide additional insights into the effects of solution viscosity on the filtrate flux and conversion in SPTFF, it could also help identify new strategies for improving the performance of SPTFF modules for specific applications. It would also be interesting to design an SPTFF module that provided opportunities to directly measure the local filtrate flux along the length of the module, thereby providing more detailed validation of the model predictions than is possible based on data only for the overall filtrate flux / conversion.

Future experimental studies of pH shifts and excipient partitioning in SPTFF would enable the validation of the model equations presented in Chapter 7. Again, having an SPTFF module with permeate sampling along the channel length would enable much more rigorous validation of the model, including the development of a more accurate description of mixing in the permeate channel. These experimental studies should also be extended to the type of multistage countercurrent diafiltration processes discussed in Chapter 2 with the goal of determining whether

the pH shifts and excipient partitioning in the countercurrent staged diafiltration are greater than those encountered in batch diafiltration processes. It would also be helpful to extend the model framework to the analysis of the countercurrent dialysis process described in Chapter 3. Side-by-side experiments (batch DF, countercurrent staged DF, and countercurrent dialysis) could be used to highlight the relative advantages / differences between these platforms for buffer exchange and final formulation of monoclonal antibody products.

References

(1) Kelley, B. D. Bioprocessing of Therapeutic Proteins. *Curr. Opin. Biotechnol.* **2001**, *12* (2), 173–174. https://doi.org/10.1016/S0958-1669(00)00195-6.

(2) Ecker, D. M.; Jones, S. D.; Levine, H. L. The Therapeutic Monoclonal Antibody Market. *MAbs* **2015**, *7* (1), 9–14. https://doi.org/10.4161/19420862.2015.989042.

(3) Hernandez, I.; Bott, S. W.; Patel, A. S.; Wolf, C. G.; Hospodar, A. R.; Sampathkumar, S.; Shrank, W. H. Pricing of Monoclonal Antibody Therapies: Higher If Used for Cancer? *Am. J. Manag. Care* **2018**, *24* (2), 109–112.

(4) Roque, A. C. A.; Lowe, C. R.; Taipa, M. Â. Antibodies and Genetically Engineered Related Molecules: Production and Purification. *Biotechnol. Prog.* **2004**, *20* (3), 639–654. https://doi.org/10.1021/bp030070k.

(5) Sommerfeld, S.; Strube, J. Challenges in Biotechnology Production - Generic Processes and Process Optimization for Monoclonal Antibodies. *Chem. Eng. Process. Process Intensif.* **2005**, *44* (10), 1123–1137. https://doi.org/10.1016/j.cep.2005.03.006.

(6) Pollock, J.; Ho, S. V.; Farid, S. S. Fed-Batch and Perfusion Culture Processes: Economic, Environmental, and Operational Feasibility under Uncertainty. *Biotechnol. Bioeng.* **2013**, *110* (1), 206–219. https://doi.org/10.1002/bit.24608.

(7) Ayturk, E.; Forespring, C. Simplifying Bioprocessing with Single-Pass TFF Aiming for Robust, Flexible Bioprocesses with Solutions That Deliver Consistent Product Quality Benefits of Continuous Processing. *GEN Genet. Eng. Biotechnol. News* **2016**, *36* (4), 24–25.

(8) Zobel, S.; Helling, C.; Ditz, R.; Strube, J. Design and Operation of Continuous Countercurrent Chromatography in Biotechnological Production. *Ind. Eng. Chem. Res.* **2014**, *53* (22), 9169–9185. https://doi.org/10.1021/ie403103c.

(9) Zydney, A. L. Continuous Downstream Processing for High Value Biological Products: A Review. *Biotechnol. Bioeng.* **2016**, *113* (3), 465–475. https://doi.org/10.1002/bit.25695.

(10) Kurnik, R. T.; Yu, A. W.; Blank, G. S.; Burton, A. R.; Smith, D.; Athalye, A. M.; van Reis, R. Buffer Exchange Using Size Exclusion Chromatography, Countercurrent Dialysis, and Tangential Flow Filtration: Models, Development, and Industrial Application. *Biotechnol. Bioeng.* **1995**, *45* (2), 149–157. https://doi.org/10.1002/bit.260450209.

(11) Dizon-Maspat, J.; Bourret, J.; D'Agostini, A.; Li, F. Single Pass Tangential Flow Filtration to Debottleneck Downstream Processing for Therapeutic Antibody Production. *Biotechnol. Bioeng.* **2012**, *109* (4), 962–970. https://doi.org/10.1002/bit.24377.

(12) Abel, J.; Kosky, A.; Ball, N.; Bacon, H.; Kaushik, R.; Kleemann, G. R. A Small-Scale Process for Predicting Donnan and Volume Exclusion Effects During Ultrafiltration/Diafiltration Process Development. *J. Pharm. Sci.* **2018**, *107* (5), 1296–1303. https://doi.org/10.1016/j.xphs.2018.01.010.

(13) Bolton, G. R.; Boesch, A. W.; Basha, J.; LaCasse, D. P.; Kelley, B. D.; Acharya, H. Effect of Protein and Solution Properties on the Donnan Effect during the Ultrafiltration of Proteins. *Biotechnol. Prog.* **2011**, *27* (1), 140–152. https://doi.org/10.1002/btpr.523.

(14) Baek, Y.; Yang, D.; Singh, N.; Arunkumar, A.; Ghose, S.; Li, Z. J.; Zydney, A. L. pH Variations during Diafiltration Due to Buffer Nonidealities. *Biotechnol. Prog.* **2017**, *33* (6), 1555–1560. https://doi.org/10.1002/btpr.2544.

(15) Stoner, M. R.; Fischer, N.; Nixon, L.; Buckel, S.; Benke, M.; Austin, F.; Randolph, T. W.; Kendrick, B. S. Protein-Solute Interactions Affect the Outcome of Ultrafiltration/ Diafiltration Operations. *J. Pharm. Sci.* **2004**, *93* (9), 2332–2342. https://doi.org/10.1002/jps.20145.

(16) Baek, Y.; Singh, N.; Arunkumar, A.; Borwankar, A.; Zydney, A. L. Mass Balance Model with Donnan Equilibrium Accurately Describes Unusual pH and Excipient Profiles during Diafiltration of Monoclonal Antibodies. *Biotechnol. J.* **2019**, *14* (7). https://doi.org/10.1002/biot.201800517.

(17) Miao, F.; Velayudhan, A.; Dibella, E.; Shervin, J.; Felo, M.; Teeters, M.; Alred, P. Theoretical Analysis of Excipient Concentrations during the Final Ultrafiltration/Diafiltration Step of Therapeutic Antibody. *Biotechnol. Prog.* **2009**, *25* (4), 964–972. https://doi.org/10.1002/btpr.168.

(18) Teeters, M.; Bezila, D.; Benner, T.; Alfonso, P.; Alred, P. Predicting Diafiltration Solution Compositions for Final Ultrafiltration/Diafiltration Steps of Monoclonal Antibodies. *Biotechnol. Bioeng.* **2011**, *108* (6), 1338–1346. https://doi.org/10.1002/bit.23067.

(19) van Reis, R.; Zydney, A. Bioprocess Membrane Technology. *J. Memb. Sci.* **2007**, *297* (1–2), 16–50. https://doi.org/10.1016/j.memsci.2007.02.045.

(20) Rucker-Pezzini, J.; Arnold, L.; Hill-Byrne, K.; Sharp, T.; Avazhanskiy, M.; Forespring, C. Single Pass Diafiltration Integrated into a Fully Continuous MAb Purification Process. *Biotechnol. Bioeng.* **2018**, *15* (8), 1948–1957. https://doi.org/10.1002/bit.26708.

(21) Nambiar, A. M. K.; Li, Y.; Zydney, A. L. Countercurrent Staged Diafiltration for Formulation of High Value Proteins. *Biotechnol. Bioeng.* **2018**, *115* (1). https://doi.org/10.1002/bit.26441.

(22) Schwartz, L. Diafiltration: A Fast, Efficient Method for Desalting or Buffer Exchange of Biological Samples. *Pall Sci. Tech. Rep.* **2003**.

(23) Jaffrin, M. Hemodialysis (HD) Membranes. In *Encyclopedia of Membranes*; 2016. https://doi.org/10.1007/978-3-662-44324-8_1242.

(24) Ronco, C.; Clark, W. R. Haemodialysis Membranes. *Nat. Rev. Nephrol.* **2018**, *14*, 394–410. https://doi.org/10.1038/s41581-018-0002-x.

(25) Scarpioni, R.; Ricardi, M.; Albertazzi, V.; De Amicis, S.; Rastelli, F.; Zerbini, L. Dialysis-Related Amyloidosis: Challenges and Solutions. *Int. J. Nephrol. Renovasc. Dis.* **2016**, *9*, 319–328. https://doi.org/10.2147/IJNRD.S84784.

(26) Bowry, S. K. Dialysis Membranes Today. *Int. J. Artif. Organs* **2002**, *25* (5), 447–460.

https://doi.org/10.1177/039139880202500516.

(27) Michaels, A. S. Operating Parameters and Performance Criteria for Hemodialyzers and Other Membrane-Separation Devices. *Trans Am Soc Artif Intern Organs* **1966**, *12*, 387–392.

(28) Wickramasinghe, S. R.; Semmens, M. J.; Cussler, E. L. Mass Transfer in Various Hollow Fiber Geometries. *J. Memb. Sci.* **1992**, *69* (3), 235–250. https://doi.org/10.1016/0376-7388(92)80042-I.

(29) Chuang, F. R.; Lee, C. H.; Chang, H. W.; Lee, C. N.; Chen, T. C.; Chuang, C. H.; Chiou, T. T. Y.; Wu, C. H.; Yang, C. C.; Wang, I. K. A Quality and Cost-Benefit Analysis of Dialyzer Reuse in Hemodialysis Patients. *Ren. Fail.* **2008**, *30* (5), 521–526. https://doi.org/10.1080/08860220802064747.

(30) Kelley, B. Industrialization of MAb Production Technology: The Bioprocessing Industry at a Crossroads. *MAbs* **2009**, *1* (5), 443–452. https://doi.org/10.4161/mabs.1.5.9448.

(31) *Monoclonal Antibodies (MAbS) Global Market Report 2021: COVID 19 Impact And Recovery To 2030*; 2021.

(32) Van Reis, R.; Zydney, A. Membrane Separations in Biotechnology. *Curr. Opin. Biotechnol.* **2001**, *12* (2), 208–211. https://doi.org/10.1016/S0958-1669(00)00201-9.

(33) Dizon-Maspat, J.; Bourret, J.; D'Agostini, A.; Li, F. Single Pass Tangential Flow Filtration to Debottleneck Downstream Processing for Therapeutic Antibody Production. *Biotechnol. Bioeng.* **2012**, *109* (4), 962–970. https://doi.org/10.1002/bit.24377.

(34) Casey, C.; Gallos, T.; Alekseev, Y.; Ayturk, E.; Pearl, S. Protein Concentration with Single-Pass Tangential Flow Filtration (SPTFF). *J. Memb. Sci.* **2011**, *384* (1–2), 82–88. https://doi.org/10.1016/j.memsci.2011.09.004.

(35) Elich, T.; Goodrich, E.; Lutz, H.; Mehta, U. Investigating the Combination of Single-Pass Tangential Flow Filtration and Anion Exchange Chromatography for Intensified MAb Polishing. *Biotechnol. Prog.* **2019**, *35* (5), e2862. https://doi.org/10.1002/btpr.2862.

(36) de los Reyes, G.; Mir, L. Method and Apparatus for the Filtration of Biological Solutions. US7384549B2, 2008.

(37) C. Casey, E. A. Application Note Scalability of Cadence™ Inline Concentrator Modules for Bovine IgG Processing https://www.pall.com/content/dam/pall/biopharm/lit-library/non-gated/application-notes/14.9534_USD3004_Scalability_Cadence_ILC_Bovine_IgG_AN_EN.pdf.

(38) MilliporeSigma. Pellicon® Single-Pass Tangential Flow Filtration Versatile ultrafltration technology for biopharmaceutical processes requiring flexibility, capacity, and efficiency http://www.emdmillipore.com/Web-US-Site/en_CA/-/USD/ShowDocument-Pronet?id=201810.092.

(39) Huter, M.; Strube, J. Model-Based Optimization of SPTFF Ultrafiltration for Integration in Continuous Biopharmaceutical Processing. *Chemie Ing. Tech.* **2018**, *90* (9), 1251. https://doi.org/10.1002/cite.201855263.

(40) Huter, M. J.; Jensch, C.; Strube, J. Model Validation and Process Design of Continuous Single Pass Tangential Flow Filtration Focusing on Continuous Bioprocessing for High Protein Concentrations. *Processes* **2019**, *7* (11), 781. https://doi.org/10.3390/pr7110781.

(41) Binabaji, E.; Ma, J.; Rao, S.; Zydney, A. L. Theoretical Analysis of the Ultrafiltration Behavior of Highly Concentrated Protein Solutions. *J. Memb. Sci.* **2015**, *494*, 216–233. https://doi.org/10.1016/j.memsci.2015.07.068.

(42) Baek, Y.; Singh, N.; Arunkumar, A.; Borys, M.; Li, Z. J.; Zydney, A. L. Ultrafiltration Behavior of Monoclonal Antibodies and Fc-Fusion Proteins: Effects of Physical Properties. *Biotechnol. Bioeng.* **2017**, *114* (9), 2057–2065. https://doi.org/10.1002/bit.26326.

(43) Binabaji, E.; Rao, S.; Zydney, A. L. The Osmotic Pressure of Highly Concentrated Monoclonal Antibody Solutions: Effect of Solution Conditions. *Biotechnol. Bioeng.* **2014**, *111* (3), 529–536. https://doi.org/10.1002/bit.25104.

(44) Pal, R. Evaluation of the Mooney Viscosity/Concentration Equation for Liquid-Liquid Emulsions. *Chem. Eng. Commun.* **1990**, *89* (1), 209–214. https://doi.org/10.1080/00986449008940571.

(45) Vilker, V. L.; Colton, C. K.; Smith, K. A. The Osmotic Pressure of Concentrated Protein Solutions: Effect of Concentration and pH in Saline Solutions of Bovine Serum Albumin. *J. Colloid Interface Sci.* **1981**, *79* (2), 548–566. https://doi.org/10.1016/0021-9797(81)90106-5.

(46) Wu, J.; Prausnitz, J. M. Osmotic Pressures of Aqueous Bovine Serum Albumin Solutions at High Ionic Strength. *Fluid Phase Equilib.* **1999**, *155* (1), 139–154. https://doi.org/10.1016/S0378-3812(98)00435-X.

(47) Da Costa, A. R.; Fane, A. G.; Wiley, D. E. Spacer Characterization and Pressure Drop Modelling in Spacer-Filled Channels for Ultrafiltration. *J. Memb. Sci.* **1994**, *87* (1–2), 79–98. https://doi.org/10.1016/0376-7388(93)E0076-P.

(48) Yeh, H. M.; Cheng, T. W.; Wu, H. H. Membrane Ultrafiltration in Hollow-Fiber Module with the Consideration of Pressure Declination along the Fibers. *Sep. Purif. Technol.* **1998**, *13* (3), 171–180. https://doi.org/10.1016/S1383-5866(98)00041-0.

(49) Brinkmann, A.; Elouafiq, S.; Pieracci, J.; Westoby, M. Leveraging Single-Pass Tangential Flow Filtration to Enable Decoupling of Upstream and Downstream Monoclonal Antibody Processing. *Biotechnol. Prog.* **2018**, *34* (2). https://doi.org/10.1002/btpr.2601.

(50) Perry, C.; Rayat, A. C. M. E. Lentiviral Vector Bioprocessing. *Viruses* **2021**, *13* (2), 268. https://doi.org/10.3390/v13020268.

(51) Yehl, C. J.; Zydney, A. L. Single-Use, Single-Pass Tangential Flow Filtration Using Low-Cost Hollow Fiber Modules. *J. Memb. Sci.* **2020**, *595*. https://doi.org/10.1016/j.memsci.2019.117517.

(52) Krippl, M.; Kargl, T.; Duerkop, M.; Dürauer, A. Hybrid Modeling Reduces Experimental Effort to Predict Performance of Serial and Parallel Single-Pass Tangential Flow Filtration. *Sep. Purif. Technol.* **2021**, *276*. https://doi.org/10.1016/j.seppur.2021.119277.

(53) Usach, I.; Martinez, R.; Festini, T.; Peris, J. E. Subcutaneous Injection of Drugs: Literature Review of Factors Influencing Pain Sensation at the Injection Site. *Advances in Therapy*. 2019, pp 2986–2996. https://doi.org/10.1007/s12325-019-01101-6.

(54) Gokarn, Y. R.; Kras, E.; Nodgaard, C.; Dharmavaram, V.; Fesinmeyer, R. M.; Hultgen, H.; Brych, S.; Remmele, R. L.; Brems, D. N.; Hershenson, S. Self-Buffering Antibody Formulations. *J. Pharm. Sci.* **2008**, *97* (8), 3051–3066. https://doi.org/10.1002/jps.21232.

(55) Bahrenburg, S.; Karow, A. R.; Garidel, P. Buffer-Free Therapeutic Antibody Preparations Provide a Viable Alternative to Conventionally Buffered Solutions: From Protein Buffer Capacity Prediction to Bioprocess Applications. *Biotechnol. J.* **2015**, *10* (4), 610–622. https://doi.org/10.1002/biot.201400531.

(56) Jachimska, B.; Wasilewska, M.; Adamczyk, Z. Characterization of Globular Protein Solutions by Dynamic Light Scattering, Electrophoretic Mobility, and Viscosity Measurements. *Langmuir* **2008**, *24* (13), 6866–6872. https://doi.org/10.1021/la800548p.

(57) Menon, M. K.; Zydney, A. L. Measurement of Protein Charge and Ion Binding Using Capillary Electrophoresis. *Anal. Chem.* **1998**, *70* (8), 1581–1584. https://doi.org/10.1021/ac970902r.

(58) Tanford, C.; Hauenstein, J. D. Hydrogen Ion Equilibria of Ribonuclease. *J. Am. Chem. Soc.* **1956**, *78* (20). https://doi.org/10.1021/ja01601a036.

(59) Menon, M. K.; Zydney, A. L. Determination of Effective Protein Charge by Capillary Electrophoresis: Effects of Charge Regulation in the Analysis of Charge Ladders. *Anal. Chem.* **2000**, *72* (22), 5714–5717. https://doi.org/10.1021/ac000752b.

(60) Voet. D; J.G, V. *Biochemistry*, 3rd Editio.; John Wiley & Sons, Inc, 2011.

(61) Hunter, R. J. *Zeta Potential in Colloid Science*; 1981. https://doi.org/10.1016/c2013-0-07389-6.

(62) Burns, D. B.; Zydney, A. L. Contributions to Electrostatic Interactions on Protein Transport in Membrane Systems. *AIChE J.* **2001**, *47* (5), 1101–1114. https://doi.org/10.1002/aic.690470517.

(63) Hückel, E.; Debye, P. Zur Theorie Der Elektrolyte. I. Gefrierpunktserniedrigung Und Verwandte Erscheinungen. *Phys. Z.* **1923**, *24* (185), 305.

(64) Tanford, C.; Swanson, S. A.; Shore, W. S. Hydrogen Ion Equilibria of Bovine Serum Albumin. *J. Am. Chem. Soc.* **1955**, *12* (1), 77–80. https://doi.org/10.1021/ja01629a002.

(65) Blatt, W. F.; Robinson, S. M.; Bixler, H. J. Membrane Ultrafiltration: The Diafiltration Technique and Its Application to Microsolute Exchange and Binding Phenomena. *Anal. Biochem.* **1968**, *26*, 151–173. https://doi.org/10.1016/0003-2697(68)90039-0.

(66) Ladwig, J. E.; Zhu, X. X.; Rolandi, P.; Hart, R.; Robinson, J.; Rydholm, A. Mechanistic Model of pH and Excipient Concentration during Ultrafiltration and Diafiltration Processes of Therapeutic Antibodies. *Biotechnol. Prog.* **2020**, *36* (5), e2993. https://doi.org/10.1002/btpr.2993.

(67) Hebbi, V.; Roy, S.; Rathore, A. S.; Shukla, A. Modeling and Prediction of Excipient and pH Drifts during Ultrafiltration/Diafiltration of Monoclonal Antibody Biotherapeutic for High Concentration Formulations. *Sep. Purif. Technol.* **2020**, *238*. https://doi.org/10.1016/j.seppur.2019.116392.

(68) Loeb, M.; Nernst, W. Zur Kinetik Der in Lösung Befindlichen Körper. *Zeitschrift für Phys. Chemie* **1888**, *2U* (1), 613–637. https://doi.org/10.1515/zpch-1888-0295.

(69) Coffman, J.; Brower, M.; Connell-Crowley, L.; Deldari, S.; Farid, S. S.; Horowski, B.; Patil, U.; Pollard, D.; Qadan, M.; Rose, S.; et al. A Common Framework for Integrated and Continuous Biomanufacturing. *Biotechnol. Bioeng.* **2021**, *118* (4), 1735–1749. https://doi.org/10.1002/bit.27690.

(70) Coffman, J.; Bibbo, K.; Brower, M.; Forbes, R.; Guros, N.; Horowski, B.; Lu, R.; Mahajan, R.; Patil, U.; Rose, S.; et al. The Design Basis for the Integrated and Continuous Biomanufacturing Framework. *Biotechnol. Bioeng.* **2021**, *118* (9), 3323–3333. https://doi.org/10.1002/bit.27697.

(71) Kheddo, P.; Tracka, M.; Armer, J.; Dearman, R. J.; Uddin, S.; Van Der Walle, C. F.; Golovanov, A. P. The Effect of Arginine Glutamate on the Stability of Monoclonal Antibodies in Solution. *Int. J. Pharm.* **2014**, *473* (1–2), 126–133. https://doi.org/10.1016/j.ijpharm.2014.06.053.

VITA

Mario Jabra
83 Farwell St, Newtonville, MA, 02460
mgjabra@gmail.com
+1 814 810 0012

Education:

PhD, Chemical Engineering
Pennsylvania State University - University Park *August 2017-August 2022*

B.S., Chemical Engineering
The University of Balamand - Al-Koura, Lebanon *June 2017*

Professional Experiences:

Scientist, Genomic Medicine Downstream Purification Development, Sanofi *12/13/2021 – Present*
Lead downstream process development for all the downstream processing steps for AAV. I was involved in pilot runs, tech transfer and as a pipeline project lead. Processes include affinity chromatography, ion exchange chromatography, tangential flow filtration, cell lysis and viral filtration.

Research Assistant, Zydney's Research Group, Penn State University *08/21/2017 – 11/04/2022*
Downstream bioprocessing for the recovery of high valued biological products mainly monoclonal antibodies
My main projects include studying and designing continuous monoclonal antibodies formulation processes using hollow-fiber membrane and modelling Single Pass Tangential flow filtration.
Another major project consists of modelling of the diafiltration process in terms of excipient and pH prediction for an optimal design including the self-buffering effects using molecular modelling of the monoclonal antibody.

Applied Biomanufacturing Laboratory, Pennsylvania State University *08/19/2020 – 10/31/2021*
Served as a student then a lecturer for an extensive course and workshop covering the theory and hands-on experience for upstream and downstream fermentation of E.coli cultures at Penn State's fermentation facility. Course includes cell plating, bioreactor cell growth, cell lysis, centrifugation, ion exchange, protein A chromatography, tangential flow and sterile filtration.

Teaching Assistantship, Pennsylvania State University *2018 - 2019*
TA for CHE360 Biomolecular engineering. The course involved using kinetic and mass models for Bioreactor design using genetic banks in order to design an upstream process typically found in biopharmaceutical companies.
TA for ChE480 lab course. I mentored and guided students through the calculations and designs of chemical engineering based processed including process control, distillation, kinetics and liquid-liquid extraction.

Research Assistant, University of Balamand, Lebanon *2016 - 2017*
Modelling and designing cross (tangential) flow filtration in binary and tertiary solutions

Instructor Assistant, University of Balamand, Lebanon *2015 - 2016*
Took responsibility in hosting teaching sessions for more than 100 students covering differential equations, advanced calculus and linear algebra.